# THE EFFECTS OF IONIC LIQUIDS ON THE PROPERTIES OF EPOXIDIZED NATURAL RUBBER BASED POLYMER ELECTROLYTE SYSTEMS

**NORAZLIN BINTI ZAINAL**

**INSTITUTE OF GRADUATE STUDIES**
**UNIVERSITY OF MALAYA**
**KUALA LUMPUR**

**2018**

# THE EFFECTS OF IONIC LIQUIDS ON THE PROPERTIES OF EPOXIDIZED NATURAL RUBBER BASED POLYMER ELECTROLYTE SYSTEMS

**NORAZLIN BINTI ZAINAL**

**THESIS SUBMITTED IN FULFILMENT OF THE REQUIREMENTS FOR THE DEGREE OF DOCTOR OF PHILOSOPHY**

**INSTITUTE OF GRADUATE STUDIES**
**UNIVERSITY OF MALAYA**
**KUALA LUMPUR**

**2018**

**UNIVERSITY OF MALAYA**

**ORIGINAL LITERARY WORK DECLARATION**

Name of Candidate : **NORAZLIN BINTI ZAINAL**

I.C/Passport No

Registration/Matric No : **HHC090005**

Name of Degree **DOCTOR OF PHILOSOPHY**

Title of Project Paper/Research Report/Dissertation/Thesis ("this Work"):

**THE EFFECTS OF IONIC LIQUIDS ON THE PROPERTIES OF EPOXIDIZED NATURAL RUBBER BASED POLYMER ELECTROLYTE SYSTEMS**

Field of Study : **ADVANCED MATERIALS**

I do solemnly and sincerely declare that:

(1) I am the sole author/writer of this Work;
(2) This Work is original;
(3) Any use of any work in which copyright exists was done by way of fair dealing and for permitted purposes and any excerpt or extract from, or reference to or reproduction of any copyright work has been disclosed expressly and sufficiently and the title of the Work and its authorship have been acknowledged in this Work;
(4) I do not have any actual knowledge nor do I ought reasonably to know that the making of this work constitutes an infringement of any copyright work;
(5) I hereby assign all and every rights in the copyright to this Work to the University of Malaya ("UM"), who henceforth shall be owner of the copyright in this Work and that any reproduction or use in any form or by any means whatsoever is prohibited without the written consent of UM having been first had and obtained;
(6) I am fully aware that if in the course of making this Work I have infringed any copyright whether intentionally or otherwise, I may be subject to legal action or any other action as may be determined by UM.

Candidate's Signature Date:

Subscribed and solemnly declared before,

Witness's Signature Date:

Name:

Designation:

**THE EFFECTS OF IONIC LIQUIDS ON THE PROPERTIES OF EPOXIDIZED NATURAL RUBBER BASED POLYMER ELECTROLYTE SYSTEMS**

## ABSTRACT

The objective of this research work is to investigate the effect of ionic liquid on epoxidized natural rubber 50 added with lithium imide salt system. Electrolyte films were prepared using two different methods, namely, the wet method and dry method. Attenuated total reflectance-Fourier transform infrared spectroscopic analyses showed evidence of interaction between epoxidized natural rubber 50, ionic liquid and lithium salt. X-ray photoelectron spectroscopy study was done to strengthen those results. The thermogravimetric analyses of the films containing ionic liquid showed good thermal stability up to 350 °C. Glass transition temperatures for the electrolyte films containing ionic liquid were lower than that of ionic liquid free electrolyte films. Addition of lithium salt to the epoxidized natural rubber-ionic liquid systems, with increasing of salt content, increased the glass transition temperature values. The increasing trend of glass transition temperature with increase in salt concentration indicated reduction in flexibility of the polymer chains due to the formation of transient cross-linking between the polymer chains and lithium cation. However, the trend of variation of ionic conductivity showed that the increase in glass transition temperature did not give adverse effect on ionic conductivity. Ionic conductivity of the films increased with salt content. Electrolyte film containing ionic liquid, prepared by wet method showed the highest value in the order $10^{-4}$ S $cm^{-1}$ at ambient temperature. Electrolyte film prepared by dry method could withstand high temperature (for elevated temperature measurement) compared with the electrolyte film prepared by wet method. It was observed from this study that the addition

of ionic liquid to polymer-salt system could reduce glass transition temperature and improve ionic conductivity of the electrolyte films.

**Keywords:** epoxidized natural rubber, ionic liquid

**KESAN CECAIR IONIK TERHADAP CIRI-CIRI BAGI SISTEM ELEKTROLIT POLIMER BERASASKAN GETAH ASLI TEREPOKSI**

## ABSTRAK

Objektif kerja penyelidikan ini adalah untuk menyiasat kesan cecair ionik terhadap sistem getah asli terepoksi 50 yang ditambah dengan garam litium imide. Filem elektrolit telah disediakan dengan dua kaedah berbeza, yang dinamakan kaedah basah dan kaedah kering. Analisis-analisis spektroskopi pantulan keseluruhan dikecilkan-inframerah transformasi Fourier menunjukkan bukti interaksi di antara getah asli terepoksi 50, cecair ionik dan garam litium. Kajian spektroskopi fotoelektron sinar-X telah dilakukan untuk mengukuhkan keputusan-keputusan tersebut. Analisis-analisis termogravimetrik bagi filem-filem yang mengandungi cecair ionik menunjukkan kestabilan terma yang baik sehingga ke suhu 350 °C. Suhu peralihan kaca bagi filem-filem elektrolit yang mengandungi cecair ionik adalah lebih rendah daripada filem-filem yang tidak mengandungi cecair ionik. Penambahan garam litium kepada sistem getah asli terepoksi – cecair ionik, dengan penambahan kandungan garam, meningkatkan nilai-nilai bagi suhu peralihan kaca. Aliran peningkatan bagi suhu peralihan kaca dengan peningkatan kepekatan garam menunjukkan penurunan kelenturan rantai polimer disebabkan oleh pembentukkan rangkaian silang sementara di antara rantai polimer dan kation litium. Walaubagaimanapun, perubahan aliran bagi kekonduksian ion menunjukkan bahawa peningkatan dalam suhu peralihan kaca tidak memberikan kesan penurunan kepada kekonduksian ion. Kekonduksian ion bagi filem-filem meningkat dengan peningkatan kandungan garam. Filem elektrolit yang mengandungi cecair ionik, yang disediakan dengan kaedah basah menunjukkan nilai tertinggi diperolehi adalah dalam julat $10^{-4}$ S $cm^{-1}$ pada suhu sekitaran. Filem elektrolit yang disediakan dengan kaedah kering boleh bertahan dengan suhu tinggi (untuk pengukuran suhu tinggi) berbanding filem elektrolit

yang disediakan dengan kaedah basah. Daripada kajian ini, telah didapati bahawa penambahan cecair ionik kepada sistem polimer-garam boleh menurunkan suhu peralihan kaca dan meningkatkan kekonduksian ion bagi filem-filem elektrolit.

**Katakunci**: getah asli terepoksi, cecair ionik

## ACKNOWLEDGEMENTS

I would like to thank Allah s.w.t for giving me the opportunity to complete this research project successfully. I wish to extend my sincere gratitude to my supervisor Prof. Dr. Nor Sabirin Mohamed for her tremendous invaluable guidance, comments and support throughout the study. She offered me so much advice, patiently supervising me and always guiding me in the right direction.

Special thanks to Assoc. Prof. Dr Razali Idris for his ideas and comments. His encouragement and help made me feel confident to overcome the difficulties that I encountered in my research work. I am also very grateful to the staff and the postgraduate students of the Electrochemical Materials & Devices Research Group in Centre for Foundation Studies in Science for their help.

Utmost appreciation to my beloved husband, children and parents for their continuous support, sacrifices and love. Finally, my special appreciation to Centre for Foundation Studies in Science which has given me the opportunity to do my PhD and also to University of Malaya for providing the financial support.

## TABLE OF CONTENTS

## LIST OF FIGURES

## LIST OF TABLES

## LIST OF SYMBOLS AND ABBREVIATIONS

| | | |
|---|---|---|
| $A$ | : | Surface area of the film |
| $B$ | : | Conduction activation energy (VTF) |
| $E$ | : | Energy of photon |
| $E_a$ | : | Activation energy |
| $h$ | : | Plank constant |
| $n$ | : | Number of charge carrier |
| $q$ | : | Charge of ion |
| $R_B$ | : | Bulk resistance |
| $t$ | : | Thickness of the film |
| $T$ | : | Temperature |
| $T_d$ | : | Degradation temperature |
| $T_g$ | : | Glass transition temperature |
| $T_o$ | : | Equilibrium glass transition temperature |
| *wt. %* | : | Weight percent |
| $\mu$ | : | Mobility of ion |
| $\sigma$ | : | Conductivity |
| $\sigma_o$ | : | Pre-exponential conductivity |

| | | |
|---|---|---|
| $(CF_3SO_2)_2N^-$ | : | Bis(trifluoromethane sulfonyl) anion |
| ATR-FTIR | : | Attenuated total reflection-Fourier transform infrared |
| $BF_4^-$ | : | Tetrafluoroborate anion |
| BMITFSI | : | 1-butyl-3-methylimidazolium bis(trifluoromethanesulfonyl) imide |
| $CF_3SO_3^-$ | : | Trifluoromethanesulfonic anion |
| DMC | : | Dimethyl carbonate |
| DMF | : | Dimethylformamide |
| DSC | : | Differential scanning calorimetry |
| DTG | : | Differential thermal gravimetry |
| EC | : | Ethylene carbonate |
| EIS | : | Electrochemical impedance spectroscopy |
| $EMIBF_4$ | : | 1-ethyl-3-methylimidazolium tetrafluoroborate |
| EMITFSI | : | 1-ethyl-3-methylimidazolium bis(trifluoromethanesulfonyl) imide |
| ENR | : | Epoxidized natural rubber |
| HDPE | : | High density polyethylene |
| IL | : | Ionic liquid |
| IS | : | Impedance spectroscopy |
| LDPE | : | Low density poly ethylene |
| $Li^+$ | : | Lithium ion |
| $LiBF_4$ | : | Lithium tetrafluoroborate |
| LiTFSI | : | Lithium imide |
| LSV | : | Linear sweep voltammetry |
| MNR | : | Modified natural rubber |
| NR | : | Natural rubber |
| PAN | : | Polyacrylonitrile |
| PC | : | Propylene carbonate |
| PEO | : | Poly (ethylene oxide) |
| $PF_6^-$ | : | Hexafluorophosphate anion |
| PMMA | : | Poly (methyl methacrylate) |
| PP | : | Polypropylene |
| PS | : | Polystyrene |

| | | |
|---|---|---|
| PVA | : | Poly (vinyl alcohol) |
| PVC | : | Polyvinyl chloride |
| PVDF | : | Polyvinylidene fluoride |
| $SiO_2$ | : | Silicon dioxide |
| SPE | : | Solid polymer electrolyte |
| $TFSI^-$ | : | Bis(trifluoromethane sulfonyl)imide ion |
| TGA | : | Thermogravimetric analysis |
| THF | : | Tetrahydrofuran |
| VTF | : | Vogel-Tammann-Fulcher |
| XPS | : | X-ray photoelectron spectroscopy |

# CHAPTER 1: INTRODUCTION

## 1.1 Overview

Polymer electrolytes are of current interest due to their potential applications in various electrochemical devices such as solar cells, batteries, sensors and electrochromic devices (Cheng *et al*, 2018; Rudziah *et al*, 2015; Deraman *et al*, 2013; Rao *et al*, 2012; Gowda *et al*, 2010; Wang *et al*, 2011; Nejati *et al*, 2011; Nguyen *et al*, 2011). This type of electrolyte materials offer many advantages including high ionic conductivity, solvent free condition, wide electrochemical stability window, light and easy processability.

Many studies have been done using synthetic polymers as host polymers in polymer electrolytes (Rajendran *et al*, 2006; Rajendran *et al*, 2003; Gorecki *et al*, 1995). However, the use of natural polymers especially natural rubber has not been widely investigated. This does not indicate that natural rubber is inferior in properties to be host polymer for the development of polymer electrolytes. In contrast the derivatives of natural rubber posses some excellent properties comparable to synthetic polymers. With the easily available source of natural rubbers and their derivatives here in Malaysia, it is vital to explore the potential of the natural resources for the development of polymer electrolytes.

Various methods have been employed to enhance the performance of polymer electrolytes such as blending with other polymers, addition of ceramic fillers and plasticization (Wang & Alexandridis, 2016; Mohamed *et al*, 2008; Idris *et al*, 2007; Wilson *et al*, 2006). The addition of plasticizer to a polymer leads to an improvement in ionic conductivity, but they usually suffer from significant problems of flammability, volatility, and instability in terms of mechanical, electrochemical and thermal properties

(Agrawal & Pandey 2008). Therefore, it is important to develop alternative electrolyte systems, which consist of non-volatile solvents with better and stable properties.

In recent years, ionic liquids (ILs) have received attention from both academic and industrial research groups because of their wide range of applications and also environmentally-friendly alternatives to organic solvents. Their unique and excellent characteristics such as negligible vapor pressure, non-flammable and non-corrosive, high thermal stability, large electrochemical window and high electrochemical stability make them suitable for applications as electrolytes for energy conversion and storage devices (Macfarlane *et al*, 2007; Shin *et al*, 2003).

This work is dedicated to the development of polymer electrolytes using modified natural rubber, namely epoxidized natural rubber (ENR), as the host polymer. In order to enhance conductivity and to get films that physically stable, ionic liquids are added to the electrolytes.

### 1.2 Problem Statements

Development of materials based on natural product such as natural rubber for use in different devices or appliances is essential to diversify its application in technical and engineering field. With this aim, and also because of the unique properties of ENR such as low $T_g$, soft elastomer characteristics, good elasticity and adhesion to solid substrates, ENR has been chosen as host polymer in electrolyte systems.

Previous studies focused on enhancing the conductivity of ENR based polymer electrolytes by employing plasticizers. However, the use of plasticizer leads to some unfavorable effects such as flammability and volatility (Long *et al*, 2016). Ionic liquids (ILs) are thought to be more suitable due to its unique and excellent characteristics.

Therefore, in this study, ILs will be used to obtain polymer electrolytes with enhanced properties and thus are more suitable for application in electrochemical devices.

Conventional polymer-salt electrolytes studies have been mainly focused on dissolving salt in polymer hosts to prepare solid or gel polymer electrolyte materials. In this method, solvents such as dimethylformamide (DMF) and tetrahydrofuran (THF) are used to dissolve the polymers and salts. However, most of the solvents are toxic and hazardous. Therefore, the dry method can be an alternative method to prepare solid polymer electrolytes (Gonzalez *et al*, 2018). Internal mixer system is the equipment that can be used to prepare the mixing process between species by considering the time dependence of the torque. This mixing process involves momentum and heat transfer. The torque trajectory can be used to monitor the mixing process between polymer and any additives. The electrolyte films can be prepared by compression moulding at certain temperature. Since it is safer and more environmental friendly compared to the wet method, it is interesting to find out the viability of this method for preparing ENR based electrolytes.

ENR based polymer electrolytes are among promising materials for application in electrochemical devices such as batteries and electrochromic devices. The rubbery films which are prepared, characterized and fabricated in the laboratory show reasonable ionic and electrochemical behavior suitable for these applications. ENR based polymer electrolyte also shows good adhesive property that can form excellent interfacial contact with electrode materials in electrochemical devices.

## 1.3 Research Objectives

The main aim of this work is to obtain ENR-ionic liquid polymer electrolyte films with high conductivity and good mechanical and electrochemical properties. As such, works were done:

(i) to improve conductivity of ENR based polymer electrolyte by using ionic liquid, at least by one order of magnitude.

(ii) to identify the effect of ionic liquid to the spectroscopic response, binding energy, thermal properties, ionic conductivity and electrochemical stability.

(iii) to obtain ENR-50 based polymer electrolyte using dry method.

(iv) to identify the characteristics of materials prepared using dry method in order to determine the viability of this method.

## 1.4 Thesis outline

The scope of this research work is briefly given as follows:

I. A literature review, which includes an overview of previous studies on polymer electrolytes; some fundamental aspects of epoxidized natural rubber and ionic liquid (that used in this work); an overview of previous studies on polymer electrolytes based on epoxidized natural rubber; and some fundamental theory on characterization techniques of polymer electrolyte.

II. Preparation of polymer electrolyte samples by wet and dry methods.

III. Study of the properties of the polymer electrolyte samples (prepared by wet method) by attenuated total reflectance-Fourier transform infrared (ATR-FTIR) spectroscopy, X-ray photoelectron spectroscopy (XPS), differential scanning calorimetry (DSC) and thermogravimetric analysis (TGA). Ionic conductivity is carried out using impedance spectroscopy measurement and

the electrochemical stability is investigated by linear sweep voltammetry (LSV).

IV. Study of the properties of the polymer electrolyte samples (prepared by dry method) by ATR-FTIR spectroscopy, XPS, DSC and TGA. Ionic conductivity is carried out using impedance spectroscopy.

V. Conclusions, which are presented in the final part.

# CHAPTER 2: LITERATURE REVIEW

## 2.1 Polymer Electrolytes

The discovery of polymer electrolytes (conducting polymers by ionic species) in the 1970s by Peter Wright and Michael Armand introduced the first new class of solid ionic conductors since the phenomenon of ionic conductivity in the solid state was first identified by Michael Faraday in the 1800s. The earliest polymer electrolytes, which remain one of the most important classes of polymer electrolytes to this day, consist of a salt dissolved in a high molecular weight polymer. The latter must contain donor atoms capable of acting as ligands coordinating the cations of the salt and hence providing the key solvation enthalpy to promote formation of the polymer electrolyte.

In solid polymer electrolytes (SPEs), cation migration is associated with the segmental mobility of the polymer chains (MacCallum and Vincent, 1989). Polymer segmental motion arising from bond rotations provides only for short range motion of coordinated cations within limited region of space. The flexibility of polymers may be considered to understand the ionic transportation in SPEs. It is believed that the ion transport occurred above the glass transition temperature, $T_g$. Above $T_g$, local segmental motion of the polymer chains occurs and thus facilitates the ionic motion through the polymer. However, segmental motion of the polymer is being in some way reduced at higher salt concentrations.

In SPEs, the combination of ionic conductivity in the solid state with mechanical flexibility, making them ideal replacements for liquid electrolytes in electrochemical cell because of their ability to form good interfaces with solid electrodes. Furthermore, the choice of solid electrolyte materials implies several advantages such as the absence of

liquids or gases which may leach out, damaging the cell and the utilization temperature range larger than for liquid electrolyte-based systems. Besides safety performance, SPEs are also promising candidate as they are easy to configure in any shape due to their high flexibility of polymer matrix, high potential for electrode application and light in weight.

Although the dry and composite types of SPEs are highly desirable in view of their mechanical/handling strength and safety, they possess relatively low ionic conductivity (typically $<10^{-4}$ S $cm^{-1}$) at room temperature which limits their practical applications. However the gel PEs exhibit higher ionic conductivity (~$10^{-3}$ S $cm^{-1}$ at 25ºC), but are less advantageous with regard to mechanical strength and safety. Thus, researchers keep on working in this field to find suitable materials to prepare solid polymer electrolytes for various applications especially in electrochemical devices.

One of the methods that can be used to obtain high ionic conductivities is by introducing plasticizers, which are often low molecular weight aprotic organic solvents such as ethylene carbonate (EC), propylene carbonate (PC), dimethylformamide (DMF) or low molecular weight polymers and their derivatives (Chintapalli & Frech, 1996; Appetecchi *et al*,1995). Introducing plasticizers into polymer electrolyte lowers the glass transition temperature ($T_g$), increases the amorphicity and free volume of the polymers. Moreover, it reduces the viscosity of polymer system and then facilitates the ionic migration within the polymer matrix. Besides, it weakens the interactions within the polymer chains and thus improves the flexibility of polymer chains in the polymer matrix (Ganesan *et al*, 2008).

A new approach to increase amorphicity as well as the number of ionic charge carriers in polymer electrolytes is to incorporate ionic liquids into the polymer matrix (Ueki & Watanabe, 2008; Lewandowski & Swiderska, 2004).

Most of the studies in polymer electrolytes reported in the literature employed synthetic polymers such as PEO, PMMA, PVC and PVDF (Eschen *et al*, 2012; Chew & Tan, 2011; Karan *et al*, 2008; Miao *et al*, 2008; Rajendran *et al*, 2008) as host. Poly(ethylene oxide) (PEO) is one of the most commonly studied host polymer for developing polymer electrolytes because of its good solvation property and its ability to dissolve high concentrations of a wide variety of dopant salts. On the other hand, there are limited number of studies used natural polymers or semi-natural polymers as hosts (Ahmad *et al*, 2012; Kumutha *et al*, 2005). Modified natural rubber (MNR) is one of the semi-natural polymers that recently have been used as host in polymer electrolyte technology.

## 2.2 Modified natural rubber

Natural rubber is an elastomer that is originally derived from a milky colloidal suspension or latex found in the sap of some plants. The most common natural rubber (NR) originated from the plant *Hevea brasillensis*, possesses excellent physical properties for general purpose rubber with its chemical structure of cis-1,4-polyisoprene. Natural rubber can easily soften with heat or hardened by cold. It has tacky, odorous and perishable properties (Gelling & Porter, 1985). The use of natural rubber ranging from household to industrial products, but the applications are limited in technical and engineering fields. However, the properties of natural rubber can be improved via modifications (Goonctilleke *et al*,1991). Chemical modifications of natural rubber have been attempted to improve the performance for specific application and to convert natural

rubber into new materials. This is possible because of the presence of double bonds (C=C) in the natural rubber polymer chain that act as simple olefin. Chemical modification can alter and enhance the physical properties of NR. One of the important products of chemically modified natural rubber is the epoxidized natural rubber (ENR).

## 2.3 Epoxidized natural rubber

ENR is a product that chemically modified form of the cis-1,4-polyisoprene rubber, whereby some of the unsaturated is converted into epoxide groups, which are randomly distributed along the polymer chain (Ismail, *et al*, 2001).

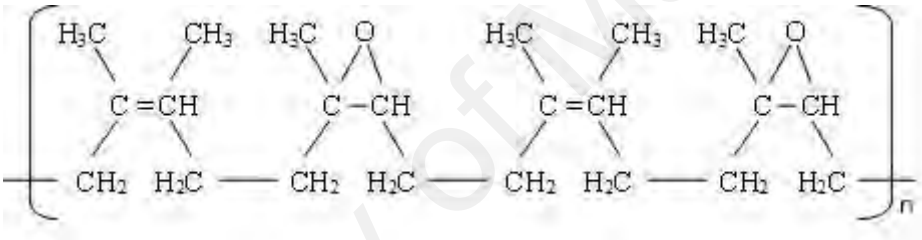

**Figure 2.1:** Chemical structure of ENR-50

ENR is produced by epoxidation reaction on the polyisoprene backbone of NR at the latex stage. This reaction goes back to 1922 when it was first discovered by Pummerer and Burkard. In spite of the process being extensively studied by many workers, it was not until Gelling and Porter, 1985 controlled the reaction to eliminate ring opening that a useful material was discovered. Although in theory any degree of epoxidation may be achieved, two grades of ENR, ENR-25 and ENR-50 with 25 and 50 mole% of epoxidation respectively, have attained commercial importance.

ENR exhibits both rubber and special elastomer characteristics that can be tailored for various usages. Some of the potential commercial uses of ENR are tires, coatings and

adhesives. Besides, ENR also has the potential for use in polymer electrolytes technology. ENR is one of the semi-natural polymers that recently have been used as host in polymer electrolyte technology mainly because of its several advantages such as good mechanical and thermal properties. The ionic conductivity in the ENR based electrolytes is expected to occur by interaction between the cation (such as $Li^+$) and the oxygen atoms of the epoxy bond (Klinklai *et al*, 2006; Kim *et al*, 2004).

**Table 2.1:** Some research works on epoxidized natural rubber based polymer electrolyte systems

| Systems | Ionic conductivity, σ (S cm$^{-1}$) | References |
|---|---|---|
| (ENR-50/PEMA)/ $LiCF_3SO_3$ | ~$10^{-5}$ | Sukri *et al* (2017) |
| (ENR-50/PEMA)/$BF_4$/$NH_4CF_3SO_3$ | ~$10^{-5}$ | Mohammad *et al* (2013) |
| (ENR-50)/EC or PC/$LiCF_3SO_3$ | ~$10^{-4}$ | Mohamed *et al* (2008) |
| (ENR-50)/EC:PC/$LiN(SO_2CF_3)_2$ | ~$10^{-4}$ | Razali & Wan Siti Nor (2007) |
| ENR/EC:PC/$LiN(SO_2CF_3)_2$ | ~$10^{-4}$ | Kim *et al* (2004) |
| (ENR/PEO)/$LiCF_3SO_3$ | ~$10^{-5}$ | Glasse *et al* (2002) |
| (ENR/PEO)/EC:PC/$LiCF_3SO_3$ | ~$10^{-4}$ | Glasse *et al* (2002) |
| (ENR-25)/EC:PC/$LiCF_3SO_3$ | ~$10^{-4}$ | Idris *et al* (2001) |
| (ENR-50)/EC:PC/$LiCF_3SO_3$ | ~$10^{-4}$ | Idris *et al* (2001) |

Studies on ENR based polymer electrolytes have been reported by a few groups of researchers, as listed in Table 2.1. They used ENR as host polymer or by blending it with other polymers and added with various types of lithium salts and plasticizers to form solid polymer electrolyte or gel polymer electrolyte systems. They reported conductivity in the

order of $10^{-4}$ S $cm^{-1}$ for polymer electrolyte system containing lithium salts and plasticizers (such as EC and PC). Plasticizing the host polymer (that is increasing the segmental motion and dropping the glass transition temperature by adding a small-molecule solvent such as ethylene carbonate or propylene carbonate) is generally recognized as one of the effective methods in enhancing the amorphous fraction and changing the local electric field distribution in the polymer matrix, thus increasing the ionic conductivity (Mustafa *et al*, 2012; Ahmad *et al*, 2011; Pradhan *et al*, 2008). However, the use of plasticizers in polymer electrolyte systems leads to some disadvantages associated with them such as poor thermal stability, volatility, flammable and low electrochemical stability. The use of plasticizers can also result in instabilities when lithium metal anodes are used in actual cells (Shin *et al*, 2005). Therefore, to overcome this limitation, the use of non-volatile organic solvents such as ionic liquids (ILs) may be considered.

### 2.4 Ionic liquids

An alternative method of achieving high ionic conductivity in polymer electrolytes technology is the use of ionic liquids (ILs). ILs can either contribute as the main conductivity medium supported in a polymer membrane or as a plasticizing component in polymer electrolytes. Addition of ionic liquids is expected to reduce the viscosity of the polymer system and facilitates the ionic migration within the polymer matrix. Besides, the ILs weaken the interactions within the polymer chains and thus improves the flexibility of polymer chains in the polymer matrix. This increases the free volume of polymer and enhances the long-range segmental motion of the polymer system leading to ionic conductivity improvement.

The ILs generally consist of bulky, asymmetric organic cations and inorganic/organic anions (Triolo *et al*, 2009). The ILs are generally liquid at room temperature. They are intriguing solvents due to their negligible vapour pressures, non-volatile, non-flammable, excellent chemical and thermal stability and also environmental compatibility. One of the advantages of using ILs is reported by Peng *et al* (2007). They found that the aluminium corrosion was not occurred in room temperature ionic liquids (RTILs) electrolytes containing lithium salt but occurred in EC+DMC solution containing lithium salt.

From an electrochemical point of view, ILs offer a high ionic conductivity and a wide potential window (Fernicola *et al*, 2007; Galinski *et al*, 2006). For these reasons, ILs have attracted much attention for their potential application in electrochemical capacitors (Balducci *et al*, 2004; McEwen *et al*, 1997) and non-aqueous batteries (Sato *et al*, 2004; Sakaebe and Matsumoto, 2003). Furthermore, because of their excellent characters they are also applicable in fuel cell and actuators. Cho *et al* (2007) reported that the displacement rate in their solid polymer actuator containing ionic liquids was greater than that observed in conventional electrolyte systems containing propylene carbonate (PC).

It has also been noted that ionic liquids have strong interactions with many polymers (Noda & Watanabe, 2000; Watanabe & Mizumura, 1996). Shin *et al* (2005) have reported that the dry solid polymer electrolyte consisting of high molecular weight PEO, LiTFSI and ionic liquid $P_{13}$TFSI reaches an ionic conductivity of ~$10^{-4}$ S $cm^{-1}$ at 20 ºC which is almost two orders of magnitude higher than that of ionic- liquid-free PEO/LiTFSI electrolyte.

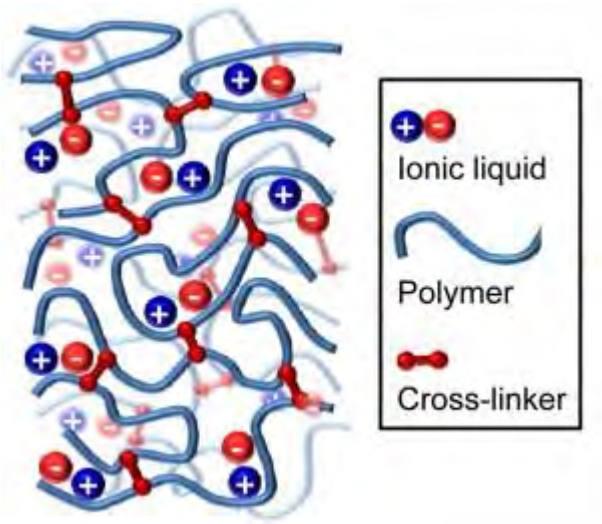


**Figure 2.2:** Schematic illustration of IL-incorporated polymers (Park *et al*, 2013)

The new prospect of using IL in polymer electrolytes applications is developed by Park *et al* (2013) as shown in Figure 2.2, who explored few ways to improve ion transport properties in solid polymer electrolytes using ionic liquids. They worked on lithium batteries, high temperature fuel cells, and electro-active actuators and showed that the devices performance enhanced upon incorporation of ionic liquid into polymer electrolyte system.

Ionic liquids are expected to provide a similar plasticizing effect to conventional organic solvent electrolyte at as a low temperature as room temperature regardless of their viscosities. Chaurasia *et al* (2011) found in their studies that ionic liquid acted as plasticizer even though at low percentage. Furthermore, Lewandoski & Swiderska (2004) found that the ionic liquids serve both as plasticizer and a source of charge carriers when they incorporated the ionic liquids into the polymer matrix (PAN, PEO and PVA).

Generally, the most popular ILs consist of quartenary ammonium cations such as imidazolium, pyridinium, pyrrolidinium, ammonium, sulfonium and phosphonium, and of anions with low Lewis basicities, e.g., $BF_4$, $PF_6$, $CF_3SO_3$ and $(CF_3SO_2)_2N$ anions. In

the imidazolium cations, the geometric packing constraints of the planar imidazolium ring, its dangling alkyl groups, and the delocalization of the charge over the N-C-N moiety in the ring all serve to decrease ion-ion interactions and lower the melting points (Tsuzuki *et al*, 2005). ILs comprising an imidazolium cation and an organic anion show mechanical strength, chemical stability and excellent ionic conductivity.

Scott *et al* (2003) found that the ionic liquids based on imidazolium salts have been found to serve as excellent plasticizers with improved thermal stability and ability to significantly reduce the glass transition temperatures. Furthermore, imidazolium salts have high thermal stability which begins to decompose at ~400 °C. Imidazolium ion also shows good behaviour in actuator studies. Cho *et al* (2007) reported that the imidazolium ion showed slightly higher displacement than the pyrrolidinium ion in their PEDOT/NBR actuator. Vuk *et al* (2008) studied the imidazolium-based ionic liquid derivatives for application in electrochromic devices which showed the improvement of the photopic transmittance

One of the most effective anions in producing low melting points appears to be the bis(trifluoromethane sulfonyl)imide $(CF_3SO_2)_2N$ (TFSI) ion. TFSI is a weakly interacting and flexible anion, and there is strong evidence of delocalization of the charge from the nitrogen atom onto the neighboring sulphur atoms. This results in a little delocalization onto oxygens, so that the delocalized charge is shielded, thereby diminishing the strength of ion-ion interactions with nearby cations (McFarlane *et al*, 2000). In addition, the delocalization of the negative charge of the TFSI with the nearby cation might allow better mobility than other anions. Ionic liquids containing TFSI have advantages such as wide electrochemical potential window, acceptable ionic conductivity, high thermal stability and negligible vapour pressure (Turner *et al*, 2005, Zhengxi *et al*, 2005). The

effectiveness of the TFSI anion in enhancing the kinetic stability toward the Li electrode of an imidazolium based IL has been proven by Koch *et al* (1995).

### 2.4.1 Ionic liquid: 1-butyl-3-methylimidazolium bis(trifluoromethanesulfonyl) imide

One of the suitable imidazolium based ionic liquid candidates for preparing polymer electrolyte material is 1-butyl-3-methylimidazolium bis(trifluoromethanesulfonyl)imide (BMITFSI). This IL is constructed by BMI cation and TFSI anion, as shown in Figure 2.3. Some physical properties such as conductivity, viscosity and glass transition temperature of BMITFSI are listed in Table 2.2. This type of ionic liquid has been used in polymer electrolytes by many groups of researchers since it has potential uses in device applications (Tong *et al*, 2017;Kim *et al*, 2009; Cho *et al*, 2007; Choi *et al*, 2007). Peng *et al* (2007) suggested that BMITFSI could be used as candidate to replace organic solvent (plasticizer) in order to inhabit the corrosion of aluminium current collector in the electrolytes containing LiTFSI in practical advanced lithium ion batteries.

The use of BMITFSI with natural polymer based has been explored by Cho *et al* (2007), as shown in Table 2.3, who fabricated a dry-type conducting polymer actuator using nitrile rubber (NBR). Their works showed the compatibility between the ionic liquid, BMITFSI and the NBR polymer. Moreover, there are few other researchers, as listed in Table 2.3, who used BMITFSI with synthetic polymers.

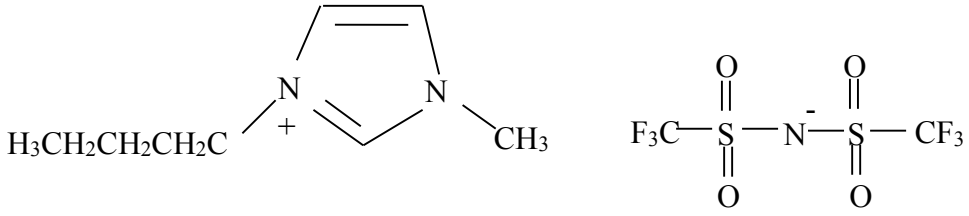


**Figure 2.3:** Chemical structure of BMITFSI

**Table 2.2:** Physical properties of BMITFSI

| Parameters | Values | References |
|---|---|---|
| Conductivity, σ (S $cm^{-1}$) | $2.23 \times 10^{-3}$ (at 25 ºC) | Zhengxi *et al* (2005) |
| Viscosity (mPa s) | 38.9 (at 30 °C<br>45 (at 25 ºC) | Osada *et al* (2009)<br>Zhengxi *et al* (2005) |
| Glass transition temperature (ºC) | -87 | Tokuda *et al* (2004) |

**Table 2.3:** Some research works on BMITFSI

| Applications | Systems | Ionic conductivity, σ (S $cm^{-1}$) | References |
|---|---|---|---|
| Actuator | NBR/BMITFSI | $2.08 \times 10^{-4}$ | Cho *et al* (2007) |
| Actuator | NBR/BMITFSI | $2.54 \times 10^{-4}$ (at 20 ºC) | Cho *et al* (2007) |
| Lithium battery | P(VdF-HFP)/ BMITFSI/$SiO_2$ | $4.3 \times 10^{-3}$ (at 25 ºC) | Kim *et al* (2008) |
| Lithium battery | PEO/LiTFSI/BMITFSI | $3.2 \times 10^{-4}$ (at 25 ºC) | Choi *et al* (2007) |

### 2.4.2 Ionic Liquid: 1-ethyl-3-methylimidazolium bis(trifluoromethanesulfonyl) imide

1-ethyl-3-methyl imidazolium bis(trifluromethanesulfonyl) imide (EMITFSI), as shown in Figure 2.4 is one of the most versatile ionic liquids which has high conductivity and low viscosity (one of the least viscous ionic liquids) at room temperature (Wang *et al*, 2007; Ishikawa *et al*, 2006). Table 2.4 listed some physical properties of EMITFSI.

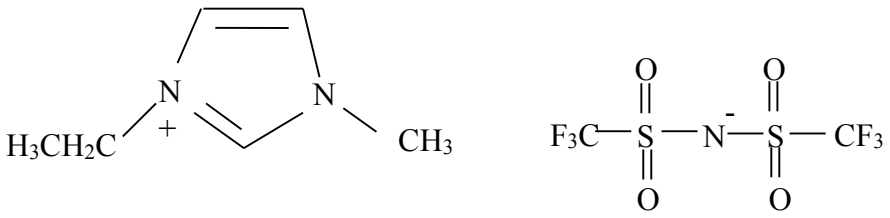

**Figure 2.4:** Chemical structure of EMITFSI

**Table 2.4:** Physical properties of EMITFSI

| Parameters | Values | References |
|---|---|---|
| Conductivity, σ (S $cm^{-1}$) | $8.7 \times 10^{-3}$ (at RT) | An *et al* (2011) |
| Viscosity (mPa s) | 26 (at RT) | Zhengxi *et al* (2005) |
| Glass transition temperature (ºC) | -87 | Zhengxi *et al* (2005) |

Zhu *et al* (2008) reported that incorporation of EMITFSI in PEO-based polymer electrolyte resulted in change of the phase structure of PEO leading to formation of more amorphous phase. The IL also weakened the association between $Li^+$ and $TFSI^-$ (from LiTFSI) causing more free $Li^+$. The $TFSI^-$ anion from the ionic liquid plays a main plasticizing role in the PEO/LiTFSI system. In term of thermal stability behaviour, Nakajima & Ohno (2005) reported that EMITFSI ionogel showed decomposition temperature at ~400 °C due to excellent thermal stability of TFSI anion compared with $EMIBF_4$ –containing polymer, which started to decrease in weight at ~300 °C.

According to Gracia *et al* (2004), the combination of EMI cation and TFSI anion in a test cell containing LiTFSI had better capacity stability than test cells containing $LiBF_4$-

$EMIBF_4$ or LiTFSI-EC/DMC. Thus, it can be suggested that the selection of anion is important to determine the thermal and capacity stabilities of the polymer electrolyte system. Table 2.5 listed other researchers who used EMITFSI with PMMA and PEO in their research works.

**Table 2.5:** Some research works on EMITFSI

| Systems | Ionic conductivity | References |
|---|---|---|
| PVdF-HFP/EMITFSI/LiTFSI | ~$10^{-3}$ S $cm^{-1}$ (at room temperature) | Bai *et al* (2017) |
| PMMA/EMITFSI | ~$10^{-2}$ S $cm^{-1}$ (at 30 ºC) | Seki *et al* (2005) |
| (PEO-PMA)/$Mg(TFSI)_2$/EMITFSI | $1.1 \times 10^{-4}$ S $cm^{-1}$ (at 20 ºC) | Morita *et al* (2005) |

## 2.5 Characterizations of polymer electrolytes

### 2.5.1 Attenuated total reflectance – Fourier transform infrared

ATR-FTIR is developed to determine the optical constant and to obtain intense spectra from samples. In ATR the radiation incident on an interface between the sample and an analysing crystal will be totally reflected at those wavelengths where the sample shows no absorption. However, at wavelengths where the sample absorbs, part of incident radiation will be absorbed causing an attenuated of the reflected radiation. Such an effect produces a spectrum which strongly resembles the transmission spectra. ATR-FTIR analysis in SPE is done to investigate ion-polymer interaction and possible conformational changes due to the addition of salt and other additives in the host polymer.

Figure 2.5 shows the transmission (in percent) versus wavelength spectra of chitosan and carboxymethyl chitosan. From the shift of the certain peaks observed in the spectra between pure chitosan and carboxymethyl chitosan (which have been labelled in the spectra), the interaction between constituents in the sample can be determined.

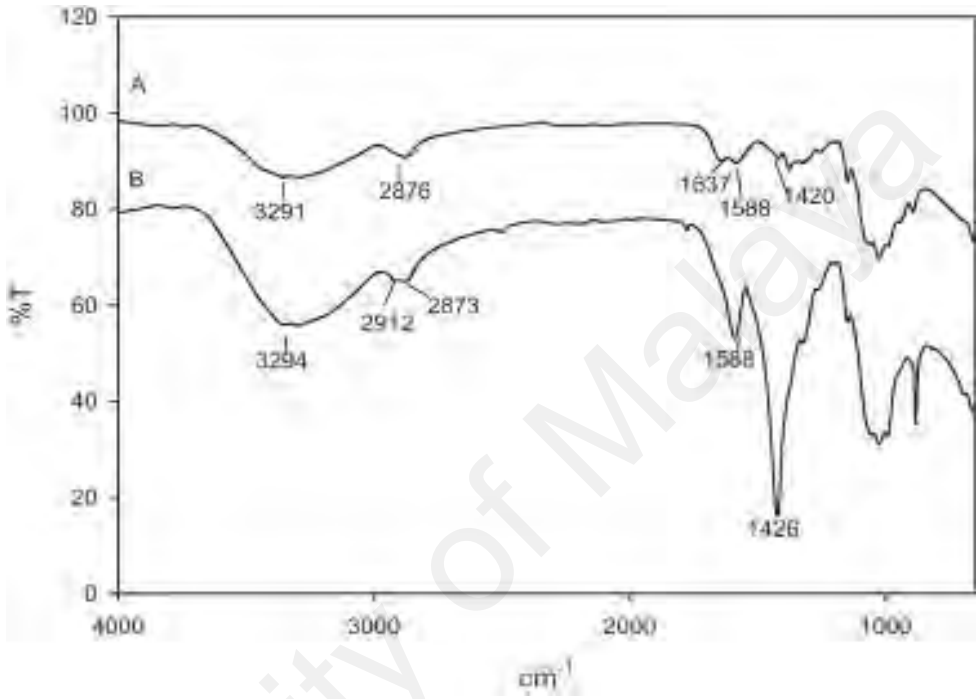


**Figure 2.5:** Transmittance spectra of powder (A) chitosan and (B) carboxymethyl chitosan (Mobarak *et al*, 2013)

### 2.5.2 X-ray photoelectron spectroscopy

XPS is a powerful technique widely employed to study surfaces of solid materials. The binding energies of various core-level electrons from different elements present in the solid material can be obtained from the result of this study. The value can be interpreted in terms of bonding between elements under consideration with their neighbours.

Photoelectron spectroscopy is based upon a single photon in/electron out process. The energy of a photon of all types of electromagnetic radiation is given by the Einstein relation,

$$E = h\upsilon \tag{2.1}$$

where $h$ is Planck constant ($6.62\times10^{-34}$ J s) and $\upsilon$ is frequency (Hz) of the radiation.

In XPS, the photon is absorbed by an atom in a molecule or solid, leading to ionization and the emission of a core (inner shell) electron. The kinetic energy distribution of the emitted photoelectrons can be measured using electron energy analyzer and thus the result can be recorded in term of photoelectron spectrum.

Binding energy is the energy required to remove the electron from its initial level to the vacuum level. The relationship between kinetic energy (KE) and binding energy (BE) can be given as,

$$\mathrm{KE} = h\upsilon - \mathrm{BE} \tag{2.2}$$

Each element reveals a characteristic binding energy associated with each core atomic orbital. It will give rise to a characteristic set of peaks in the photoelectron spectrum at kinetic energies determined by the photon energy and the respective binding energies. The presence of peaks at particular energies indicate the presence of specific element in the sample. Furthermore, the intensity of the peaks is related to the concentration of the element within the sample region.

Figure 2.6 shows intensity versus binding energy of C1s core level spectra of pristine $SiO_2$ and functionalized $SiO_2$. The appearance of new group (C-O-C) as shown in Figure 2.6 (b) confirmed that reaction between carbon and oxygen had occured.

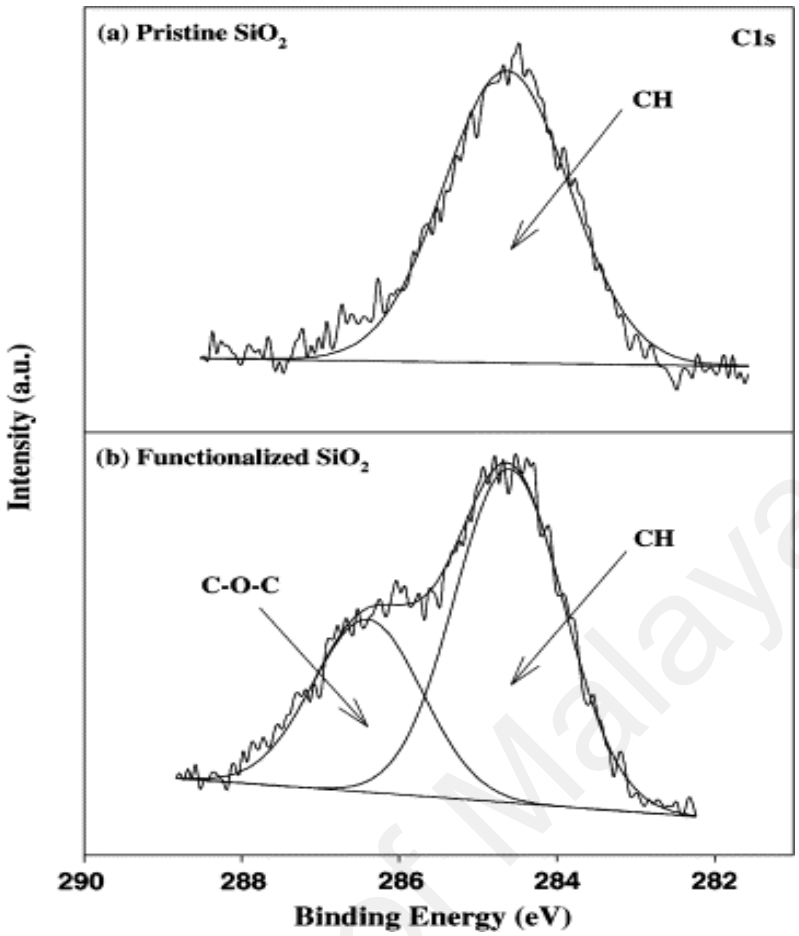


**Figure 2.6:** XPS C1s spectra of (a) pristine SiO2 and (b) functionalized $SiO_2$ (Liu *et al*, 2002)

### 2.5.3 Thermogravimetric analysis

TGA is an analytical technique to determine thermal stability of a material. It is based on the measurement of mass loss of material as a function of temperature. In TGA, a continuous graph of mass change against temperature is obtained when a substance is heated at a uniform rate under an inert atmosphere such as Helium or Argon.

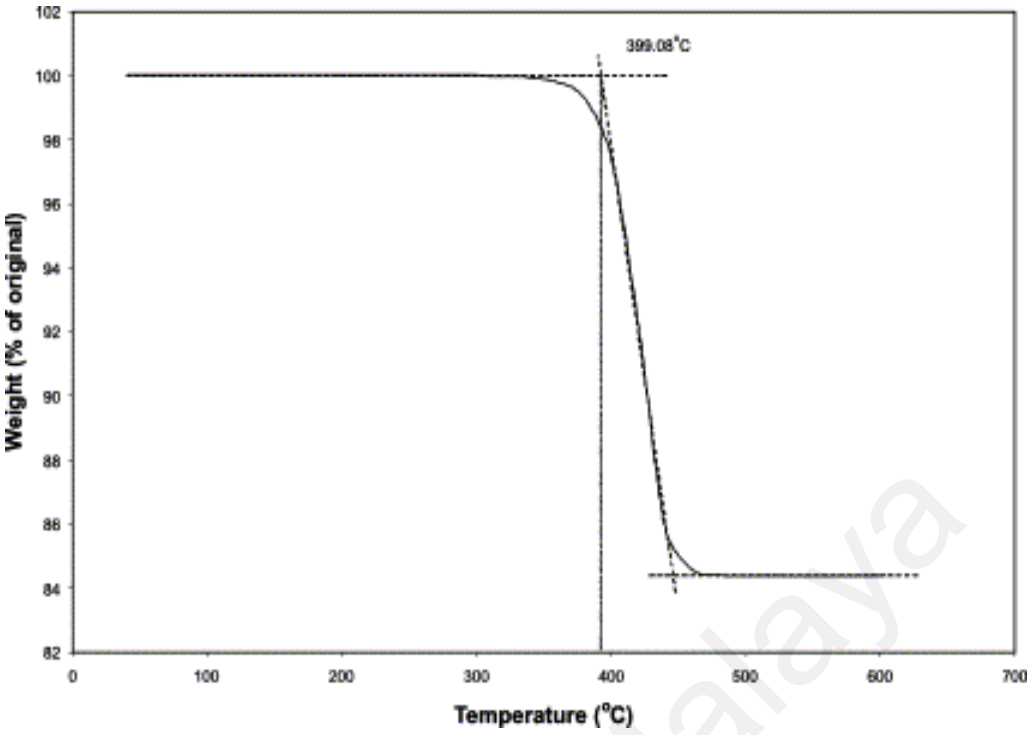


**Figure 2.7:** Onset temperature from TGA curve (Goodrum & Geller, 2002)

In a TG curve of single stage decomposition, there are two characteristic temperatures; the initial and the final temperature. Initial temperature is defined as the lowest temperature at which the onset of a mass change can be detected by thermo balance operating under particular conditions and the final temperature is the temperature at which the particular decomposition appears to be complete. To characterize the samples, the extrapolated onset temperature ($T_{onset}$) can be calculated to denote the temperature at which the weight loss begins as shown in Figure 2.7.

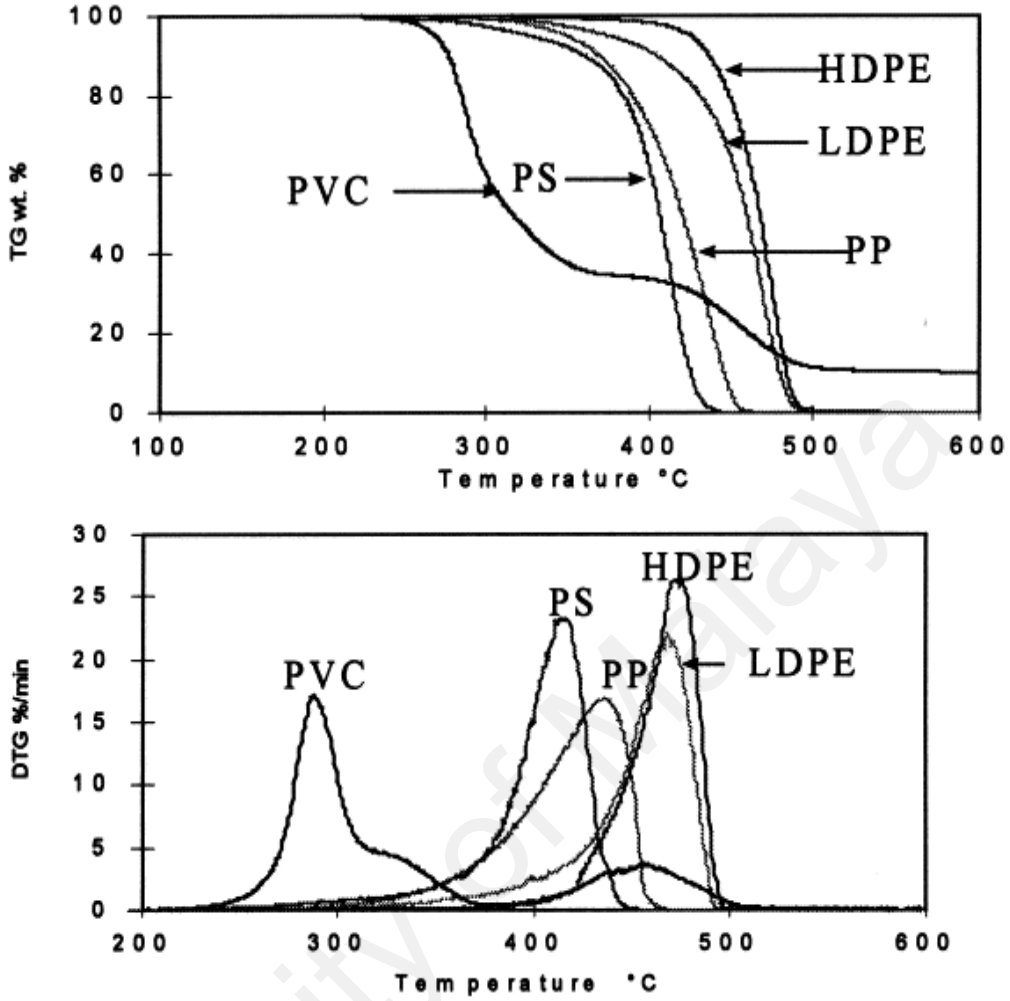


**Figure 2.8:** TG and DTG curves of some polymers: PVC=polyvinyl chloride; PS=polystyrene; PP=polypropylene; LDPE=low density polyethylene; and HDPE=high density poly ethylene (Miranda *et al*, 2001)

Figure 2.8 shows TG and DTG curves of PVC, PS, PP, LDPE and HDPE. From TG curves, the thermal stability of the polymers can be compared. The TG curve can help to elucidate decomposition mechanism. TG and DTG curves can be used to "fingerprint" materials for identification or quality control. From Figure 2.8, it can be seen that HDPE shows the most thermally stable among those polymers while PVC is the least thermally stable.

### 2.5.4 Differential scanning calorimetry

DSC is used to study the thermal responses of materials. When the materials are heated, thermal changes are bound to occur. At the point of thermal change in a sample, heat energy is either absorbed (endothermic) or released (exothermic) can be detected. Figure 2.9 shows the DSC thermogram for glass transition temperature, $T_g$. $T_g$ is defined as the transition of temperature from glassy state to rubbery state. Beyond this transition, a long range molecular motion occurs and thus the degree of rotational freedom increases. A decrease in $T_g$ helps in softening polymer chains and improving segmental movement.

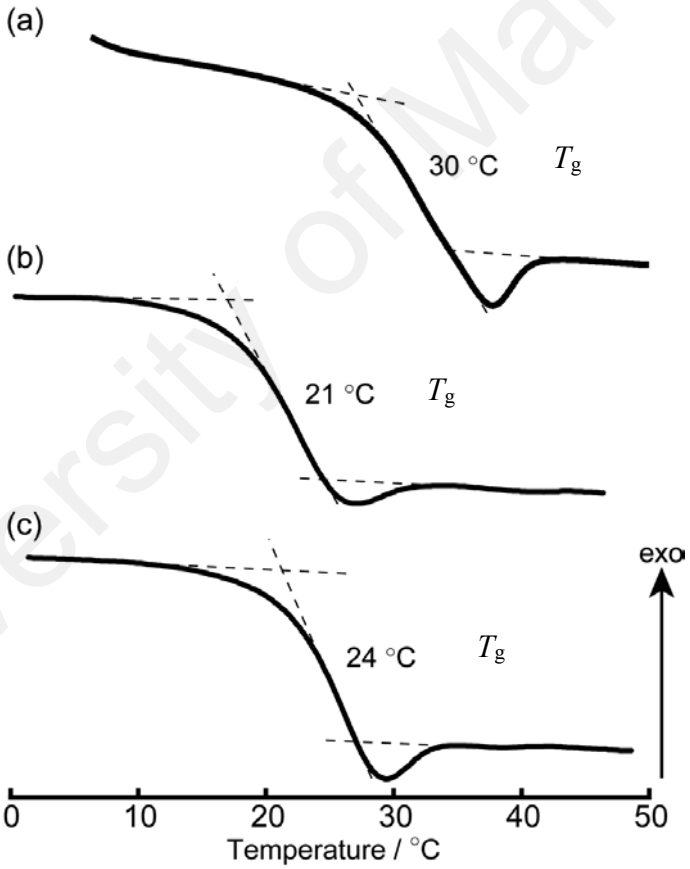


**Figure 2.9:** DSC thermograms in the glass transition temperature range (Yoshida *et al* 2014)

### 2.5.5 Ionic conductivity study

The fundamental of ionic conduction in the polymer electrolytes is due to transport of cations and anions in a polymer matrix. It is known that the ionic mobility is promoted by segmental motion of the polymer host. General expression of ionic conductivity of a homogenous polymer electrolyte is given below:

$$\sigma = nq\mu \tag{2.3}$$

where $n$ is the number of charge carriers, $q$ is the charge of ions and $\mu$ is the mobility of ions. These charge carriers include free ions and ion pairs. Based on equation (2.3), the quantity and mobility of charge carriers are the main factors that could affect the ionic conductivity of polymer electrolytes.

There are few ways to increase ionic conduction; one can simply add more salt in order to increase the number of charge carrier and can also decrease the glass transition temperature $T_g$, which facilitates relaxation and therefore improves the ion transportation.

Ionic mobility or conductivity through polymer in a polymer electrolyte can take place even though without the presence of electrolytic pathways. This is related to that of the "ion hopping" or the "redistribution of free volume" mechanism within the polymer matrix. In this case, the ions can diffuse under the influence of small electric potential either by the short- range ion hopping between coordination sites, or the long-range diffusion through segmental motion of the polymer. The segmental motion either permits the ions to hop from one site to another site or provides a pathway for ions to move in an electric field. This is related to the transport mechanism which is closely dependent on the flexibility of the polymer backbone (Ratner *et al,* 2000).

Impedance spectroscopy (IS) is a tool to analyse the response of a cell, comprising of an ion conducting electrolyte sample sandwiched between two blocking or non-blocking electrodes by sinusoidal ac signal. IS measures the impedance of the sample over a wide frequency range. In general, impedance is a complex quantity which consists real part, $Z$'($x$-axis) and imaginary part, $Z$'' ($y$-axis).

The bulk ionic conductivity of polymer electrolytes is determined by the equation;

$$\sigma = \frac{t}{R_b A} \tag{2.4}$$

where $t$ is the thickness, $R_b$ is bulk resistance and $A$ is the surface area of the measured film. $R_b$ is obtained from the interception of semicircle with the real impedance axis as shown in Figure 2.10. This figure shows the semicircular portion which is mainly due to the parallel combination of both resistive and capacitive components.

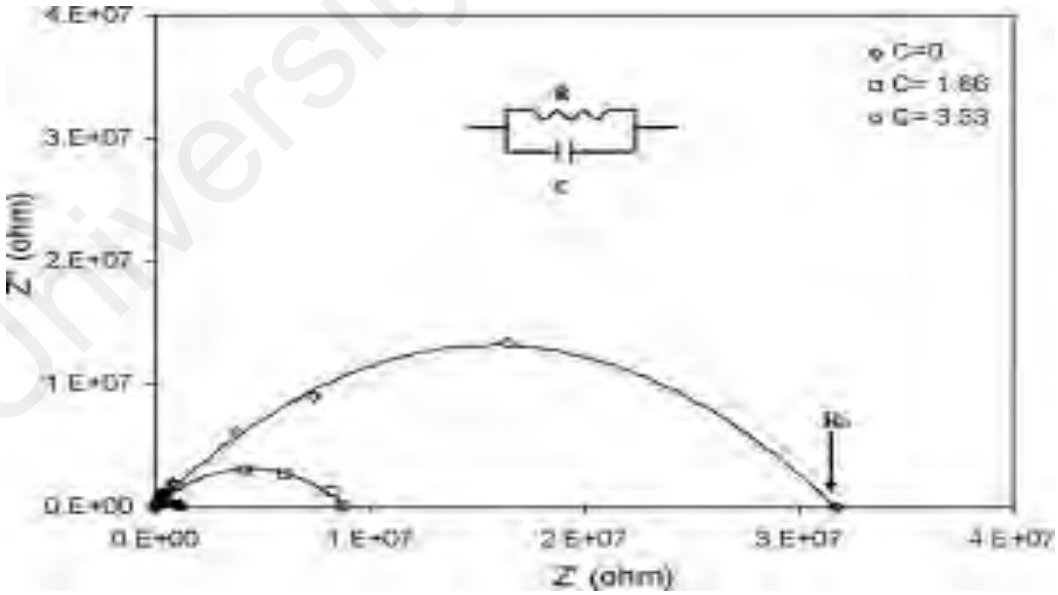


**Figure 2.10:** Bulk resistance from Cole-Cole plot (Sheha *et al*, 2012)

The temperature dependence of conductivity study is commonly done in order to investigate and understand the mechanism of ionic conduction in solid polymer electrolyte systems. There are several forms of equation such as Arrhenius equation and Vogel-Tammann-Fulcher (VTF) equation to describe the conductivity-temperature relationships.

The ceramic materials and glassy materials usually show simple Arrhenius forms for the conductivity, $\sigma$ as in Equation (2.5):

$$\sigma = \sigma_0 \exp [-E_a/kT] \quad (2.5)$$

In polymer electrolytes, on the other hand, temperature conductivity behaviour usually best fitted to an expression of the form

$$\sigma = \sigma'_0 \exp [-B/(T-T_0)] \quad (2.6)$$

This is called VTF behaviour. The VTF equation is often used to fit the properties of polymers close to their glass transition temperature. $T_0$ is normally called the equilibrium glass transition temperature and is related to the (kinetic) measured glass transition temperature roughly by

$$T_0 \approx T_g - 50 \text{ K} \quad (2.7)$$

The glass transition temperature $T_g$ is normally defined as the temperature at which the shear or macroscopic viscosity achieves the value $10^{13}$ Pa. Briefly, above $T_g$, local segmental motion of the polymer chains occurs and this facilitates the motion of ions through the polymer.

The simplest understanding of VTF behaviour is that diffusion can occur only when the diffusing particle moves from one free volume space to another. The VTF form of Equation (2.6) is based on an expansion of the free volume around the equilibrium glass transition temperature $T_0$. The free volume concept is the simplest way to understand the transport behaviour in polymer electrolytes. This concept has been developed by Cohen and Turnbull, 1959. It states that the polymer motion is not mainly thermal activated but essentially occurs by redistribution of the free volume.

The expansion of the polymer matrix with temperature produces the formation of local empty spaces and voids for the polymer segmental motion. Therefore, it facilitates the migration of ions and enhances the transport of charge carriers, inducing higher ionic conductivity. Figure 2.11 shows the temperature dependence of ionic conductivity fitted to the VTF expression. By fitting the VTF equation, conduction activation energy, $B$ can be obtained. $B$ is defined as the energy required to overcome the reorganization and reformation of the polymer chain with $Li^+$.

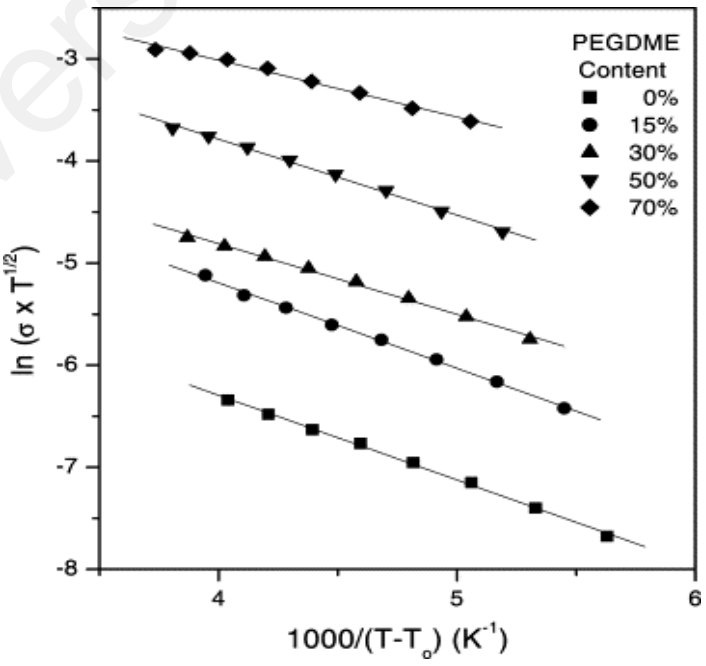


**Figure 2.11:** VTF plots of ionic conductivity for polymer electrolyte at different PEGDME content (Kang *et al*, 2003)

### 2.5.6 Linear sweep voltammetry

One of the important parameters in the characterization of polymer electrolytes is the electrochemical stability window. The electrochemical stability window, defined as a potential range where no Faradaic current flows, is limited in its cathodic and anodic parts by the polymer, plasticizer and salt reduction/oxidation at electrodes. The energy stored in a capacitor is proportional to the applied potential in the second power, and therefore, the electrochemical stability window should be as broad as possible (Lewandowski et al 2003). Two types of voltammetry are linear sweep voltammetry (LSV) and cyclic voltammetry (CV). In LSV, the voltage was swept from the open-circuit voltage of the cell toward more positive voltage values until a great current charge due to electrolytes decomposition at the inert electrode interface occurred. Figure 2.12 shows the example of LSV plot of polymer electrolytes with nano-crystalline $TiO_2$-PMMA hybrid. There is no obvious current through the working electrode from the open circuit potential to 4.5 V versus $Li^+$ /Li, and then an onset current can be observed at potentials higher than 4.5 V versus $Li^+$ /Li, which may be associated with the decomposition of the CPE. The result shows that the electrochemical stability window is at least 4.5 V for the sample (Cao, et al, 2013).

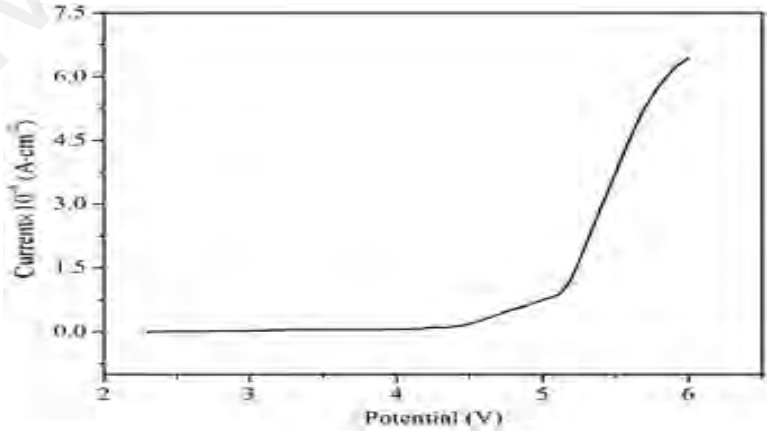


**Figure 2.12:** LSV plot of the doped CPE (PVDF-HFP doped with $TiO_2$-PMMA nanohybrid) (Cao, *et al,* 2013)

## 2.6 An alternative method to prepare solid polymer electrolyte (dry method)

Solid polymer electrolytes are usually prepared by solution casting method which involved solvent to dissolve and mix all the materials used in the systems. In this method, solvents such as dimethylformamide (DMF) and tetrahydrofuran (THF) are used to dissolve the polymers and salts. However, most of the solvents are volatile and unsafe. Therefore, alternative method has been proposed to prepare SPE which is called dry method. Internal mixer system is used in this method since this equipment is suitable in working with rubbery samples such as ENR-50.

Internal mixer is often equipped with two counter-rotating rotors in a large housing that shear the rubber charge along with the additives. The mixing can be done in three or four stages to incorporate the ingredients in the desired order. The shearing action generates considerable heat, so, both rotors and housing are water-cooled to maintain a temperature low enough to assure that vulcanization does not begin.

Mixing is the process used to obtain a thorough and uniform dispersion in the rubber stocks required by the formulation while compounding is the operation of bringing together all the ingredients required to mix a batch of rubber compound. Using internal mixer system, mixed materials can be prepared and the process can be investigated by considering the time dependence of the torque. This mixing process involves momentum and heat transfer. The torque trajectory can be used to monitor the mixing process between polymer and any additives. The electrolyte films can be prepared by compression moulding at certain temperature.

# CHAPTER 3: EXPERIMENTAL METHODS

## 3.1 Overview

In this research work, electrolyte materials were prepared using two methods; wet method and dry method. ENR-50 was used as polymer host and LiTFSI as doping salt. To improve ionic conductivity of the electrolyte, ionic liquids were added. According to our preliminary study, BMITFSI and EMITFSI showed most suitable candidate to improve conductivity. Furthermore, these ionic liquids were also found more compatible with ENR-50.

Table 3.1 shows the materials used in this work for wet and dry methods.

**Table 3.1:** Materials used for sample preparation

| Materials | Abbreviation | Supplier |
|---|---|---|
| Epoxidized Natural Rubber of 50% epoxidation level | ENR-50 | Rubber Research Institute Malaysia (RRIM) |
| Tetrahydrofuran | THF | R&M Chemicals |
| Lithium bis(trifluoromethanesulfonyl)imide | LiTFSI | Sigma-Aldrich |
| 1-butyl-3-methylimidazolium bis(trifluoromethanesulfonyl)imide | BMITFSI | Sigma-Aldrich |
| 1-ethyl-3-methylimidazolium bis(trifluoromethanesulfonyl)imide | EMITFSI | Sigma-Aldrich |
| Ethylene carbonate | EC | Sigma-Aldrich |

### 3.2 Sample Preparation Using Wet Method

The first method used in this research work for preparing the electrolyte materials was wet method. In wet method, three (3) electrolyte systems had been prepared:

(i) (ENR-50)-LiTFSI

(ii) (ENR-50)-BMITFSI-LiTFSI

(iii) (ENR-50)-EMITFSI-LiTFSI

Electrolyte materials were prepared using solution casting method. Firstly, masticated ENR-50 was cut into small pieces and dissolved in THF using magnetic stirrer (Figure 3.1). After homogeneous solutions were formed, lithium salt of desired amount, expressed as weight percent (wt.%), was then added and the solutions were stirred for another 24 h. After 24 h of stirring, viscous homogeneous solutions formed were cast into Teflon petri dishes and left for slow drying at room temperature to form electrolyte films. The films were further dried in a vacuum oven for 48 h at 40$^{o}$C to remove residual solvent. The electrolyte system was designated as (ENR-50)-LiTFSI(*X*), where *X* denotes 0, 10, 20, 30, 40 or 50 wt%. The weight percent of salt was determined by:

$$\text{wt.\% of salt} = \frac{(\text{wt.of salt})}{(\text{wt.of polymer})+(\text{wt.of salt})} \times 100\ \% \qquad (3.1)$$

To prepare (ENR-50)-ionic liquid-LiTFSI system, 20 wt% of ionic liquid (BMITFSI or EMITFSI) was mixed into the ENR-50 solutions. This amount of ionic liquid was chosen based on two factors; the compatibility with ENR-50 and it also gives reasonable ionic conductivity value. The mixture was then added with the desired amount of lithium salt, expressed as weight percent (wt.%). The stirring, casting and drying processes were the same as mentioned before. The electrolyte system was designated as (ENR-50)-ionic liquid-LiTFSI(*Y*), where *Y* denotes 0, 10, 20, 30, 40 or 50 wt%. Tables 3.2 to 3.4 show the lists of designations and LiTFSI compositions of all samples prepared by wet method.

**Figure 3.1:** Stirring process

**Table 3.2:** Designations and compositions of LiTFSI for (ENR-50)-LiTFSI system

| Designations | LiTFSI compositions (in wt. %) |
|---|---|
| WEL0 | 0 |
| WEL10 | 10 |
| WEL20 | 20 |
| WEL30 | 30 |
| WEL40 | 40 |
| WEL50 | 50 |

**Table 3.3:** Designations and compositions of LiTFSI for (ENR-50)-BMITFSI-LiTFSI system

| Designations | LiTFSI compositions (in wt. %) |
|---|---|
| WEBL0 | 0 |
| WEBL10 | 10 |
| WEBL20 | 20 |
| WEBL30 | 30 |
| WEBL40 | 40 |
| WEBL50 | 50 |

**Table 3.4:** Designations and compositions of LiTFSI for (ENR-50)-EMITFSI-LiTFSI system

| Designations | LiTFSI compositions (in wt. %) |
|---|---|
| WEEL0 | 0 |
| WEEL10 | 10 |
| WEEL20 | 20 |
| WEEL30 | 30 |
| WEEL40 | 40 |
| WEEL50 | 50 |

### 3.3 Sample Preparation Using Dry Method

The second method used in this work was dry method (solvent free method). In this method two (2) systems had been prepared:

(i) (ENR-50)-LiTFSI

(ii) (ENR-50)-BMITFSI-LiTFSI

Dry method is used as an alternative method to prepare electrolyte materials. Materials were melt-blended in a Haake internal mixer using cam blade. The required weights of masticated ENR-50 strip were fed into the mixing chamber. After the ENR-50 melt, ionic liquid, lithium salt and ethylene carbonate (as lubricant) were charged into the mixing chamber. The mix materials were blended for a few minutes until a constant torque level was reached. The electrolyte films were obtained by compression moulding. Table 3.5 and 3.6 present the parameters used in the internal mixer and hot pressing systems respectively. The electrolytes were designated as (ENR-50)-LiTFSI(*M*) and (ENR-50)-ionic liquid-LiTFSI(*N*), where *M* and *N* denote 0, 5, 10, 15, 20 wt.%. Tables 3.7 and 3.8 show the lists of designations and compositions of LiTFSI of all samples prepared by dry method.

**Table 3.5:** Internal mixer specifications

| **Parameters** | **Specifications** |
|---|---|
| Temperature (ºC) | 120 |
| Time (min) | 20 |
| Rotor speed ($min^{-1}$) | 40 |

**Figure 3.2:** Internal mixer and rotating rotor

**Table 3.6:** Hot pressing specifications

| Parameters | Specifications |
|---|---|
| Temperature (°C) | 140 |
| Pressure (bar) | 80 |
| Pressing time (min) | 20 |

**Table 3.7:** Designations and compositions of LiTFSI for (ENR-50)-LiTFSI system

| Designations | LiTFSI compositions (in wt. %) |
|---|---|
| DEL0 | 0 |
| DEL5 | 5 |
| DEL10 | 10 |
| DEL15 | 15 |
| DEL20 | 20 |

**Table 3.8:** Designations and compositions of LiTFSI for (ENR-50)-BMITFSI-LiTFSI system

| Designations | LiTFSI concentrations (in wt. %) |
|---|---|
| DBEL0 | 0 |
| DBEL5 | 5 |
| DBEL10 | 10 |
| DBEL15 | 15 |
| DBEL20 | 20 |

### 3.4 Characterizations

After the samples had been prepared, the characteristics of the samples such as the interaction between constituents, thermal behaviour (phase transition and thermal stability), ionic conductivity and electrochemical stability were studied using various techniques such as ATR-FTIR, XPS, DSC, TGA, EIS and LSV.

#### 3.4.1 Attenuated total reflectance – Fourier transform infrared

Infrared (IR) spectral analysis was done to identify the nature of bonding and different functional groups present in the sample by monitoring the vibrational energy levels of the molecules. In this technique, IR radiation is passed through a sample. Some of the IR radiation is absorbed by the sample and some of it is passes through (transmitted). The technique of using ATR is suitable for this work (rubbery sample) by placing the sample (film) directly onto the ATR crystal. An ATR operates by measuring the changes that occur in a totally internally reflected infrared beam when the beam comes into contact with a sample. This analysis was carried out using a Perkin Elmer Spectrum 400 FT-IR/FT-FIR Spectrometer in the range of 550-4000 $cm^{-1}$ at 2 $cm^{-1}$ resolution and the spectra were recorded in the transmittance mode.

#### 3.4.2 X-ray photoelectron spectroscopy

XPS is a widely used method for surface analysis of polymer materials. The information regarding to chemical state bonding can be obtained from this technique. This technique is widely used to determine localized bonding chemistry of carbon and to differentiate the oxidation states of inorganic compounds. The characteristic peaks obtained in the spectra can be used to identify the species present. The XPS studies in this work were carried out using a Omicron DAR 400 surface analysis spectrometer with a

Mg Kα X-ray source (1486.7 eV). The spectrum was taken at an operating current of 10 mA and an operating voltage of 14 kV. The survey scan was recorded in the energy range between 0 and 1400 eV. The step size energy was 0.5 eV $step^{-1}$. The sample analysis chamber was kept at ~$2 \times 10^{-8}$ mTorr.

### 3.4.3 Thermogravimetric analysis and differential scanning calorimetry

TGA had been used to study the thermal stability of electrolytes. TGA measures the amount and rate change in the mass of a sample as a function of temperature or time under argon atmosphere. In this work, LabSysevo Setaram Instrumentation was used and measurement was done in the temperature ranged from 30 to 700 ºC at a heating rate of 10 ºC $min^{-1}$.

Mettler Toledo DSC 822 equipment was employed to study the phase transitions of electrolytes. The purge gas was Nitrogen at 50 ml $min^{-1}$. The results were evaluated with the STAR$^e$ Software package. Samples of about 2-5 mg were measured in hermetically sealed 40 µl Aluminium crucibles in self-generated atmosphere. The measurements for all systems were conducted with the samples heated to 170 ºC, followed by cooling to -65 ºC, and then heating again to 250 ºC at a cooling and heating rate of 10 °C $min^{-1}$.

### 3.4.4 Electrochemical impedance spectroscopy

EIS is a technique for studying electrode processes by measuring the change in the electrical impedance of the electrode. This technique has been used to determine the ionic conductivity of electrolytes. The ionic conductivities of the electrolytes were measured by impedance spectroscopy measurement. In general, impedance is complex quantity, in which the real and imaginary parts are labelled as *Z*' and *Z*'' respectively. In the complex

impedance plot, which is called Cole-Cole plot, the real quantity $Z$' (in $x$-axis) is plotted against $Z$'' ($y$-axis). From the graph, the bulk resistance, $R_b$ of the electrolytes can be obtained. From the bulk resistance value, the ionic conductivity of the electrolyte was calculated using the relation

$$\sigma = \frac{t}{AR_b} \tag{3.2}$$

where $t$ and $A$ are the thickness of the electrolyte medium and the area of the electrode surface respectively.

The ionic conductivity measurement was done using Solartron SI 1260. The electrolyte samples were sandwiched between two copper electrodes and the impedance measurements were carried out at room temperature over the frequency range of 100 Hz to 1 MHz at 100 mV. The ionic conductivity as a function of temperature was studied in the temperature range of 30$^{o}$C to 80$^{o}$C (for wet method) and 40 °C to 100 °C (for dry method).

### 3.4.5 Linear sweep voltammetry

The electrochemical stability of the prepared electrolyte material was investigated by LSV analysis using Wonatech Zive MP2 electrochemical workstation. The measurement was done by employing inert copper as working electrode and lithium metal as reference and counter electrodes. The cell was constructed and utilized data scan rate of 10 mV $s^{-1}$ from 0 to 5 V at room temperature.

# CHAPTER 4: EXPERIMENTAL RESULTS (WET METHOD) AND DISCUSSIONS

## 4.1 System 1: (ENR-50)-LiTFSI

Figure 4.1 shows ENR-50 film prepared by solution casting method. As seen in the figure, the ENR-50 film is quite translucent. In the salted system, ENR-50 is doped with 10 to 50 wt.% of lithium bis(trifluoromethanesulfonyl)imide (LiTFSI) to form (ENR-50)-LiTFSI electrolyte system.

**Figure 4.1:** ENR-50 film

### 4.1.1 Attenuated total reflectance – Fourier transform infrared

ATR-FTIR spectra were recorded in the transmittance mode. The ATR-FTIR spectra of ENR-50 film, lithium imide salt and (ENR-50)-LiTFSI electrolyte films are presented in Figure 4.2 to Figure 4.5. In the spectrum of ENR-50 film (Figure 4.2), the main focus is the presence of epoxide group in ENR-50, located at 872 and 1255 $cm^{-1}$ which correspond to asymmetrical and symmetrical stretching vibration band of the epoxide group (Jeon *et al*, 1998, Gan & Hamid 1997). Other characteristic bands are also observed at 1378 $cm^{-1}$ (C-H deformation of $–CH_3$), 1449 (C-H deformation of $–CH_2$-) and 2859, 2921 and 2963 $cm^{-1}$ (C-H stretching).

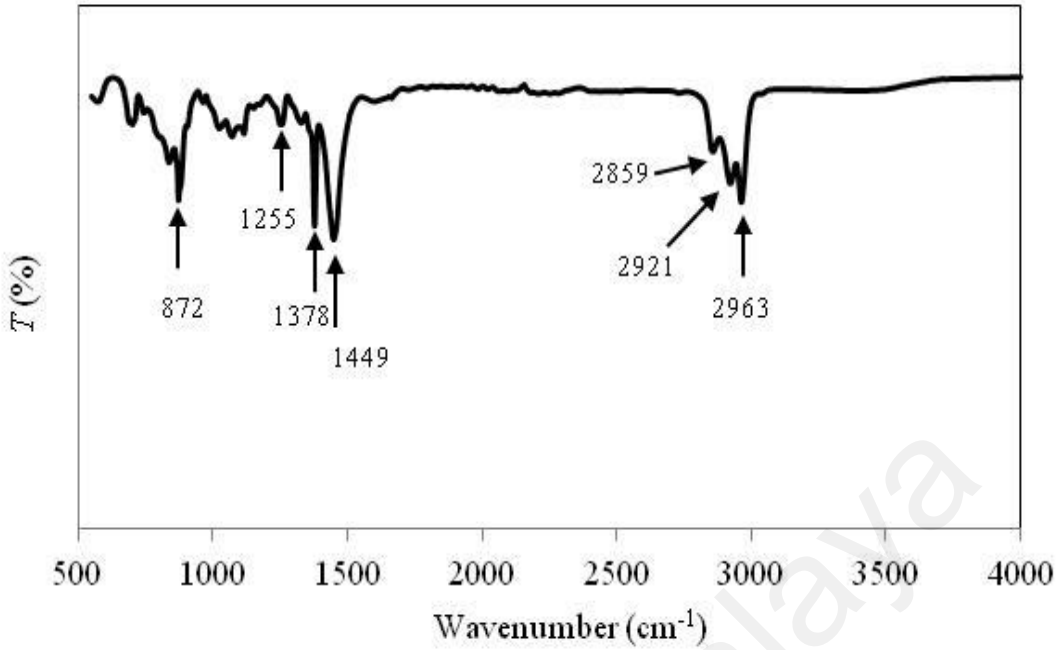


**Figure 4.2:** Transmission spectrum of WEL0 film

Figure 4.3 shows the transmission spectrum of lithium salt used in this system. The vibrational modes of the lithium salt are listed in Table 4.1.

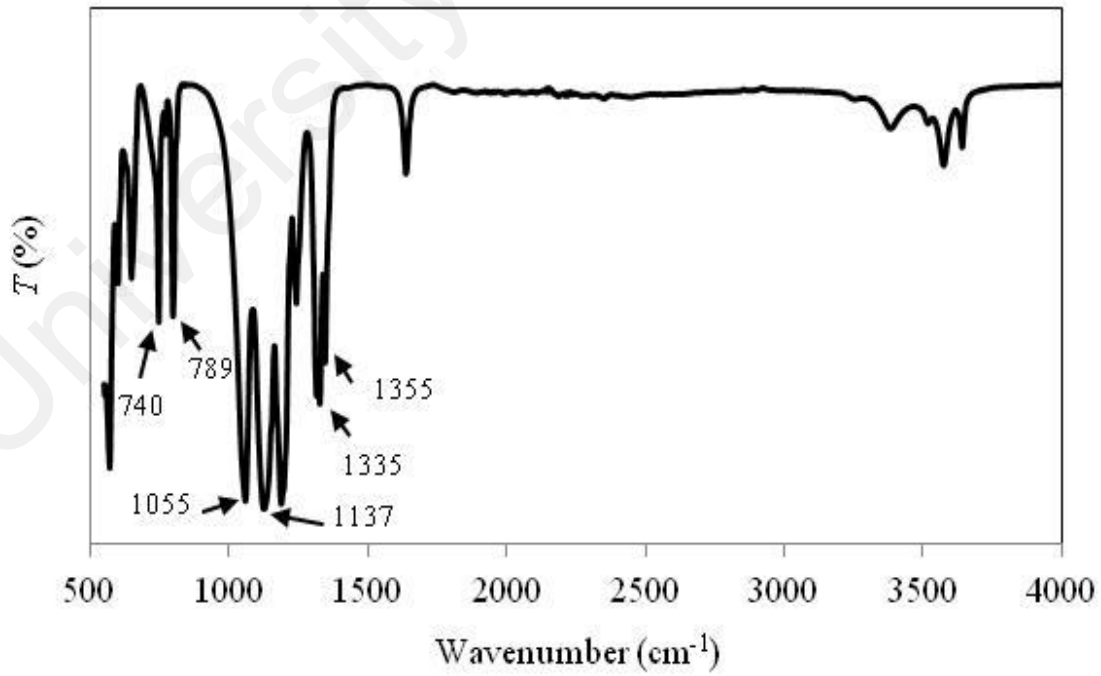


**Figure 4.3:** Transmission spectrum of LiTFSI

**Table 4.1:** Assignments of vibrational modes of LiTFSI

| Descriptions of vibration modes | Wavenumber ($cm^{-1}$) | References |
|---|---|---|
| S-N stretching mode | 740 | Deepa *et al* (2000) |
| Combination of C-S and S-N stretching mode | 789 | Ahmad *et al* (2008) |
| S-N-S asymmetric stretching mode | 1055 | Deepa *et al* (2000) |
| $SO_2$ symmetrical stretching mode | 1137 , 1335 | Ramesh & Lu (2008), Deepa *et al* (2000) |
| $SO_2$ asymmetric stretching mode | 1355 | Ahmad *et al* (2008) Deepa *et al* (2000) |

Referring to Figure 4.4, it can be seen that the asymmetrical stretching vibration band of the epoxide group at 872 $cm^{-1}$ still appears and retains its position but experience intensity reduction with increasing salt content. However, from Figure 4.5, the C-O-C band at 1255 $cm^{-1}$ disappeared after addition of lithium salt. Other bands, i.e. at 1378 and 1449 $cm^{-1}$, shifted to higher wavenumbers in the ENR-50-salt systems. Furthermore, the increase in salt content reduces the intensities of these two peaks. The disappearance and shifting of the bands, especially for epoxide group bands indicate that interactions have occurred between the epoxide group from ENR-50 and LiTFSI. This phenomenon will be discussed further in XPS analysis.

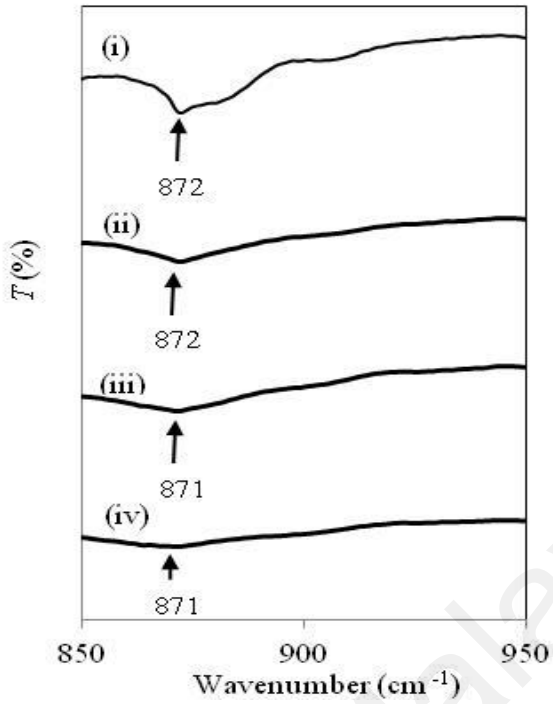


**Figure 4.4:** ATR-FTIR spectra of (i) WEL0, (ii) WEL10, (iii) WEL30 and (iv) WEL50 in the range from 850 to 950 $cm^{-1}$

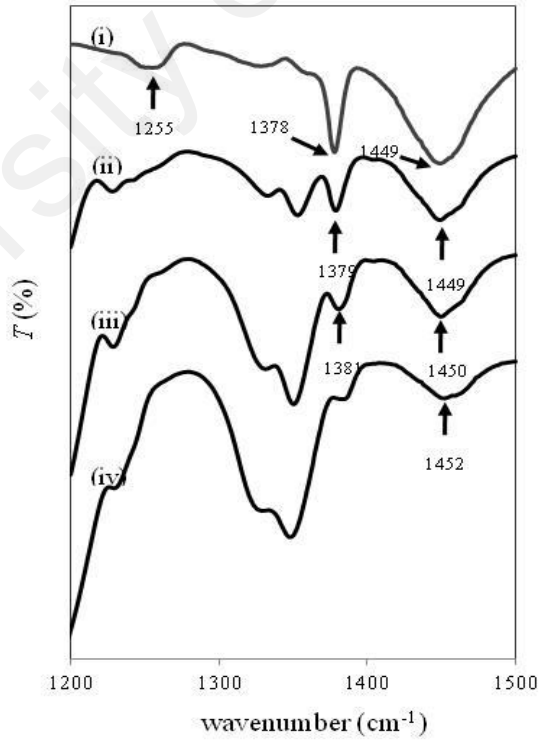


**Figure 4.5:** ATR-FTIR spectra of (i) WEL0, (ii) WEL10, (iii) WEL30 and (iv) WEL50 in the range from 1200 to 1500 $cm^{-1}$

Figures 4.6 and 4.7 show the ATR-FTIR spectra for LiTFSI and (ENR-50)-LiTFSI electrolyte films in the range from 700 – 1100 $cm^{-1}$ and 1100 – 1400 $cm^{-1}$ respectively. From Figure 4.3, S-N bonding is found at 740 $cm^{-1}$, a combination of C-S and S-N stretching is located at 789 $cm^{-1}$, S-N-S bonding at 1055 $cm^{-1}$ and $SO_2$ bonding at 1137, 1335 and 1355 $cm^{-1}$. The peak at 740 $cm^{-1}$ shifts to higher wavenumber and experiences intensity enhancement with increasing salt content. Similar observation is found for the band at 789 $cm^{-1}$ that is shifted to higher wavenumbers with increasing salt content showing the sensitivity of these peaks to salt content. Meanwhile the bands of $SO_2$ bonding at 1137, 1335 and 1355 $cm^{-1}$ are shifted to lower wavenumbers with increasing amount of LiTFSI in the salted ENR system.

This downshift in wavenumber corresponds to a weak interaction between ENR-50 and ions from lithium salt. Consequently, it provides more free ions for ionic transport (Chen-Yang *et al*, 2005). The disappearance, shifting and changes in intensity of the bands in the spectra shown in Figures 4.4 to 4.7 suggest that interactions have occurred between the ENR-50 and LiTFSI forming (ENR-50)-LiTFSI complex.

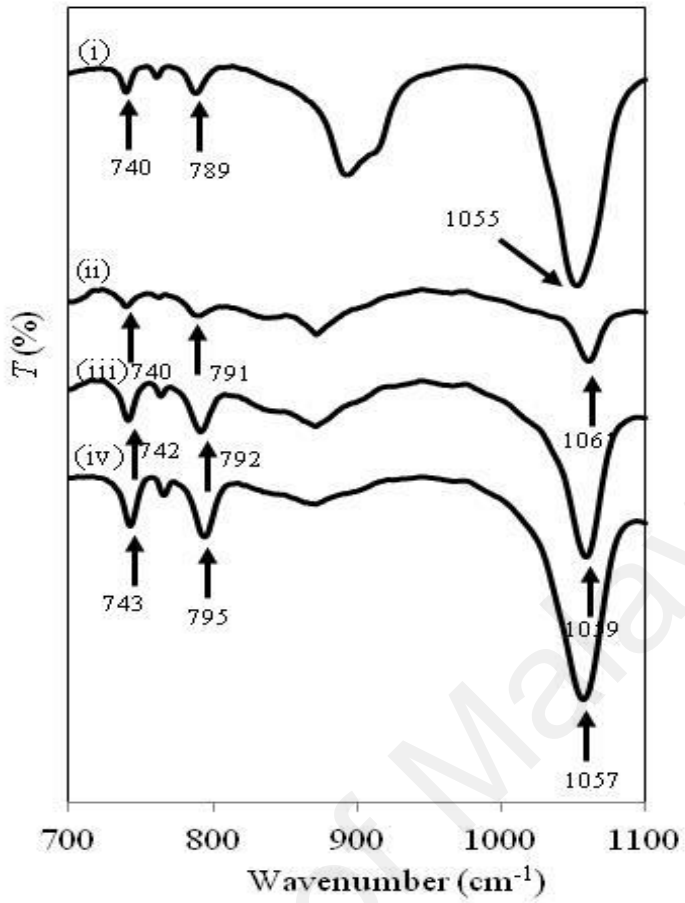


**Figure 4.6:** Transmission spectra of (i) lithium imide salt, (ii) WEL10, (iii) WEL30 and (iv) WEL50 in the range from 700 to 1100 $cm^{-1}$.

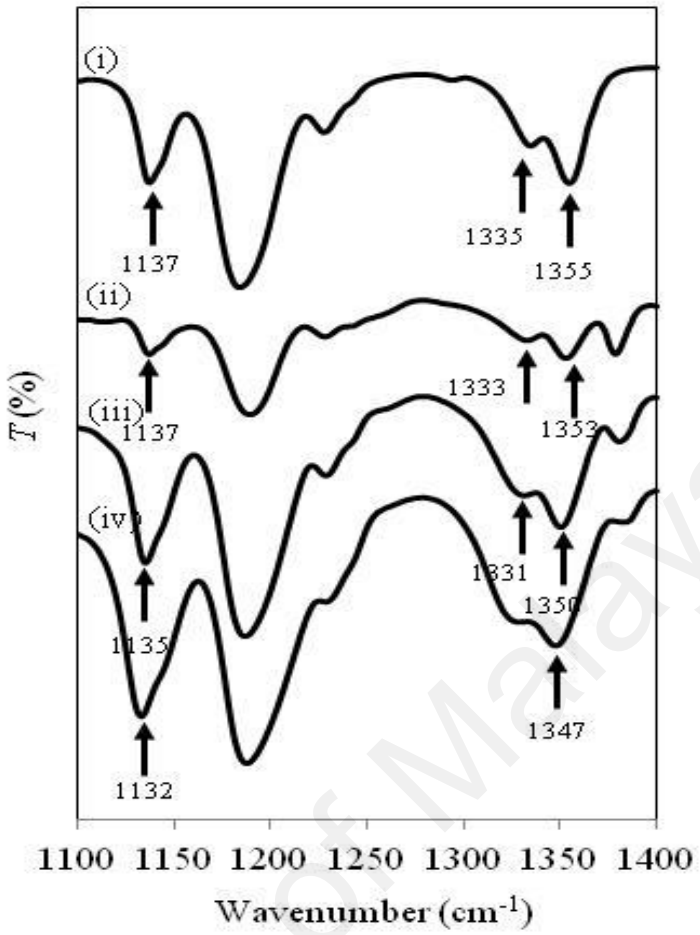


**Figure 4.7:** Transmission spectra of (i) lithium imide salt, (ii) WEL10, (iii) WEL30 and (iv) WEL50 in the range from 1100 to 1400 $cm^{-1}$

.

### 4.1.2 X-ray photoelectron spectroscopy

XPS analysis was carried out to confirm the interaction between ENR-50 and LiTFSI mentioned in the previous subsection. X-ray photoelectron spectra provide the relative frequencies of binding energies of electrons detected, measured in electron-volts (eV). The binding energies are used to identify the elements to which the peaks correspond. XPS data are given in a plot of intensity versus binding energy. For this study, the main focus is to investigate the chemical state of the epoxy group of ENR-50.

Figures 4.8 and 4.9 depict the deconvoluted carbon and oxygen spectra respectively for (ENR-50) and Figures 4.10 and 4.11 show the deconvoluted carbon and oxygen spectra respectively for (ENR-50) with 10 wt.% of LiTFSI.

The C1s spectra (Figure 4.8 and Figure 4.10) show two resolved peaks, which the strong peaks at ~284 eV represent the C-C/C-H bond (Han & Tay, 2009), whereas the lower peaks belong to C-O-C bond which corresponds to epoxy group of ENR-50.

The O1s spectrum of ENR-50 (Figure 4.9) displays a peak at 531.0 eV (Han & Tay, 2009) which refers to O-C bond of epoxy group from ENR-50. This oxygen is believed to provide coordinating site for $Li^+$ from LiTFSI. However, the O1s spectrum of ENR-50 added with lithium salt exhibits two resolved peaks.

Table 4.2 shows the C1s and O1s binding energies for ENR-50 and ENR-50 added with 10 wt.% of LiTFSI. The change in binding energy (between oxygen and carbon) with addition of lithium salt indicates that the interaction between oxygen and lithium has occurred. The appearance of peak observed at 529.6 eV (Harilal, *et al*, 2009) in Figure 4.11 is believed to correspond to the interaction between oxygen and lithium, which appeared after addition of lithium salt. This peak is not observed in ENR-50 spectrum. This is in agreement with the ATR-FTIR result, which shows the disappearance of one of the epoxy groups. This epoxy group might be coordinated with Li cations and formed oxygen and lithium bonding.

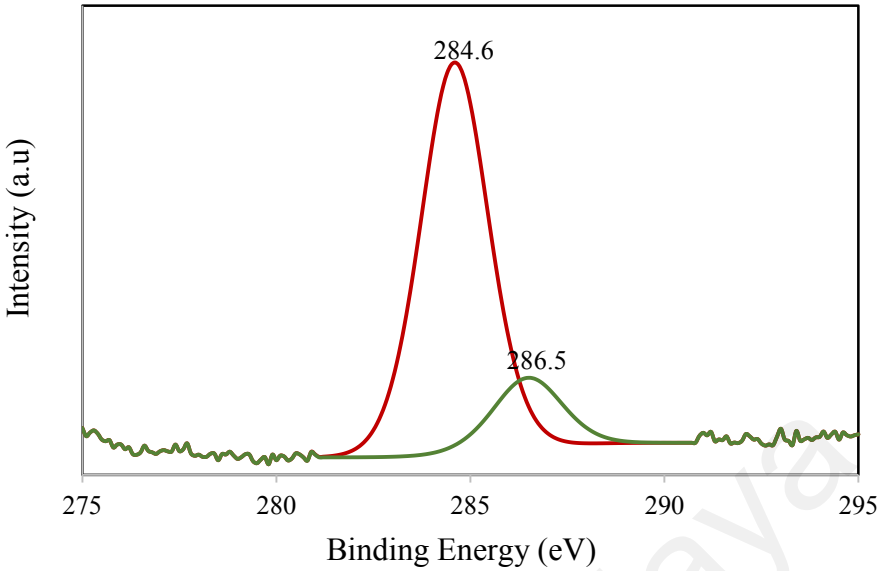


**Figure 4.8:** C1s XPS spectrum for WEL0

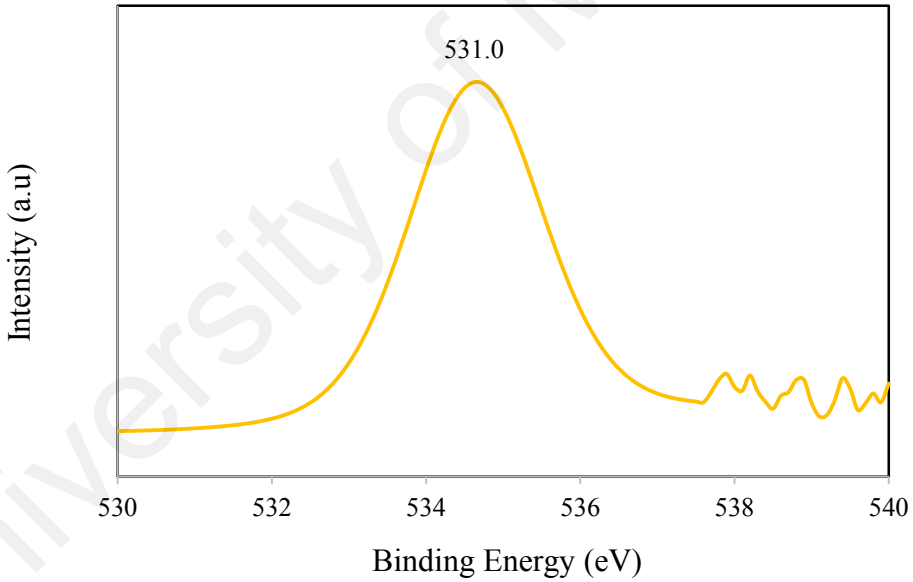


**Figure 4.9:** O1s XPS spectrum for WEL0

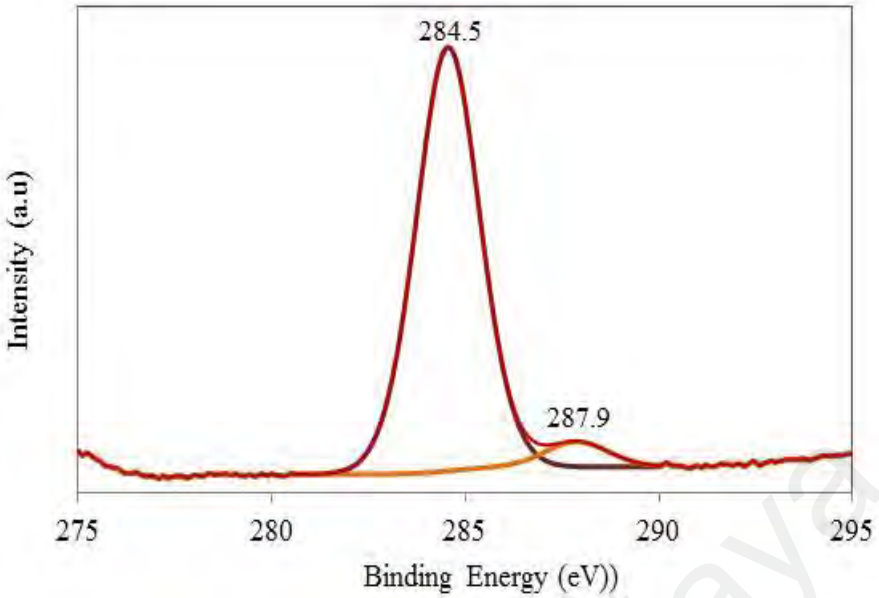


**Figure 4.10:** C1s XPS spectrum for WEL10

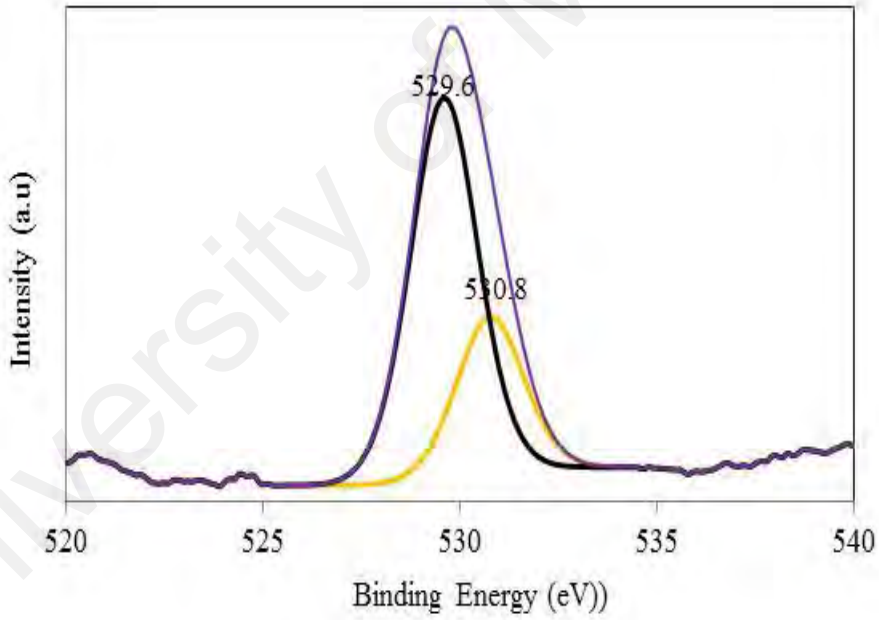


**Figure 4.11:** O1s XPS spectrum for WEL10

**Table 4.2:** C1s and O1s binding energies for ENR-50 and salted ENR-50

| Spectra | Binding Energy (eV) of WEL0 | Binding Energy (eV) of WEL10 | Peak (Chemical state) |
|---|---|---|---|
| C1s | 284.6 | 284.5 | C-C/C-H |
| | 286.5 | 287.9 | C-O-C (epoxy) |
| O1s | 531.0 | 530.8 | O-C |
| | - | 529.6 | Expected for oxygen and lithium |

### 4.1.3 Thermogravimetric Analysis

TGA was carried out to measure the weight loss as a function of temperature. The thermal stability was determined over a temperature range from 30 to 700 °C. TG curves represent the variation in the weight loss (in %) of the sample with temperature (in °C). Figure 4.12 shows the thermogravimetric response for ENR-50 film. The degradation temperature, $T_d$ of the samples was determined by onset temperature ($T_{onset}$).

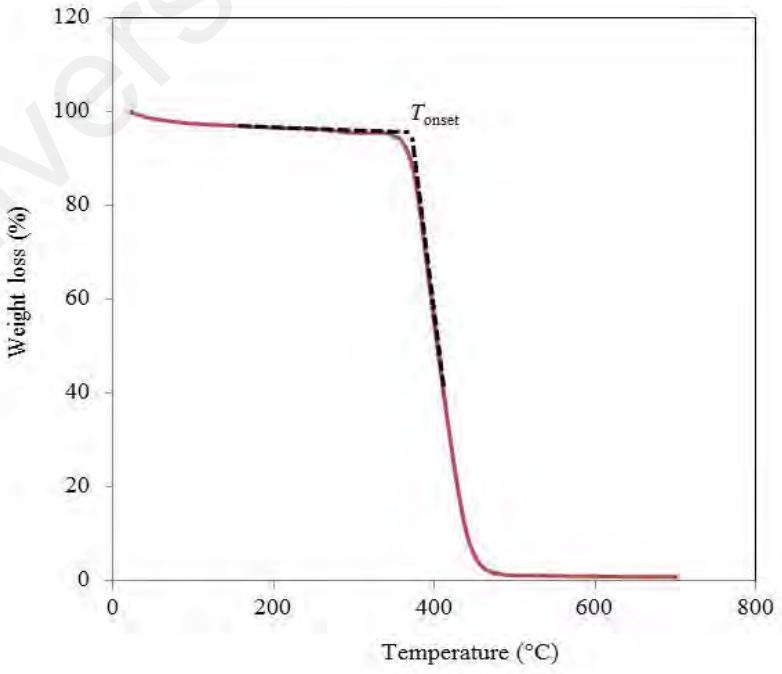


**Figure 4.12:** TGA thermogram of WEL0 film

The onset of thermal decomposition for ENR-50 film started at 370 °C, which shows that the film is quite stable up to this temperature. Beyond this temperature, the weight of polymer is drastically reduced up to 95 % and then saturated at 450 °C. However, $T_{onset}$ for salted film is lower (~ 345 ºC), indicating that the thermal stability of the polymer is weakened slightly due to the addition of salt, as shown in Figure 4.13.

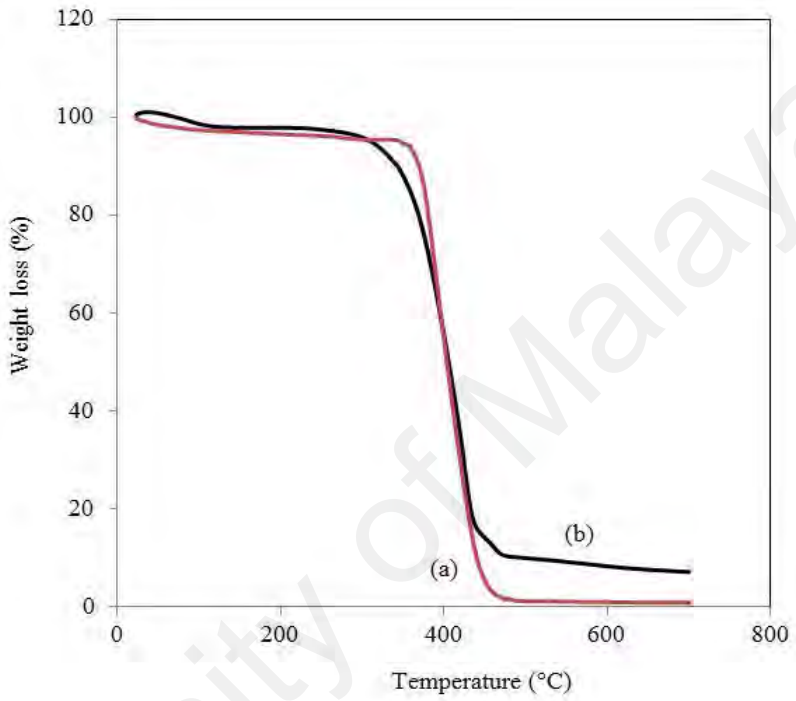


**Figure 4.13:** (a) TGA thermograms of WEL0 and (b) WEL10

### 4.1.4 Differential scanning calorimetry

Differential scanning calorimetry was used to determine the glass transition temperature, $T_g$ of the electrolyte films. Figures 4.14 (a), (b) and (c) show the DSC thermogram for ENR-50, ENR-50 added with 10 wt% of LiTFSI and ENR-50 added with 30 wt.% of LiTFSI films respectively. The $T_g$ (onset temperature of the heat capacity change) is determined from the midpoint of the gradient of this thermogram. The $T_g$ of ENR-50 film obtained from this work is -22 °C. This value is the same as that obtained by Idris *et al* (2001).

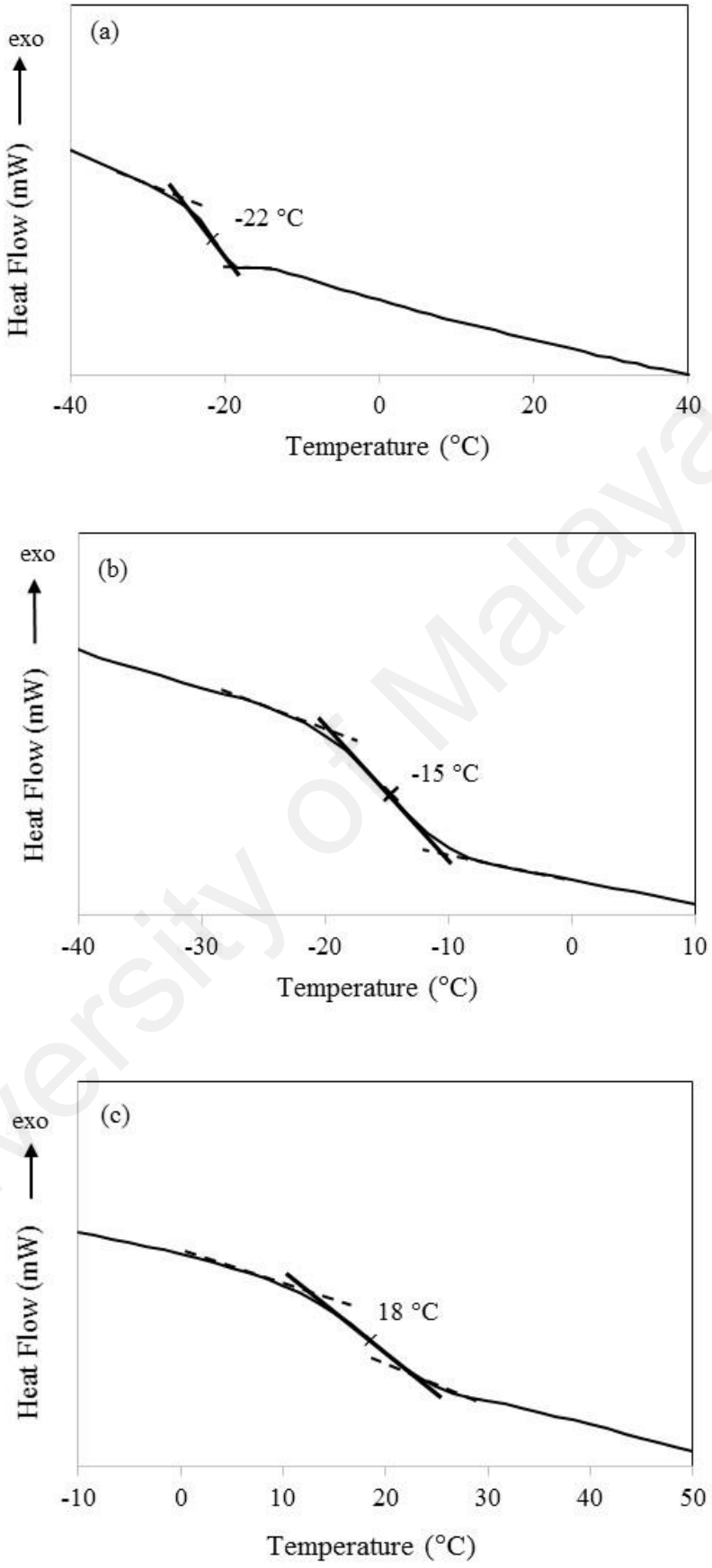


**Figure 4.14:** Glass transition temperature of (a) WEL0, (b) WEL10 and (c) WEL30

.

Figure 4.15 shows the glass transition behaviour of the (ENR-50)-LiTFSI which depends on the salt content. The increase in $T_g$ with increasing salt concentration resulting in the retardation of the motion of the polymer matrix. This implies the interaction between the lithium cation with the epoxy group of the polymer (Hussin et al, 2017), thus, indicating the formation of transient cross-linking effect (Kim *et al* (2003); Hou *et al* (2003)).

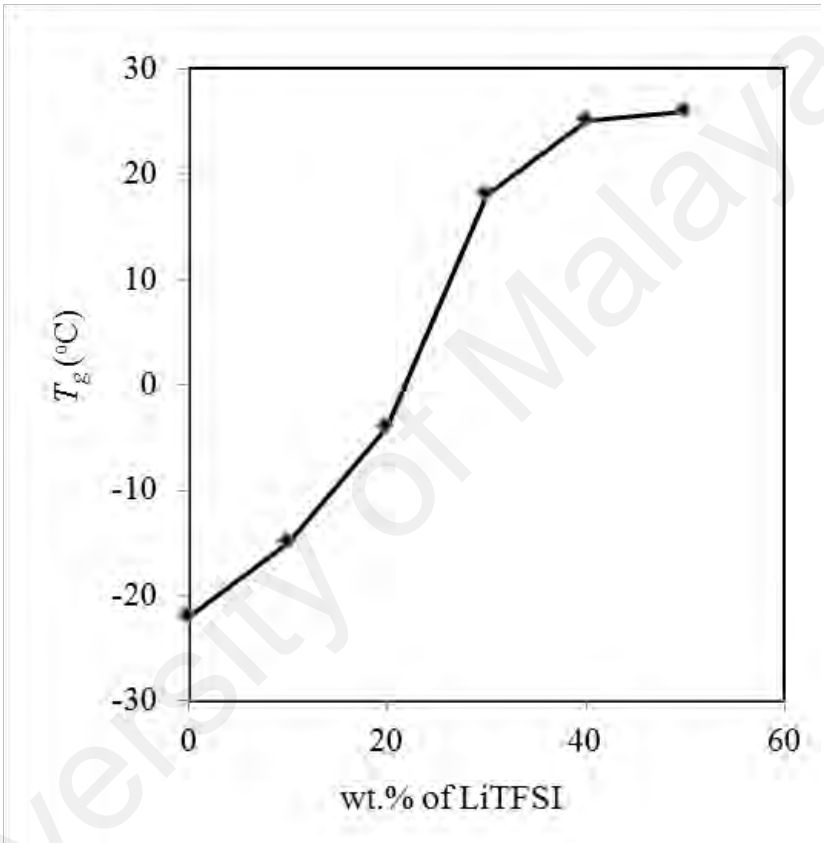


**Figure 4.15:** $T_g$ against salt concentration for (ENR-50)-LiTFSI electrolyte system

### 4.1.5 Ionic Conductivity

Figure 4.16 shows typical impedance plot of WEL10 at room temperature. Imaginary part of the impedance, $Z''$, is normally plotted against real part of the impedance, $Z'$, in a complex plane, and is referred as a Cole-Cole plot. Bulk resistance, $R_b$ of the material can be obtained from the intersecting point of arc with real axis.

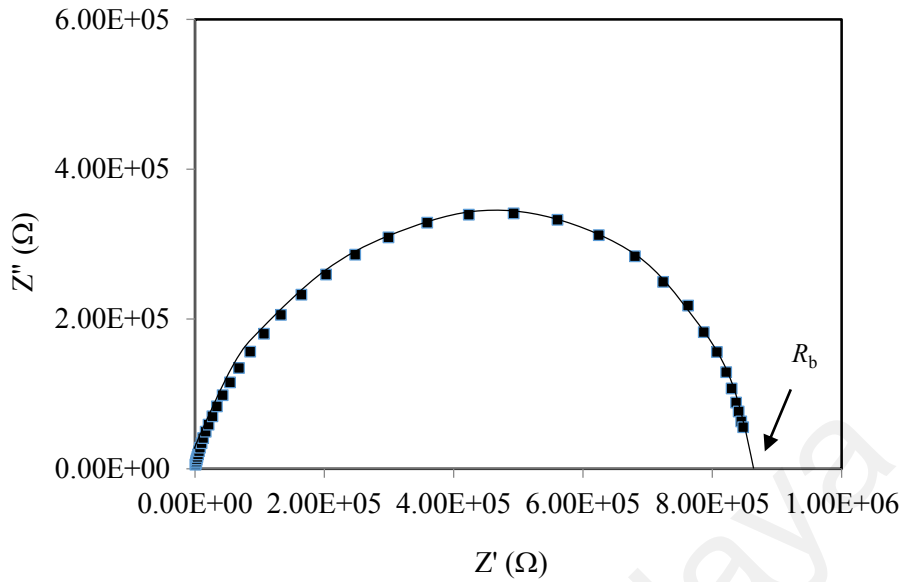


**Figure 4.16:** Impedance plot of WEL10 at room temperature

The ionic conductivity values are calculated using the following equation:

$$\sigma = \frac{t}{(R_b\ A)} \tag{4.1}$$

where $t$ is the thickness of the electrolyte film, and $A$ is the electrode-electrolyte contact area.

Figure 4.17 displays the ionic conductivity as a function of salt content for (ENR-50)-LiTFSI electrolyte system. The dependence of ionic conductivity on the salt content may provide information on the specific interaction between the polymer matrix and the salt. From Figure 4.17, it can be seen that the conductivity increases with increasing LiTFSI content and attains a maximum value of $3.24\times10^{-5}$ S cm$^{-1}$. The maximum conductivity was achieved at 50 wt.% of LiTFSI. At salt content higher that 50 wt.%, the 'salting out' effect could be seen on the surface of the sample. Hence, the measurements are limited to this concentration.

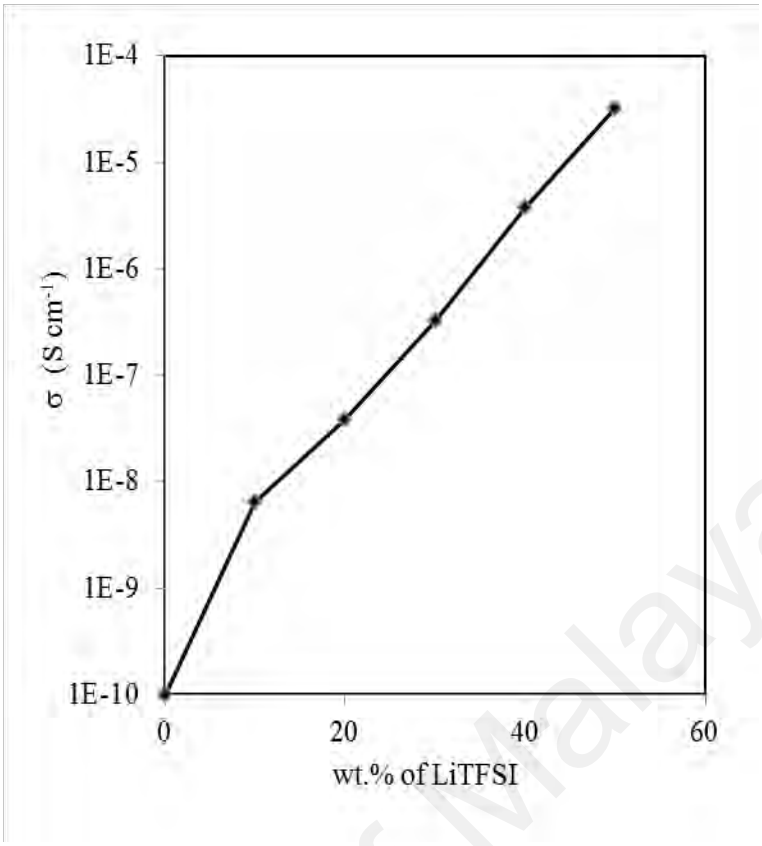


**Figure 4.17:** Ionic conductivity versus salt concentration of (ENR-50)-LiTFSI electrolyte system at room temperature

For this system, it can be stated that ionic conductivity at room temperature is not coupled with the segmental motion of the polymers. Even though the $T_g$ increases, the ionic conductivity also increases. In this system, the cross-links may be well separated in space and can move with respect to each other to a certain extent thereby contributing to ionic conductivity (Subban, 2004). The ionic conductivity may also be contributed by the anions which interact weakly with the polymer (Johansson *et al*, 1996), as mentioned earlier in ATR-FTIR section. Furthermore, the increase in ionic conductivity with increasing salt content could be related to the increase in the number of carrier ions content in the system (Nazir *et al*, 2017).

To examine the thermal dependence of the ionic conductivity of the electrolyte sample, ac impedance measurement was performed at temperatures varying from 30 to 80 ºC. The

ionic conductivity changes at those temperatures are shown in Figure 4.18. For all samples, the conductivity increases with increasing temperature.

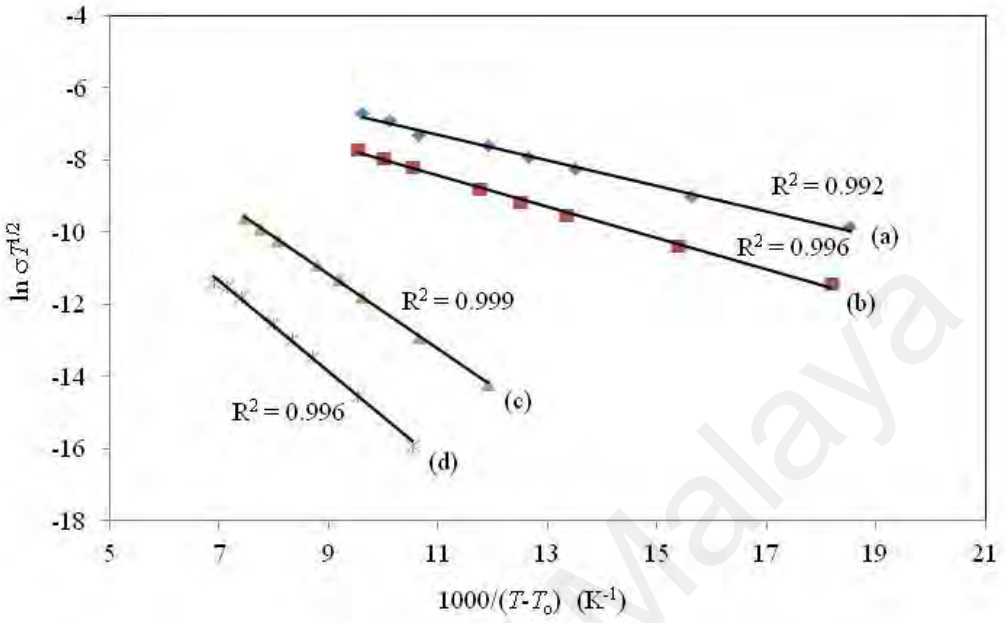


**Figure 4.18:** VTF plot of (a) WEL50 (b) WEL40 (c) WEL20 and (d) WEL10.

The electrolyte system exhibits VTF behaviour, in which ion transport is related to the segmental motion of the polymer chain. As temperature increase, thermal movement of polymer chain segments and the dissociation of salt enhances. This leads to increase in ionic conductivity. The experimental data can be fitted with the Vogel-Tammann-Fulcher (VTF) equation in the form:

$$\sigma = AT^{1/2} \exp\left[-B/(T-T_0)\right] \qquad (4.2)$$

$A$ and $B$ are the parameters related to the number of charge carriers and the conduction activation energy respectively. $T_0$ is the Vogel scaling temperature and is taken as $T_0=T_g - 50$ K where $T_g$ is the glass transition temperature.

The VTF relationship indicates the coupling of the charge carriers with the segmental motion of the polymer chain. The ionic conductivity change is dominated by the change

in ionic mobility, as predicted by the free volume theory (Cohen & Turnbull, 1959). Free volume theory states that the polymer motion is not mainly thermally activated, but essentially occurs by redistribution of the free volume. As the temperature increases, local voids are created by the expansion of the material and thus, polymer segments can move in this free volume. Since the ionic conduction occurs in the amorphous phase of the material, the increasing free volume density helps in increasing the conductivity (Aziz *et al*, 2017).

Calculated *B* values for (ENR-50)-LiTFSI electrolyte system is plotted against LiTFSI concentration and is shown in Figure 4.19. From the graph, the *B* values are affected by the conductivity. The highest conducting sample gives the lowest *B*. The lowest *B* value is 2.94 kJ $mol^{-1}$ at 50 wt.% of LiTFSI. Since activation energy represents the energy required to overcome the reorganization and reformation of the polymer chain with $Li^+$, the decrease in *B* with salt concentration implies increase in migration rate of charge carriers. The increase in migration rate of charge carriers is attributed to the enhancement of the polymer segmental motion as mentioned earlier.

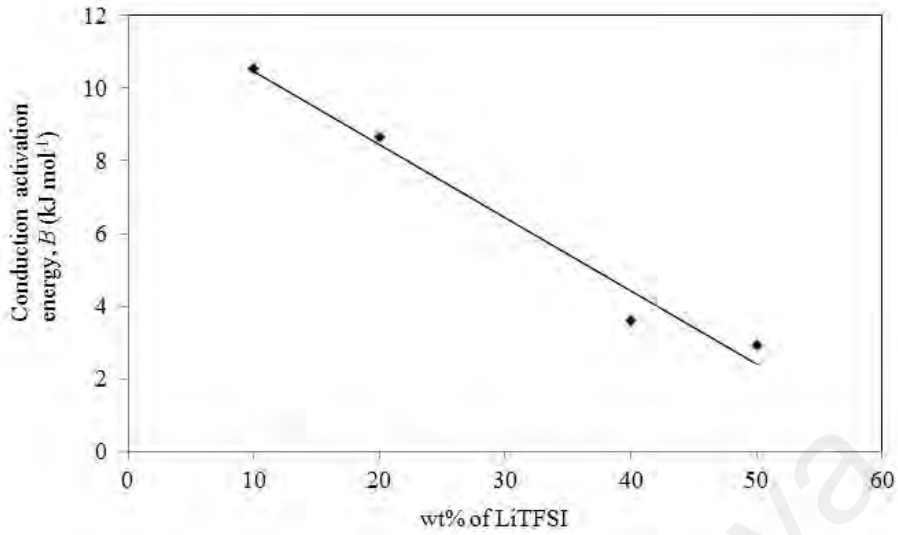


**Figure 4.19:** Conduction activation energy versus salt concentration of (ENR-50)-LiTFSI system

## 4.2 System 2: (ENR-50)-BMITFSI-LiTFSI

To improve the ionic conductivity of the electrolyte system, ionic liquid, BMITFSI was added to the (ENR-50)-LiTFSI system. One of the film obtained for this system is shown in Figure 4.20. Comparing Figure 4.20 with Figure 4.1, WEBL50 film looks more transparent than WEB0 film.

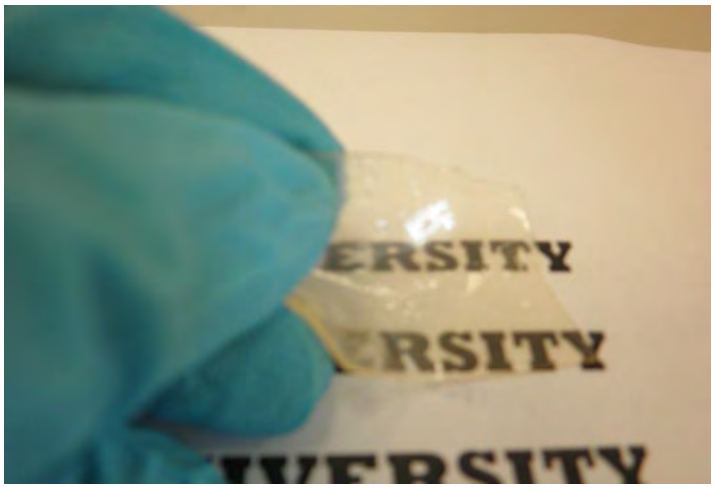

**Figure 4.20:** WEBL50 film

### 4.2.1 Attenuated total reflectance – Fourier transform infrared

Evidence of complexation of ENR-50 with the ionic liquid and lithium salt is confirmed by vibrational spectroscopy. The ATR-FTIR spectra of BMITFSI and the (ENR-50)-BMITFSI-LiTFSI electrolytes in certain spectral regions are shown in Figure 4.21 and and Figure 4.22 respectively.

Table 4.3 lists the vibration modes with the respective wavenumber of BMITFSI transmission spectrum. Peaks at 3116 and 3159 $cm^{-1}$ are assigned to the vibration of C-H for cyclic $BMI^{+}$. The stretching and deformation vibrations of $CH_2$ groups appear at the wavenumber of 2969 $cm^{-1}$, whereas the band at wavenumber of 1573 $cm^{-1}$ belongs to the vibration of C-C and C-N. The absorption peaks at 1347 $cm^{-1}$ is assigned to the vibration of $–SO_2$ of the TFSI anion.

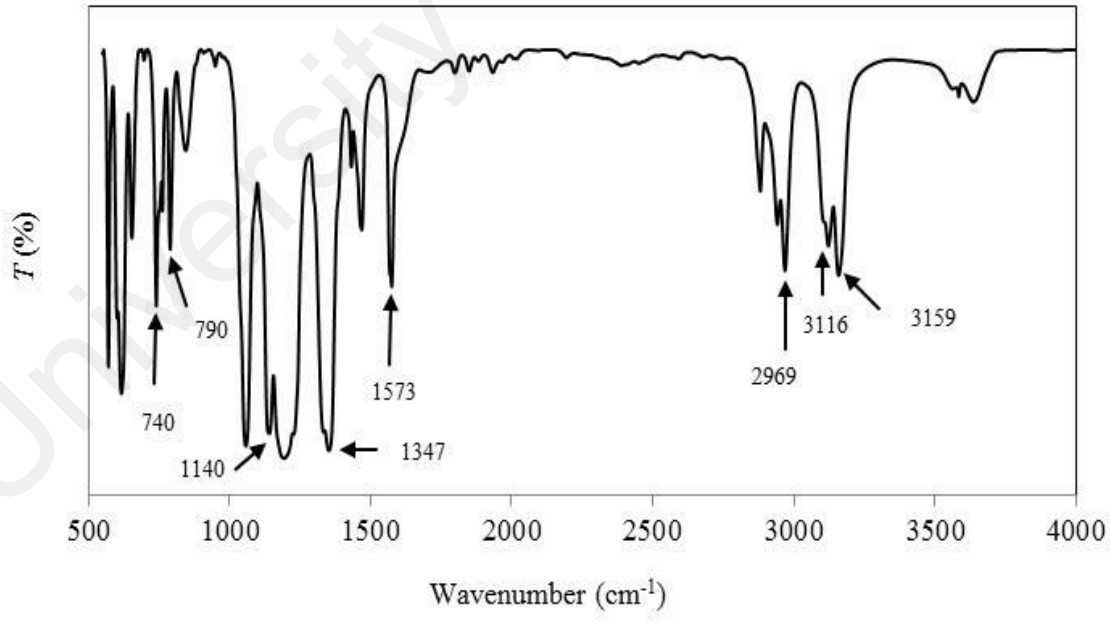


**Figure 4.21:** Transmission spectrum for BMITFSI

**Table 4.3:** Assignments of vibrational modes of BMITFSI

| Descriptions of vibration modes | Wavenumber ($cm^{-1}$) | References |
|---|---|---|
| C-H vibration mode for cyclic $BMI^+$ | 3116, 3159 | Ramesh *et al* (2011)<br>Jiang *et al* (2006) |
| $CH_2$ stretching mode | 2969 | Ramesh *et al* (2011)<br>Jiang *et al* (2006) |
| C-C and C-N bending mode | 1573 | Ramesh *et al* (2011)<br>Jiang *et al* (2006) |
| $SO_2$ symmetric and asymmetric stretching mode | 1140, 1347 | Ahmad *et al* (2008) |
| Combination of C-S and S-N stretching mode | 790 | Ahmad *et al* (2008) |
| S-N stretching mode | 740 | Lassegues *et al* (2008) |

Figures 4.22 (a), (b) and (c) show the spectra of (ENR-50)-BMITFSI-LiTFSI in the spectral range of 700-900 $cm^{-1}$, 1100-1500 $cm^{-1}$ and 1500-3500 $cm^{-1}$ respectively. The C-O-C band of ENR-50, observed at 1255 $cm^{-1}$ in Figure 4.2, does not appear in these spectra. The disappearance of this band indicates interaction between ENR-50, BMITFSI and LiTFSI. The epoxy group is believed could provide coordination site with Li cation to promote ionic conductivity. However, the asymmetrical stretching vibrational band of the epoxide group still appears in (ENR-50)-BMITFSI-LiTFSI spectra but are shifted to lower wavenumber, which indicates weak interaction between polymer and ions from both BMITFSI and LiTFSI. This promotes more free ions for ionic transport. Other characteristic bands of ENR-50 (1378 and 1449 $cm^{-1}$) shift in positions and change in intensities. These give additional evidences of interaction between ENR-50, BMITFSI and LiTFSI.

Presence of salt and its varying concentration in (ENR-50)-BMITFSI-LiTFSI electrolytes system have resulted in positional and intensity changes. The symmetrical and asymmetrical stretching vibration of $SO_2$ in imide located at 1140 and 1347 $cm^{-1}$ shifted to lower wavenumber with increased intensities.

The presence and absence of C-H vibration modes for cyclic $BMI^+$ in electrolyte system (Figure 4.22 (c)), indicates the interaction between ENR-50 and BMITFSI. The sensitivity to salt content is evident from the spectra, as the peak at 3156 $cm^{-1}$ shifts to the higher wavenumber with addition of salt and disappears at high salt content. The intensities of the characteristic peaks are reduced substantially as the salt content increases. However, the peak at 3116 $cm^{-1}$ is not observable in the spectra indicating interaction of $BMI^+$ with ENR-50. Moreover, the interaction between ENR-50, BMITFSI and LiTFSI can also be observed by the appearance of a new peak at 1657 $cm^{-1}$ after addition of 10 wt.% of LiTFSI in (ENR-50)-BMITFSI electrolyte system. This peak shifted to lower wavenumber with increase in salt content.

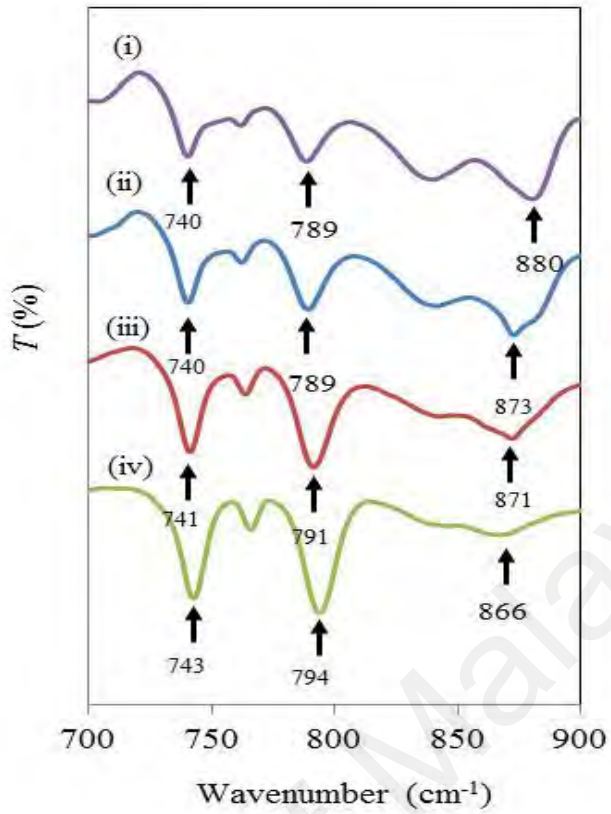


**Figure 4.22:** ATR-FTIR spectra of (i) WEBL0, (ii) WEBL10, (iii) WEBL30 and (iv) WEBL50 in the range of 700 to 900 $cm^{-1}$

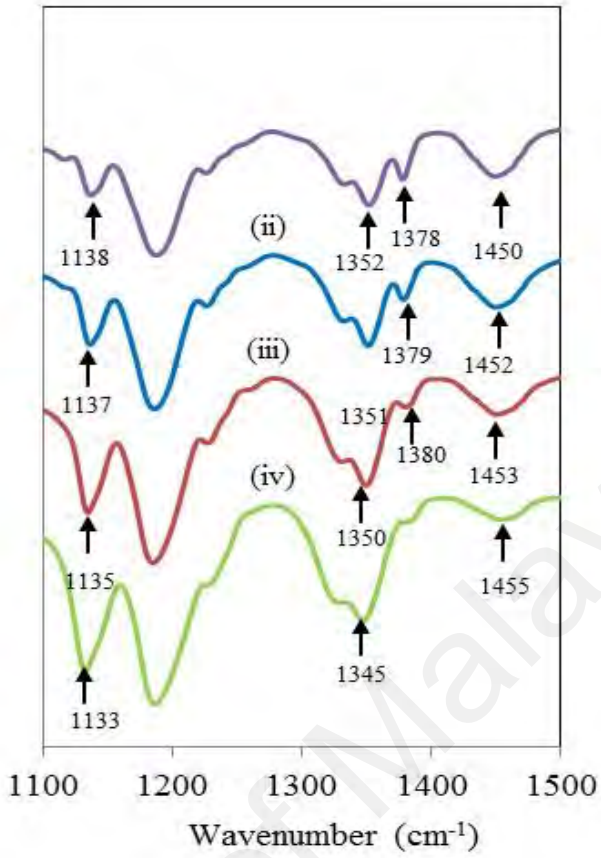


**Figure 4.23**: ATR-FTIR spectra of (i) WEBL0, (ii) WEBL10, (iii) WEBL30 and (iv) WEBL50 in the range of 1100 to 1500 $cm^{-1}$

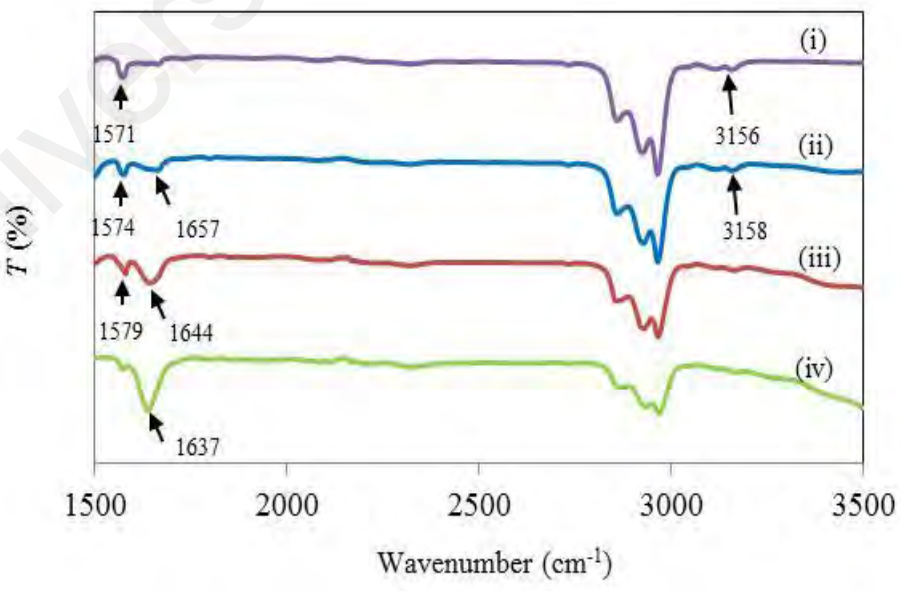


**Figure 4.24**: ATR-FTIR spectra of (i) WEBL0, (ii) WEBL10, (iii) WEBL30 and )iv) WEBL50 in the range of 1500 to 3500 $cm^{-1}$

### 4.2.2 X-ray photoelectron spectroscopy

XPS analysis was carried out to confirm the interaction between ENR-50, BMITFSI and LiTFSI mentioned in the previous section. Figures 4.25 and 4.26 show the XPS spectra of (ENR-50)-BMITFSI added with 10 wt.% of LiTFSI for C1s and O1s binding energies respectively. Three peaks are observed in each spectrum. These peaks are labelled according to the element they belong to and the binding energies of the corresponding peaks are shown in Table 4.4.

The C1s spectrum for WEBL10 displays a sharp dominant peak at 284.4 eV due to C-C/C-H bonds (Ameen *et al*, 2013; Xuan *et al*, 2011). The smallest peak is observed at 286.4 eV, which is expected belong to C-O-C bond of epoxy group. The peak of the epoxy group can also be observed in the O1s spectrum in Figure 4.19 (b), the highest peak at 530.9 eV. The binding energies for O-C- peak decreases in (ENR-50)-BMITFSI-LiTFSI film compared to that in ENR-50 film indicating that the interactions between the epoxy groups from the polymer with the cations increase. This can be shown by the appearance of peak at 529.2 eV that can probably be attributed to the interaction between oxygen and lithium cation since this peak is not observed in the ENR-50 spectrum. This result is consistent with ATR-FTIR result which shows the disappearance of one of the epoxy group that is believed to coordinate with $Li^+$. The O=S bond of imide is presented by peak at binding energy ~532.5 eV (Ensling *et al*, 2009). This peak is not observed in Figure 4.11. This means that the addition of ionic liquid increases the number of imide anion. The peak at 281.7 eV which appears in C1s spectrum may be attributed to cation or anion from ionic liquid since this peak is not observed in Figure 4.10.

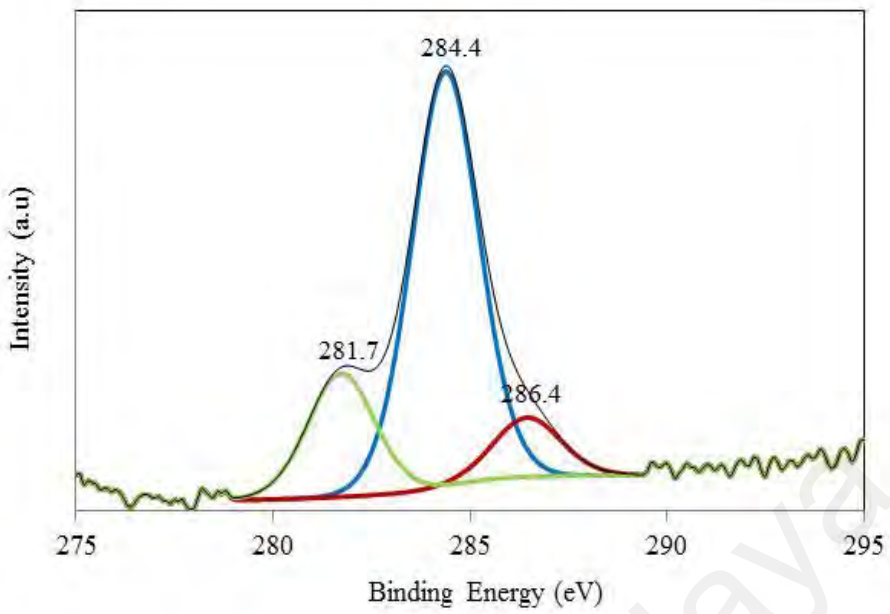


**Figure 4.25:** C1s XPS spectrum for WEBL10

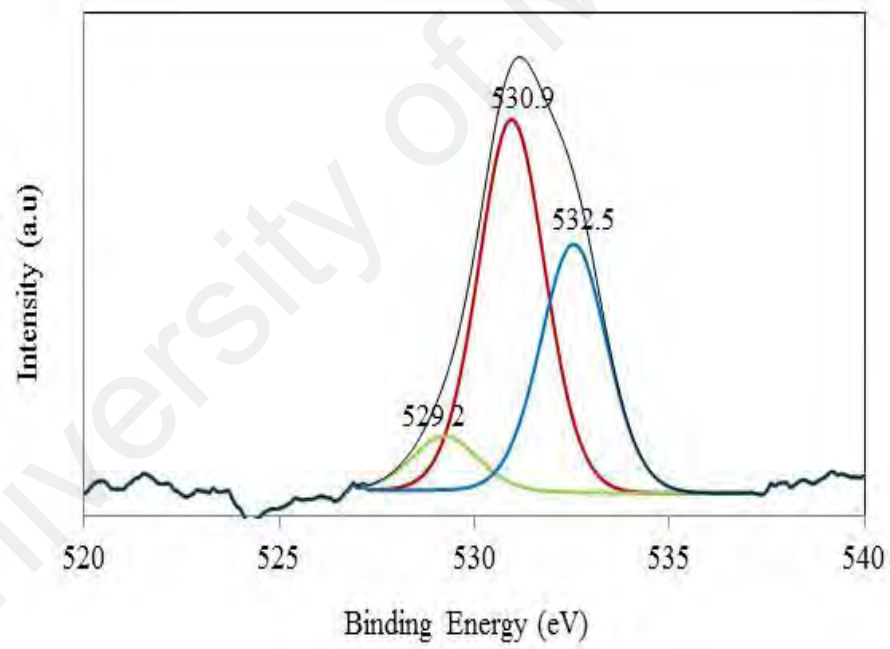


**Figure 4.26**: O1s XPS spectrum for WEBL10

**Table 4.4:** C1s and O1s binding energies for ENR-50 and salted (ENR-50)-BMITFSI

| Spectra | Binding Energy (eV) of ENR-50 | Binding Energy (eV) of WEBL10 | Peaks |
|---|---|---|---|
| C1s | 284.6 | 284.4 | C-C/C-H |
| | 286.5 | 286.4 | C-O-C (epoxy) |
| O1s | 531.0 | 530.9 | O-C |
| | - | 529.2 | Expected for oxygen and lithium |
| | - | 532.5 | O=S |

### 4.2.3 Thermogravimetric Analysis

Thermal stability of the polymer electrolyte is also an important parameter to guarantee acceptable performances in device applications. Therefore, in this work, the thermal stability of the electrolyte system containing ionic liquid was studied using TGA over a temperature range from 30-700 °C.

Figure 4.27 demonstrates the thermal stability of (ENR-50)-BMITFSI and (ENR-50)-BMITFSI added with 10 wt.% of LiTFSI. The decompose temperature of these two films are higher than 350 ºC.

Up to 350 ºC, there are no distinct weight reductions, indicating good thermal films stability in this temperature range. The degradation temperature for WEBL0 is 360 °C. Beyond this temperature, the weight drops by about 79%, reflecting the degradation of the polymer main chain. From 447 °C the weight gradually decreases and then saturates at 488 ºC.

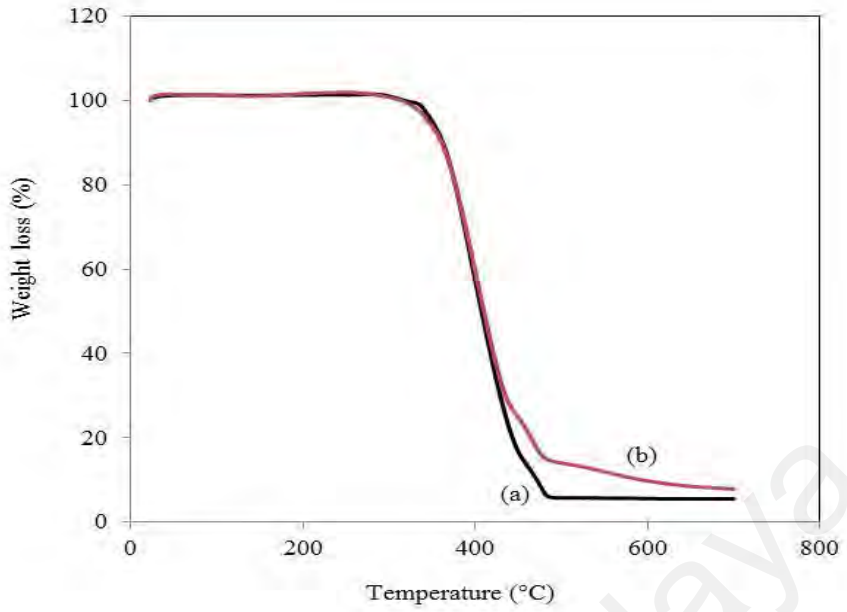


**Figure 4.27:** TGA thermograms of (a) WEBL0 and (b) WEBL10

On the other hand, the degradation of WEBL10 starts at 355 °C, which is lower than salt-free film (~360 °C). The degradation of polymer chain is shown by the weight loss of about 71 %. Comparing to WEL10 (Figure 4.13) the degradation of film without ionic liquid is lower than the film containing ionic liquid indicating that the thermal stability of the film is enhanced slightly due to the presence of ionic liquid. This is in contrast with the thermal stability of polymer electrolyte containing plasticizers such as EC and PC which shows reduction in decomposition temperature after addition of plasticizers (Stephan *et al*, 2002).

### 4.2.4 Differential scanning calorimetry

Figures 4.28 (a), (b) and (c) show the DSC thermograms of WEBL0, WEBL10 and WEBL50 respectively. As mentioned in subsection 4.1.4, the $T_g$ of ENR-50 is -22 °C. As expected, ENR-50 film containing BMITFSI shows $T_g$ at -28 °C (Figure 4.28 (a)), which is lower than that of pure ENR-50 film. BMITFSI is expected to play a role as a plasticizer

in the (ENR-50)-LiTFSI system. This statement is supported by Singh & Sekhon (2005) and Cho *et al* (2007) who reported that BMITFSI shows the best plasticizing effect among ionic liquids that they used in their solid electrolyte systems.

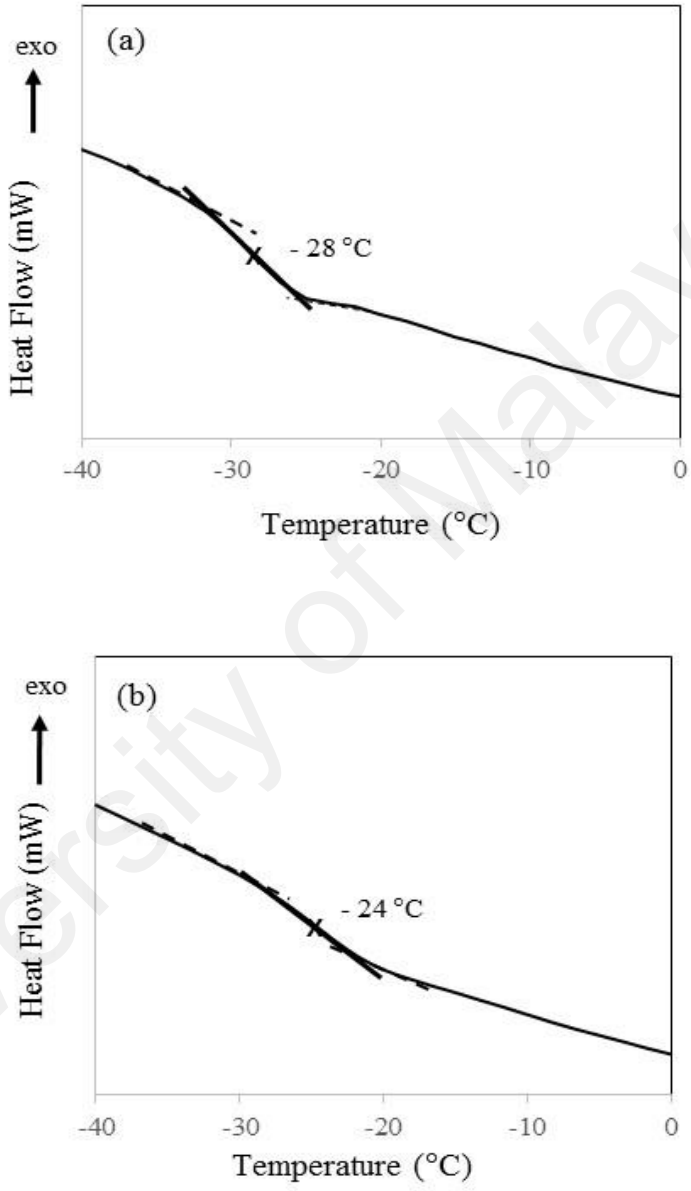


**Figure 4.28:** Glass transition temperature values for (a) WEBL0, (b) WEBL10 and (c) WEBL20

Figure 4.28, continued..

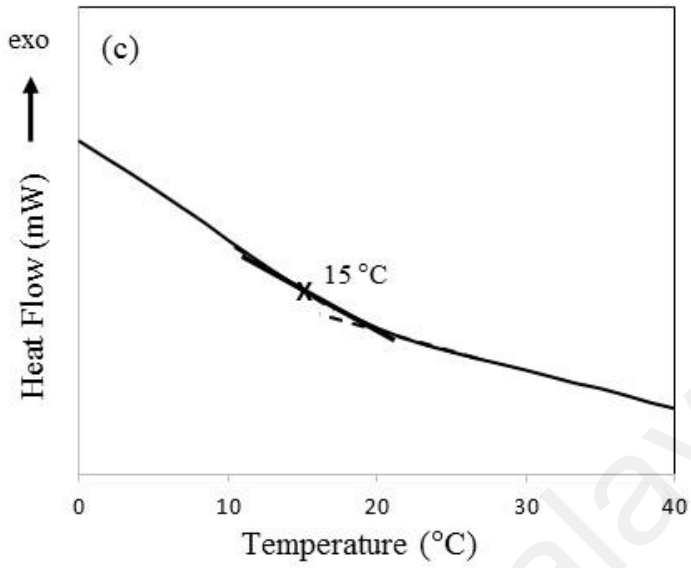


Figure 4.29 shows glass transition temperatures of the polymer electrolytes as a function of lithium salt content. The $T_g$ increases with increasing salt content, indicating the interaction between polymer chains and dopant salt arises from the formation of transient cross-links (Hou *et al*, 2003 and Kim *et al* 2003) created by coordination of lithium ions with the epoxy group of the polymer . The cross-linking reduces degree of mobility of polymer segments and hence the polymer chains become less flexible.

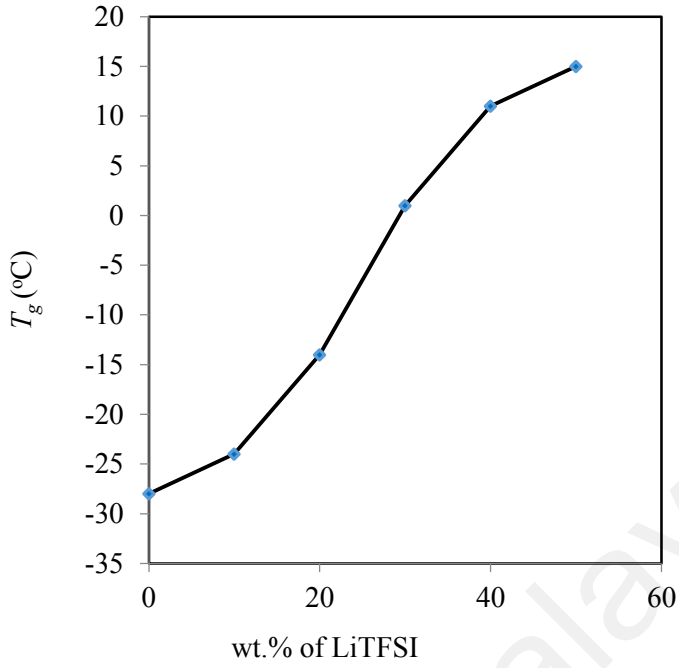


**Figure 4.29:** Graph $T_g$ against salt content of (ENR-50)-BMITFSI-LiTFSI

Comparing with the graph in Figure 4.15, the $T_g$ values in Figure 4.29 for (ENR-50)-BMITFSI added with LiTFSI are lower than the ENR-50 (BMITFSI free) containing an equivalent amount of LiTFSI. The decrease in $T_g$ helps to soften the polymer chains and improves the segmental movement of polymer chains, thus enhances the movement of ions. This result shows the role of ionic liquid as plasticizer, which improves the flexibility of the polymer chains.

### 4.2.5 Ionic Conductivity

Figure 4.30 presents the impedance plot of WEBL10 at room temperature. Considerable reduction of the resistance is observed as compared to Figure 4.16. This is ascribed to a decrease in internal resistance of (ENR-50)-LiTFSI material caused by the presence of BMITFSI molecules.

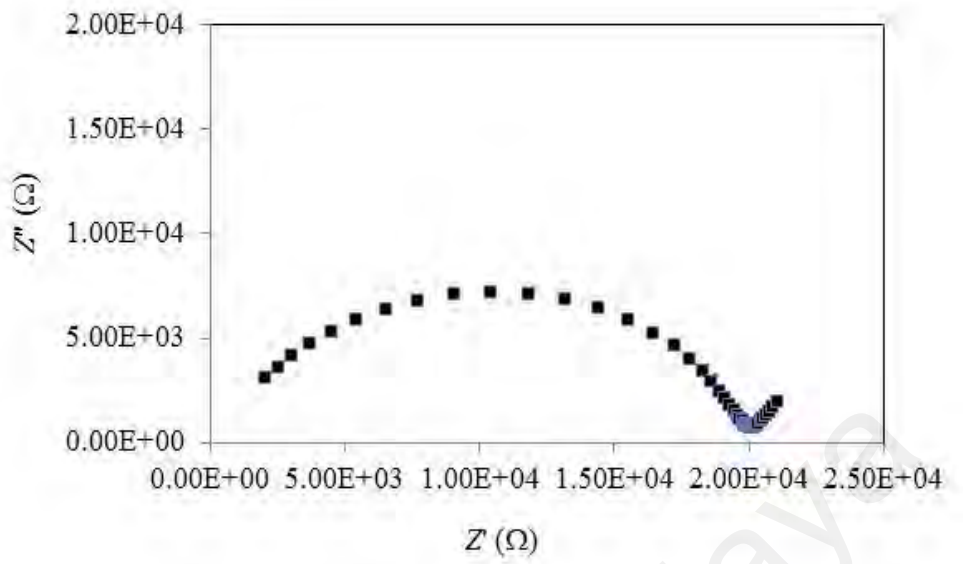


**Figure 4.30:** Impedance plot of WEBL10 at room temperature

Figure 4.31 shows the ionic conductivity of various salt contents for ENR-50 containing ionic liquid, BMITFSI. The highest ionic conductivity value is $1.03 \times 10^{-4}$ S $cm^{-1}$ at 50 wt.% of LiTFSI. This conductivity value is comparable with the value reported by Razali and Wan Siti Nor (2007) for (ENR-50)-EC/PC polymer electrolyte system. The conductivity shows an increasing trend with the salt content. This means that the increase in $T_g$ (Figure 4.29) does not give adverse effect on ionic conductivity. In this system, the cross-links that formed between the ENR-50 chains and lithium salt (as mentioned in previous section) may have certain average lifetime, after which the ions form new cross-links with the same or different polymer chains. In this bond breaking mechanism, ions are believed to be mobile (Lin & Maranas, 2013), thus contributes to the increase of ionic conductivity of the system. Furthermore, the nature of imide as plasticizing salt (Marzantowicz, *et al*, 2006) might also contribute to the enhancement of ionic conductivity (with increase in salt content), even though in cross-linking environment.

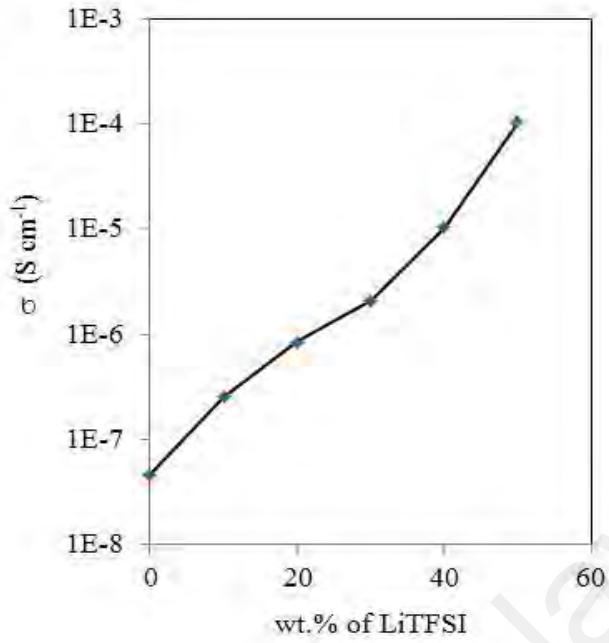


**Figure 4.31:** Ionic conductivity versus salt content of (ENR-50)-BMITFSI-LiTFSI electrolyte system at room temperature

Comparing with (ENR-50)-LiTFSI system in Figure 4.17, the increase in ionic conductivity in (ENR-50)-BMITFSI-LiTFSI system is strongly ascribed to the production of additional mobile charge carriers as ionic liquid provides $BMI^+$ and $TFSI^-$ (Misenan *et al*, 2018). Another perspective is the weakening of the interaction between the polymer matrices upon inclusion of ionic liquid. Thus, it reduces the solvation of Li cations by polymer matrix and eventually promotes the decoupling of ions due to its high self-dissociating property (Jiang *et al*, 2006). Therefore, it exhibits an increase in ionic conductivity by enhancing the ion transportation.

It can be seen that the ionic conductivity of the samples containing both BMITFSI and LiTFSI is higher than the samples containing an equivalent amount of LiTFSI alone. Therefore, it can be stated that the use of BMITFSI in the polymer electrolyte enhances the ionic conductivity.

The relationship between σ and $T_g$ is displayed in Figure 4.32. When ionic liquid is added to the salted system, $T_g$ is lowered and the ionic conductivity increases. The increase in ionic conductivity is related to the plasticizing effect of ionic liquid. It softens the polymer chain and enhances the flexibility of the polymer system, accelerating the polymer segmental mobility and ionic transportation by providing more conduction pathways (Sekhon *et al*, 2006).

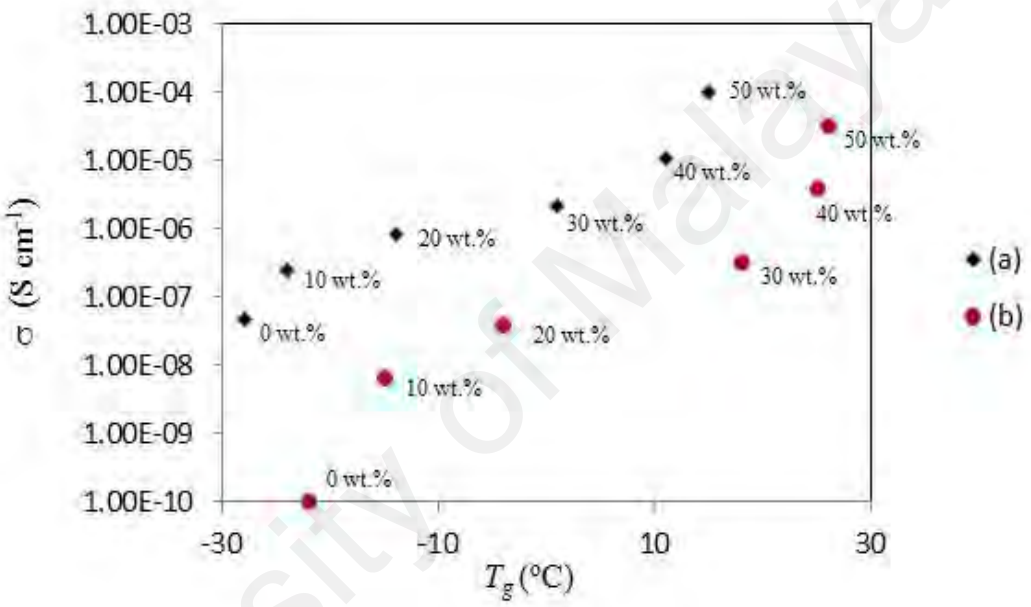


**Figure 4.32:** Relationship between ionic conductivity and glass transition temperature for (a) (ENR-50)-BMITFSI-LiTFSI system and (b) (ENR-50)-LiTFSI system at 0 – 50 wt.% of salt content

Figure 4.33 shows temperature dependence of the ionic conductivity of (ENR-50)-BMITFSI-LiTFSI films at various salt content from 30 to 80 °C. The temperature dependence of ionic conductivity is fitted by the Vogel-Tammann-Fulcher equation, indicating that ion motion is strongly coupled to segmental motion of the polymer chains. Furthermore, the addition of ionic liquid provides more voids and free spaces for ion migration and thereby enhances ionic conductivity.

The ionic conductivity of this system is slightly higher than ionic liquid-free system (Figure 4.18). It is due to the presence of BMITFSI that reduces the viscosity of the electrolyte and increase the plasticizing effect.

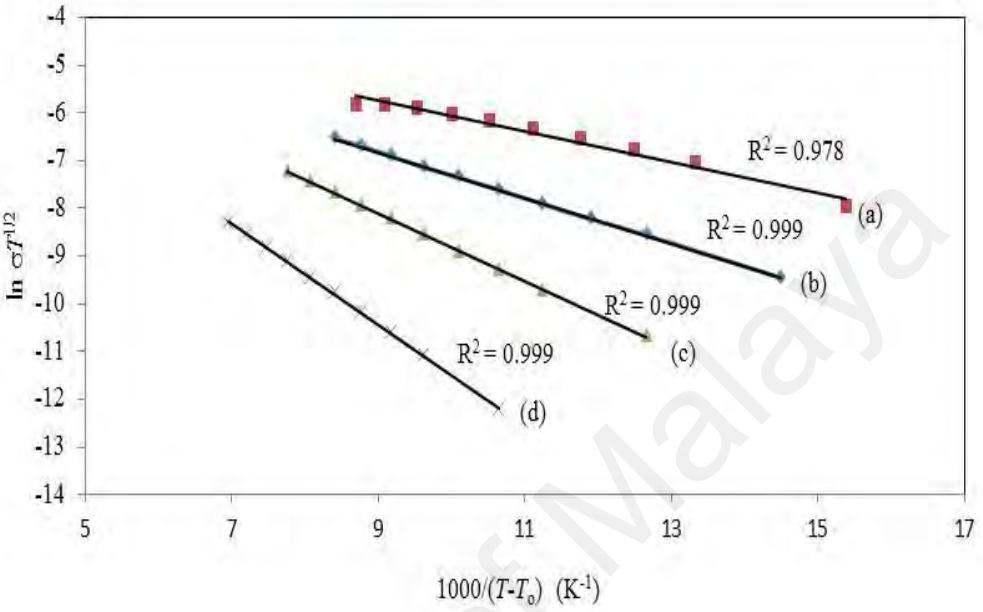


**Figure 4.33:** VTF plot of (a) WEBL50 (b) WEBL40 (c) WEBL30 and (d) WEBL20

Figure 4.34 illustrates the conduction activation energy values (calculated from equation 4.2) plotted against LiTFSI content. The lowest *B* value is 2.67 kJ $mol^{-1}$, which is slightly lower than the value in the ionic liquid-free system. In this system, BMITFSI disrupts the interaction between polymer chains and $Li^+$, thus it requires less energy to break and reform the coordination bond among the polymer matrix. Moreover, it has affected the local microstructure of the polymer, acting as plasticizer, lowering the conduction activation energy for ion transport. As a result, it enhances the migration rate of ion, and therefore, increases the ionic conductivity of the system (Diederichsen, *et al*, 2017).

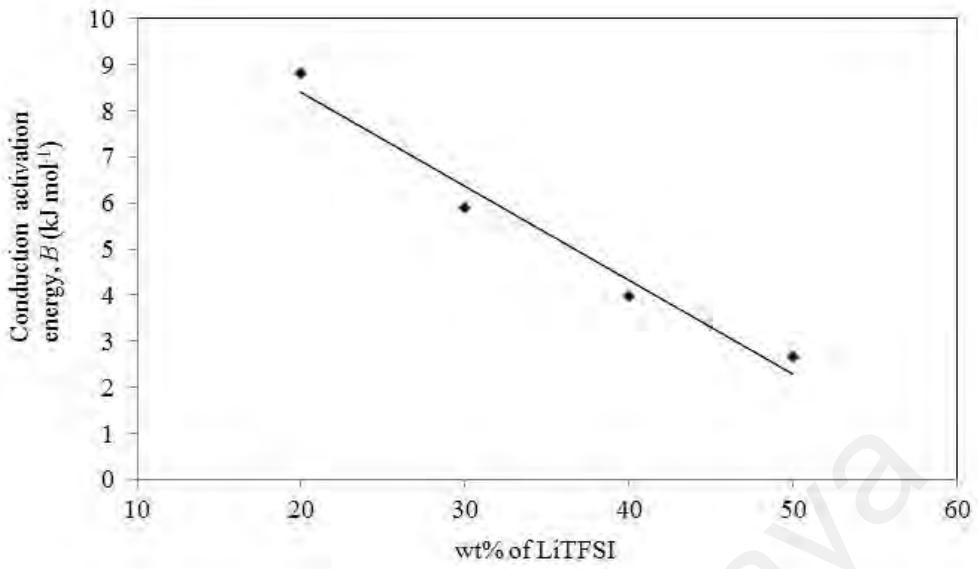


**Figure 4.34:** Conduction activation energy versus salt content of (ENR-50)-BMITFSI-LiTFSI

### 4.2.6 Linear sweep voltammetry

The electrochemical stability of (ENR-50)-BMITFSI-LiTFSI electrolyte film was investigated by LSV using copper as working electrode and lithium as counter and reference electrodes. The results is shown in Figure 4.35. An electrochemical stability up to 2.7 V was obtained for WEBL50 at ambient temperature. This sample is chosen because of its high ionic conductivity compared to other samples. However, for the first system (ionic liquid free), the electrochemical stability of WEL50 could not be determined due to the unstable condition of lithium with the sample.

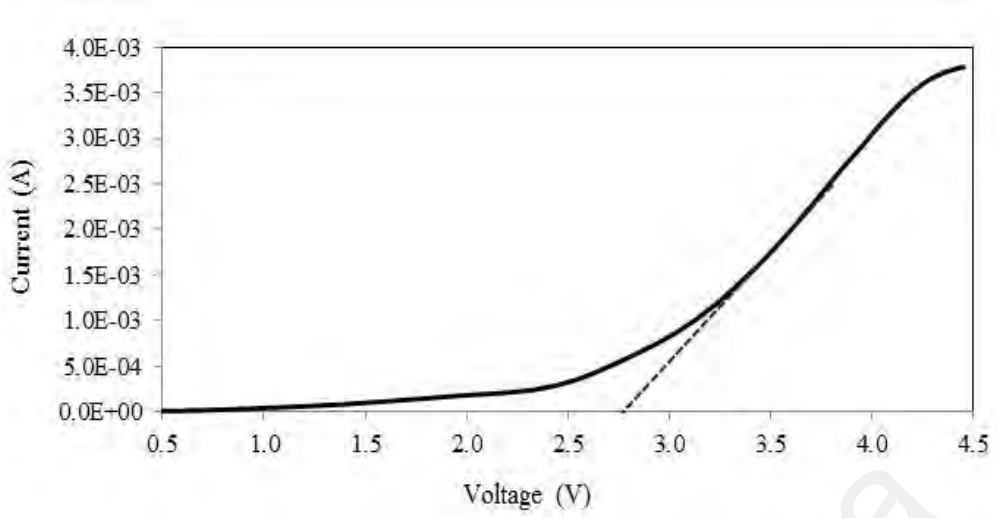


**Figure 4.35:** Linear sweep voltammetry of WEBL50

## 4.3 System 3: (ENR-50)-EMITFSI-LiTFSI

Alternatively, 1-ethyl-3-methylimidazolium bis(trifluoromethanesulfonyl) imide (EMITFSI) was added to investigate its effect to the properties of (ENR-50)-LiTFSI electrolyte system. Figure 4.36 shows (ENR-50)-EMITFSI-LiTFSI film prepared by solution casting method. The film obtained is translucent (less transparent) compared with film added with BMITFSI. This indicates that the type of ionic liquid used affects the transparency of light that passing through the film.


**Figure 4.36:** WEEL50 film

### 4.3.1 Attenuated total reflectance – Fourier transform infrared (ATR-FTIR)

The ATR-FTIR spectrum of EMITFSI is shown in Figure 4.37. Eight peaks related to EMITFSI; C-H vibrational modes of cyclic $EMI^+$ are observed at 3124 and 3162 $cm^{-1}$, $CH_3$ stretching mode at 1472 $cm^{-1}$, C-C and C-N stretching mode at 1574 $cm^{-1}$ and $SO_2$ asymmetric stretching mode from imide at 1140 and 1345 $cm^{-1}$. The vibrational modes of EMITFSI with their respective wavenumbers are listed in Table 4.5.

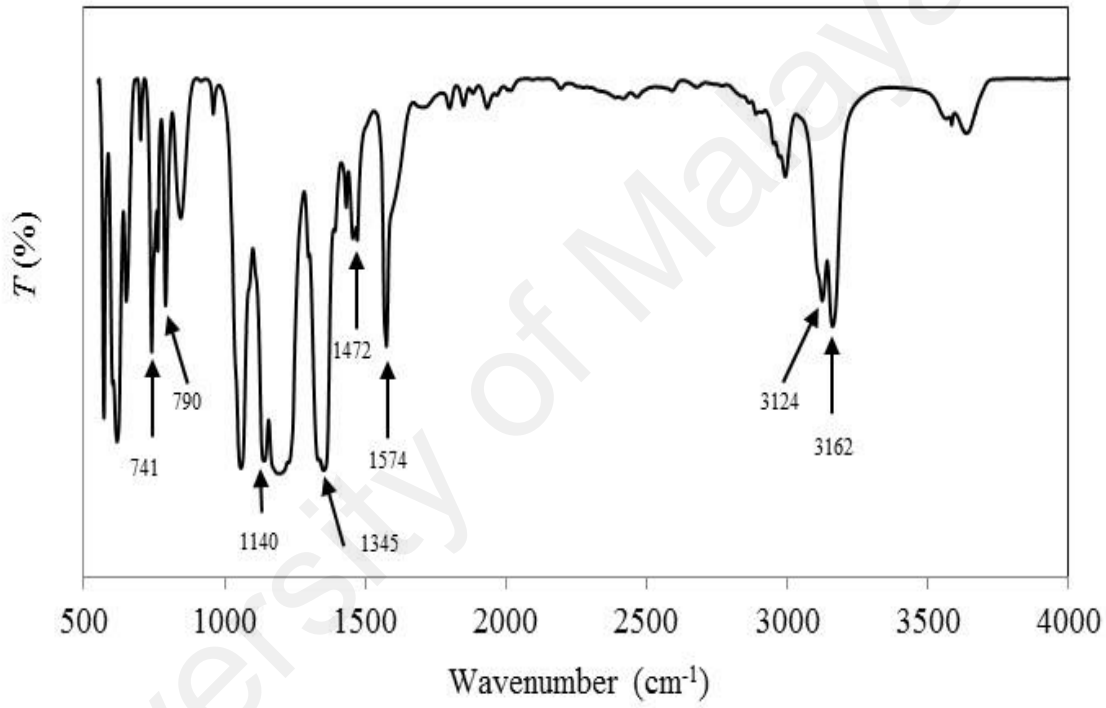


**Figure 4.37:** Transmission spectrum of EMITFSI

**Table 4.5:** Assignments of vibrational modes of EMITFSI

| Descriptions of vibration modes | Wavenumber ($cm^{-1}$) | References |
|---|---|---|
| C-H vibrational mode for cyclic $EMI^+$ | 3124, 3162 | Chaurasia *et al* (2011), Noack *et al* (2010) |
| $CH_3$ bending mode | 1472 | Noack *et al* (2010), Nanbu *et al* (2003) |
| C-C and C-N stretching mode of the imidazole ring | 1574 | Noack *et al* (2010), Nanbu *et al* (2003) |
| $SO_2$ symmetric and asymmetric stretching mode | 1140, 1345 | Dhumal *et al* (2014) |
| Combination of C-S and S-N stretching mode | 790 | Lassegues *et al* (2008) |
| S-N stretching mode | 741 | Lassegues *et al* (2008) |

Figures 4.38 and 4.39 show the ATR-FTIR spectra of (ENR-50)-EMITFSI and (ENR-50)-EMITFSI in the spectral range of 700-900 $cm^{-1}$ and 1100-1400 $cm^{-1}$ respectively. As observed from these two spectra, both epoxy groups of ENR-50 (at 872 and 1255 $cm^{-1}$) disappeared after addition of ionic liquid and lithium salt.

When ionic liquid is mixed with the polymer, there is a possibility of end groups of the imidazolium cation ($EMI^+$) of the ionic liquid to interact with the epoxy groups of ENR-50. The epoxy groups belonging to C-O-C groups of ENR-50 is most likely to form bond or complex with the ionic liquid cation aromatic ring. Furthermore, upon addition of salt, this epoxy groups interact with Li cations to promote ionic conductivity. The disappearance of bands of these epoxy groups indicates interaction between ENR-50, EMITFSI and LiTFSI.

From Figure 4.38, the peaks at 741 and 790 $cm^{-1}$ show increasing in intensities at higher salt content, even though the peaks are retained in positions. Furthermore, from Figure 4.39, the peaks which correspond to imide anion show shifting in frequency and increasing in intensities at higher salt content. These observations indicate that the interactions occurred between ENR-50, ionic liquid and lithium salt.

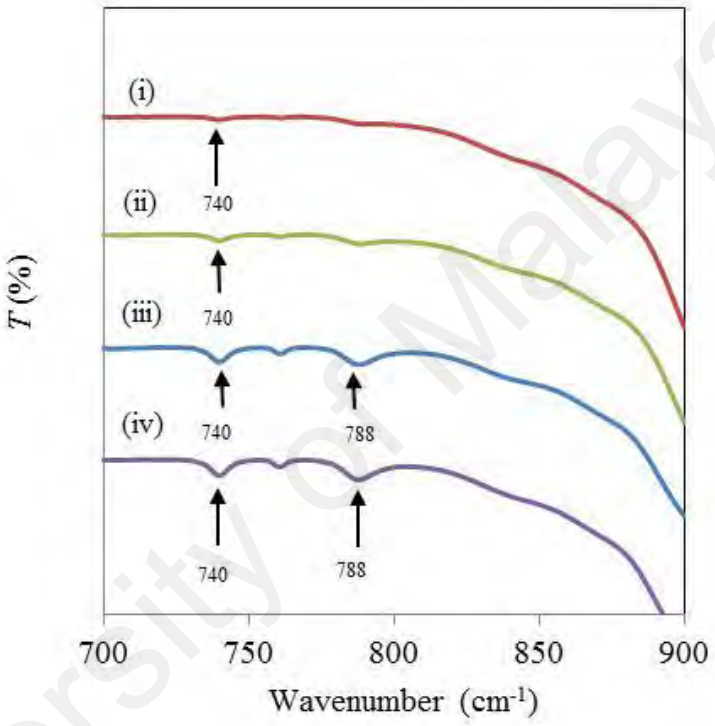


**Figure 4.38:** ATR-FTIR spectra of (i) WEEL0, (ii) WEEL10, (iii) WEEL30 and (iv) WEEL50 in the range of 700 to 900 $cm^{-1}$

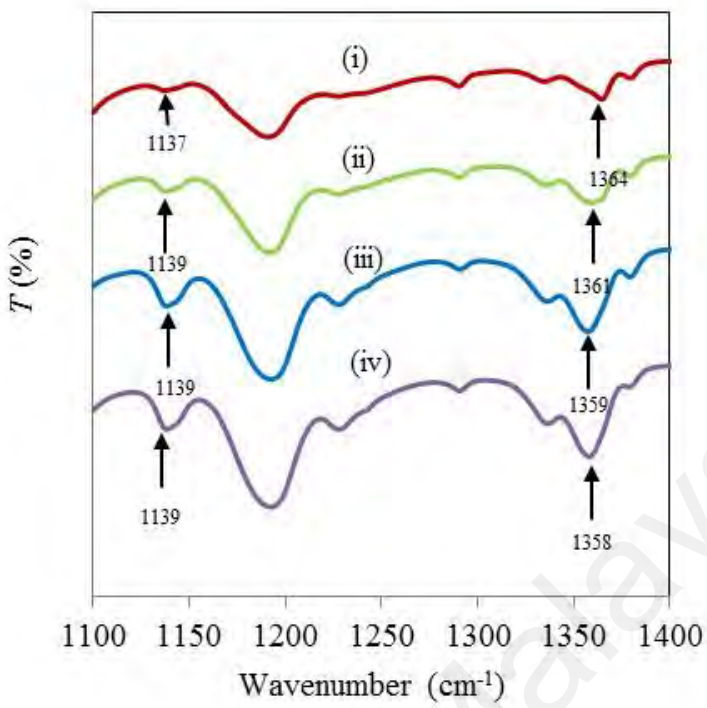


**Figure 4.39**: ATR-FTIR spectra of (i) WEEL0, (ii) WEEL10, (iii) WEEL30 and (iv) WEEL50 in the range of 1100 to 1400 $cm^{-1}$.

### 4.3.2 X-ray photoelectron spectroscopy

The deconvoluted carbon and oxygen spectra for (ENR-50)-EMITFSI-LiTFSI are depicted in Figures 4.40 and 4.41 respectively. Correlation of XPS data with the results obtained from ATR-FTIR spectroscopy is important to confirm the interaction between ENR-50, EMITFSI and LiTFSI.

The peak at 284.2 eV is attributed to carbon atoms of C-C or C-H while the peak at 286.2 eV is attributed to carbon atoms of C-O-C from epoxy group of ENR-50. Furthermore, several peaks can also be found in the O1s spectum corresponding to O-C at 530.7 eV, and O=S from imide at 532.6 eV. The interaction between oxygen from epoxy group and lithium cation is expected to have occurred at 529.2 eV (Xu, *et al*, 2013). This clarifies the complexation between oxygen and lithium. Table 4.6 shows the binding energies of the peaks observed in C1s and O1s spectra of ENR-50 and (ENR-50)-

EMITFSI added with 10 wt.% of LiTFSI. The peaks at 282.5 eV and 287.5 eV which appears in C1s spectrum may be attributed by moisture, cation or anion from ionic liquid since the peaks are not observed in Figure 4.10 for ionic liquid-free system.

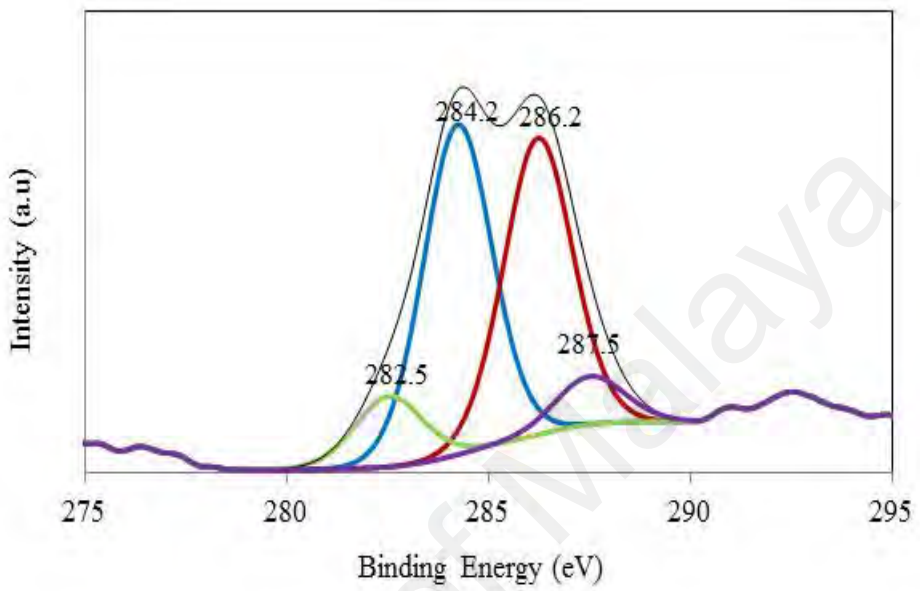


**Figure 4.40:** C1s spectrum for WEEL10

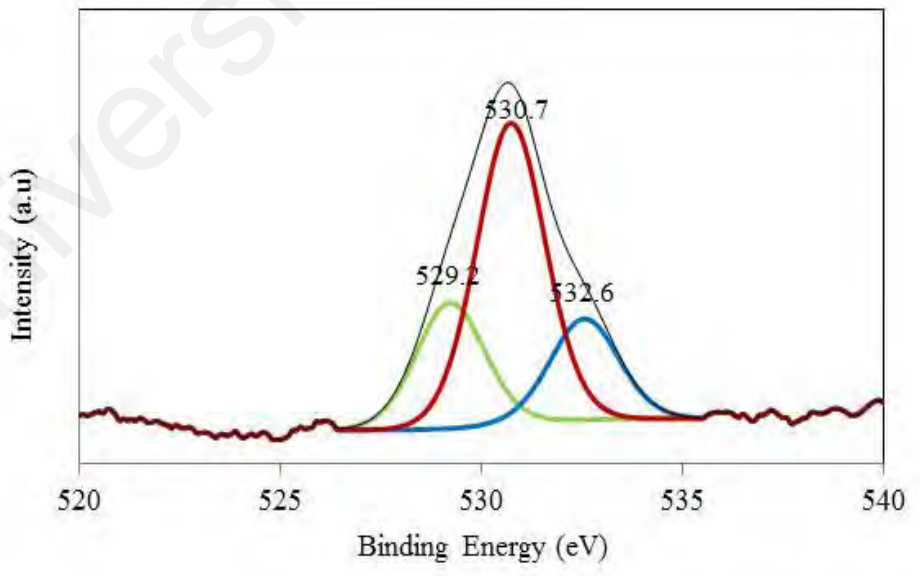


**Figure 4.41**: O1s spectrum for WEEL10

**Table 4.6:** C1s and O1s binding energies for ENR-50 and salted (ENR-50)-EMITFSI

| Spectra | Binding Energy (eV) of ENR-50 | Binding Energy (eV) of WEEL10 | Peaks |
|---|---|---|---|
| C1s | 284.6 | 284.2 | C-C/C-H |
| | 286.5 | 286.2 | C-O-C (epoxy) |
| O1s | 531.0 | 530.7 | O-C |
| | - | 529.2 | Expected for oxygen and lithium |
| | - | 532.6 | O=S |

### 4.3.3 Thermogravimetric Analysis

TGA study was further carried out to examine the thermal properties of ENR-50 containing EMITFSI ionic liquid and lithium salt.

Figure 4.42 presents thermograms of (ENR-50)-EMITFSI and (ENR-50)-EMITFSI-LiTFSI. The first weight loss (~100 °C) is ascribed to the evaporation of solvent or moisture. The ENR-50 containing EMITFSI film starts complete decomposition at ~360 °C. The degradation of salted (ENR-50)-EMITFSI film starts at temperature 1-2 °C lower than the salt-free film. According to An *et al* (2011), the decomposition temperature for EMITFSI is at 358 °C. Kim and Park (2009) reported that the thermal stability of composite electrolytes containing $EMIBF_4$ was ~320 °C. This indicates that the electrolyte system based on ENR-50 containing EMITFSI can give better thermal stability compared to the composite electrolytes containing $EMIBF_4$.

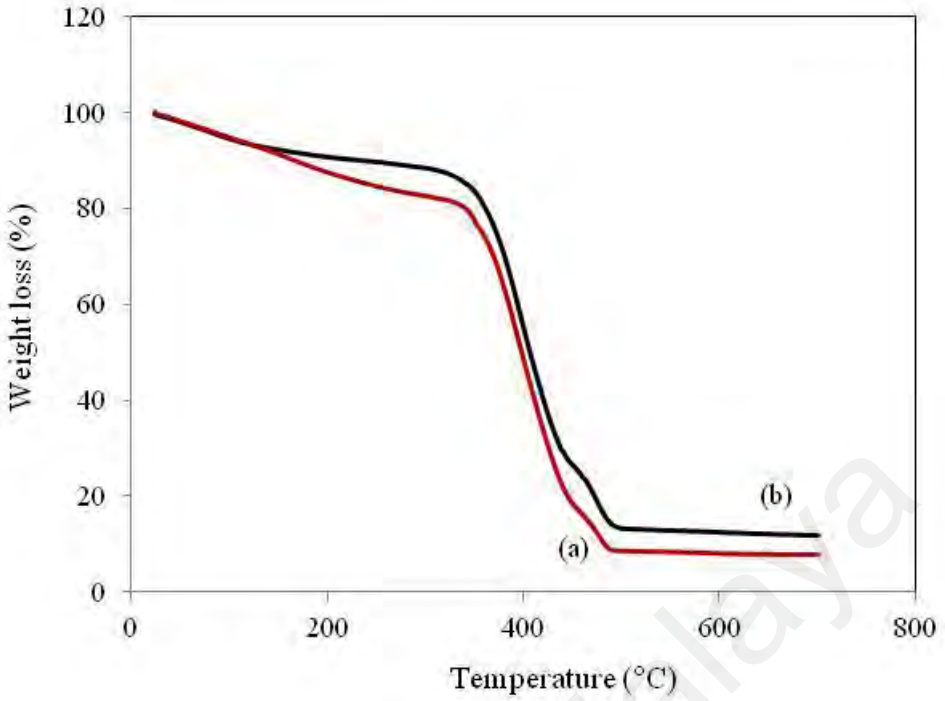


**Figure 4.42:** TG curves for (a) WEEL0 and (b) WEEL10

### 4.3.4 Differential scanning calorimetry

Figures 4.43 (a), (b) and (c) show the DSC thermograms of WEEL0, WEEL10 and WEEL50 respectively. The $T_g$ of (ENR-50)-EMITFSI is -23 °C which is almost similar with ENR-50 film. When added with salt, the glass transition temperatures of the salted films containing EMITFSI are lower than ionic liquid free system at the same amount of LiTFSI.

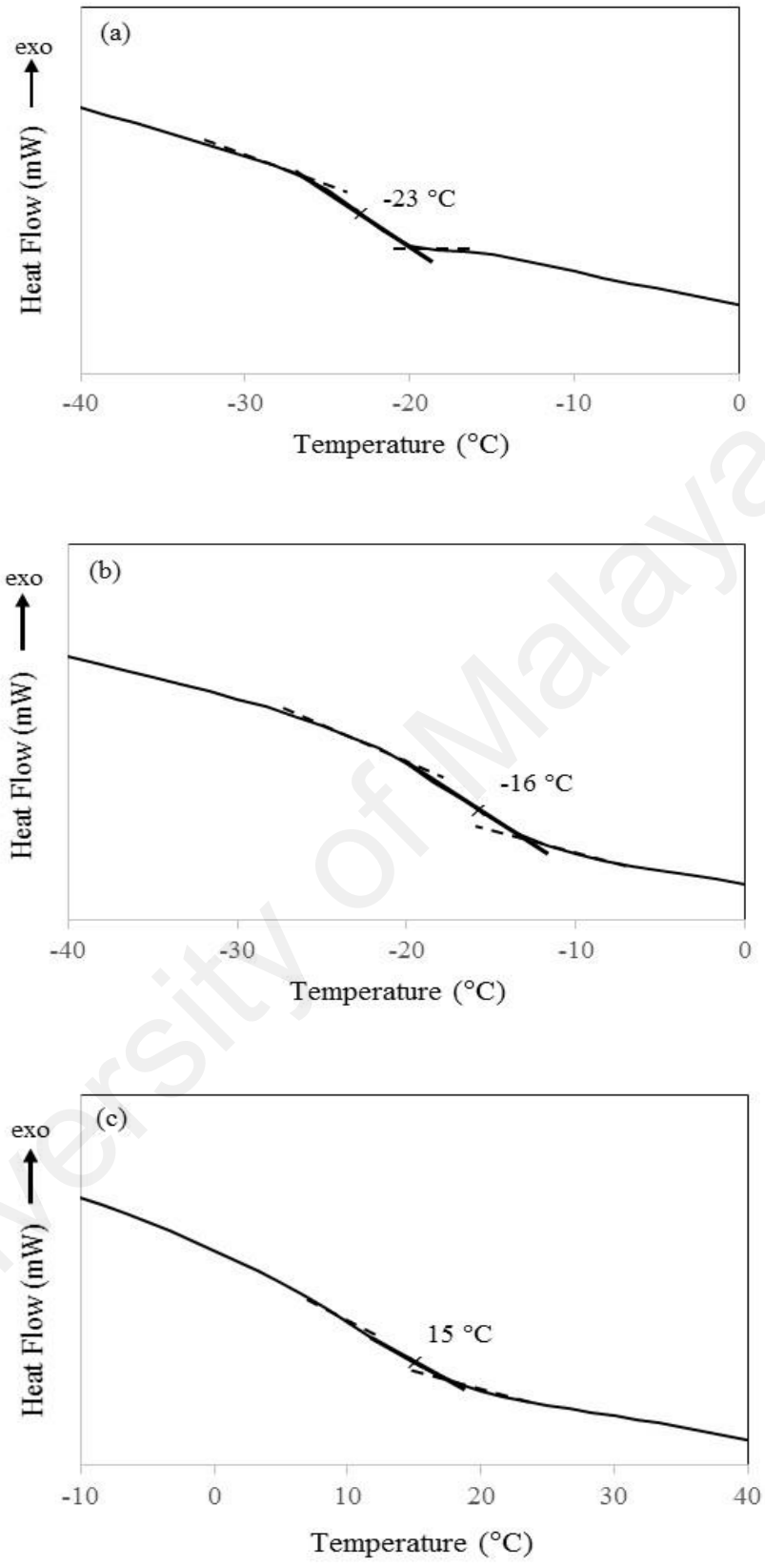


**Figure 4.43:** Glass transition temperature values for (a) WEEL0, (b) WEEL10 and (c) WEEL50

The glass transition temperature of (ENR-50)-EMITFSI-LiTFSI electrolyte system has been plotted against salt content and is shown in Figure 4.44. The increase in salt content resulted increases in the $T_g$. This is mainly due to the ion-dipole interaction of the lithium cation with the oxygen of the epoxy group in ENR-50, which may act as a transient cross-linking. In contrast, EMITFSI which consists of a cation with low Lewis acidity and an anion with low Lewis basicity, has much weaker ion-ion interaction than LiTFSI. The ion-dipole interaction between EMITFSI and ENR-50 appears to be weaker than that between LiTFSI and ENR-50. This consideration is supported by the fact that LiTFSI dissociation is facilitated by the solvation with the polymer matrix, whereas EMITFSI has a self-dissociation property (Noda, *et al*, 2001).

The trend of graph in Figure 4.35 is similar with the trend of graph in Figure 4.29 which shows the role of ionic liquid as plasticizer. EMITFSI also shows the decrease in $T_g$, values when compared with $T_g$ values in graph 4.15 at the same amount of salt content.

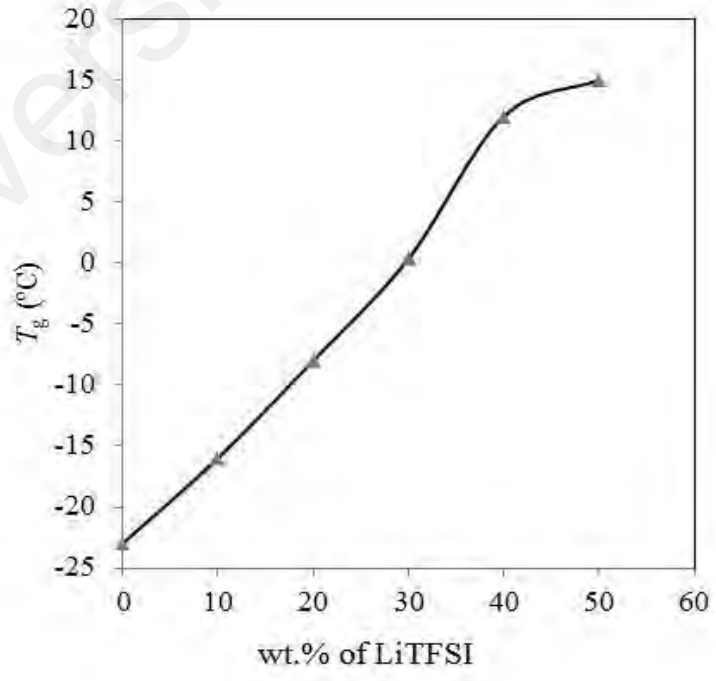


**Figure 4.44:** Graph of $T_g$ against salt content of (ENR-50)-EMITFSI-LiTFSI

### 4.3.5 Ionic Conductivity

Figure 4.45 presents the impedance plot obtained at room temperature for (ENR-50)-EMITFSI at 20 wt.% of LiTFSI. The bulk resistance, $R_b$ is obtained from the graph and the ionic conductivity, σ is calculated from equation (4.1).

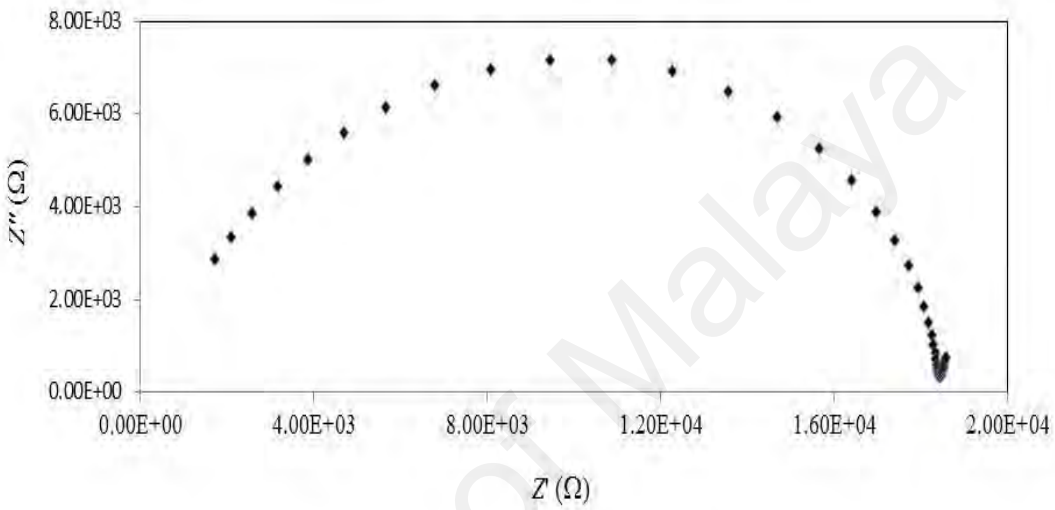


**Figure 4.45:** Impedance plot of WEEL20 at room temperature

Figure 4.46 shows ionic conductivity of (ENR-50)-EMITFSI-LiTFSI plotted against various wt.% of LiTFSI content. As shown in previous section, the ionic conductivity of the polymer itself is very poor (~$10^{-10}$ S $cm^{-1}$). However, the conductivity of ENR-50 increases with addition of EMITFSI ionic liquid (~$10^{-8}$ S $cm^{-1}$). When lithium salt was added to the (ENR-50)-EMITFSI system, the ionic conductivity increases and reaches a value of $3.66 \times 10^{-4}$ S $cm^{-1}$ at 50 wt.% of salt.

Comparing with (ENR-50)-LiTFSI system (Figure 4.17), ionic conductivity for ionic liquid added system is higher up to an order of magnitude. Addition of EMITFSI weakens the interaction within polymer chains, reduces the solvation of Li cations by polymer

matrix and hence promotes the decoupling of ions. In addition, ionic liquid has low viscosity which may help to reduce the viscosity of the electrolyte. Therefore, it provides more voids and free spaces for ion migration and thereby enhances ionic conductivity (Sekhon *et al* 2006).

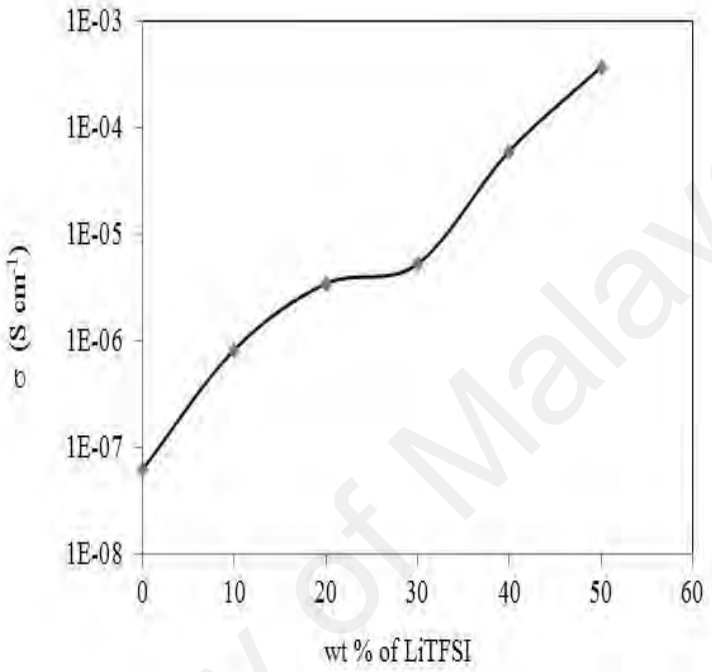


**Figure 4.46:** Ionic conductivity versus salt concentration of (ENR-50)-EMITFSI-LiTFSI

Among the three systems, this electrolyte system shows the highest value of ionic conductivity. The high ionic conductivity of the (ENR-50)-EMITFSI-LiTFSI electrolyte system is mainly attributable to the high ionic conductivity of EMITFSI itself (8.8 mS $cm^{-1}$ at 20 °C and also low viscosity (34 cP) (Galinski *et al*, 2006). In addition, the higher value of conductivity with addition of ionic liquid is probably because of increased number of charge carriers provided by ionic liquid. In pure ionic liquids both cations and anions have been shown to be nearly equally mobile (Lee *et al*, 2005, Tokuda *et al*, 2004).

It can be observed from Figure 4.46 and Figure 4.31, that the (ENR-50)-LiTFSI system containing, EMITFSI shows slightly higher value of ionic conductivity than that from the (ENR-50)-LiTFSI system containing BMITFSI. The difference between these two ionic liquids is the alkyl chain length of cation. The larger the individual molecules/ions, the lower the Coloumbic interactions and thus the less dense they are packed, which in turn results in a lower macroscopic density. Along with decreases in density, the viscosity increases. In other words, the longer alkyl chain length gives bigger cation size, higher molecular weight and viscosity. This eventually leads to a decrease in conductivity (Zhengxi *et al*, 2005).

The temperature dependence of conductivity for (ENR-50)-EMITFSI with different amount of LiTFSI at temperature ranges from 30 – 80 °C is shown in Figure 4.47. The ionic conductivity increases with the increases in temperature. The variation in ionic conductivity with temperature for this system also obeys Vogel-Tamman-Fulcher (VTF) relationship.

The change in ionic conductivity is dominated by the change in ionic mobility, as predicted by the free volume theory (Cohen and Turnbull, 1959). As the temperature increases, local voids are created by the expansion of polymer matrix and thus, polymer segments can move in this free volume. Furthermore, the addition of ionic liquid also helps to decrease the viscosity of the electrolyte. The decrease in viscosity with increasing temperature results in easier ionic transport at higher temperatures. In other words, the decrease in viscosity ($\eta$) with increase in temperature leads to increase in the ionic mobility ($\mu$) of charge carriers of ionic liquid and hence increase in conductivity ($\sigma = \eta q \mu$) (Singh and Sekhon, 2005). The polymer expansion effect is another reason for increase

in ionic conductivity. As temperature increases, the interaction between polymer and Li ion decreases. This facilitates the migration of ions.

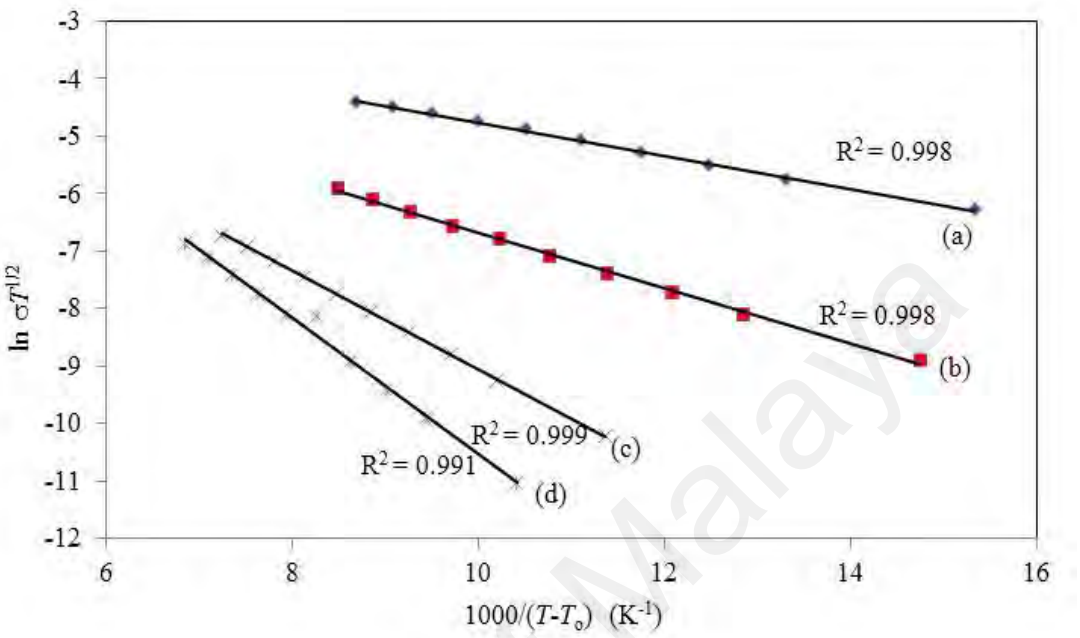


**Figure 4.47:** VTF plot of (a) WEEL50 (b) WEEL40 (c) WEEL20 and (d) WEEL10

From Figure 4.48, the parameter *B* is found to decrease with increasing salt content. The film with 50 wt% of LiTFSI shows the lowest *B* value (2.39 kJ $mol^{-1}$). As discussed earlier, the attractive bond between polymer and salt is weak and requires less energy to break the bond for reorganization and reformation processes. Thus, the lower *B* implies higher mobility of ions and hence the minimum of *B* may imply a maximum segmental motion. In addition, the least energy reveals the highest migration rate of charge carrier. It is also observed that the system with high ionic conductivity implying low conduction activation energy.

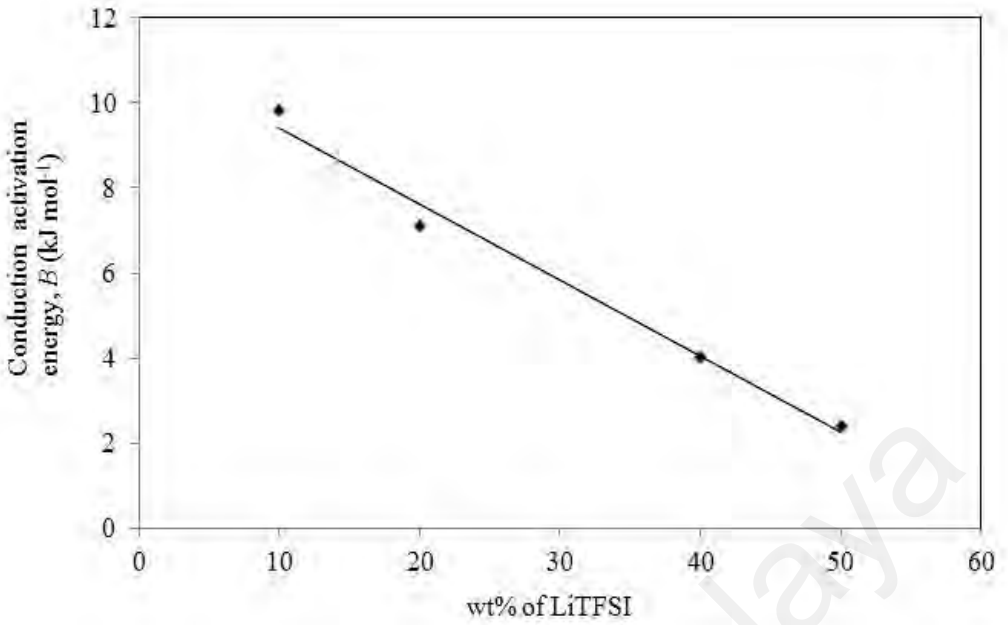


**Figure 4.48:** Conduction activation energy versus salt content for (ENR-50)-EMITFSI-LiTFSI

# CHAPTER 5: EXPERIMENTAL RESULTS (DRY METHOD) AND DISCUSSIONS

## 5.1 System 1: [(ENR-50)-LiTFSI]$_{dry}$

Figure 5.1 presents (ENR-50)-LiTFSI film prepared by dry method. In this method, ENR-50 was mixed with 5 to 20 wt.% of LiTFSI to form (ENR-50)-LiTFSI electrolyte system. The salted ENR-50 mixture is quite hard, thus difficult to form electrolyte film. Therefore, to overcome this matter, a small quantity of ethylene carbonate (EC) was added to the (ENR-50) and LiTFSI mixture purposely to soften the material. The advantage of preparing films using this method is that the film is easier to be peeled off (non-tacky film) compared to the film prepared by wet method. In other words, the films obtained by this method were easy to handle. Moreover, the samples prepared by this method are free from THF. In this method, stable films beyond 20 wt.% LiTFSI could not be prepared, and hence the measurements are limited to the films with salt concentration up to 20 wt.% only.

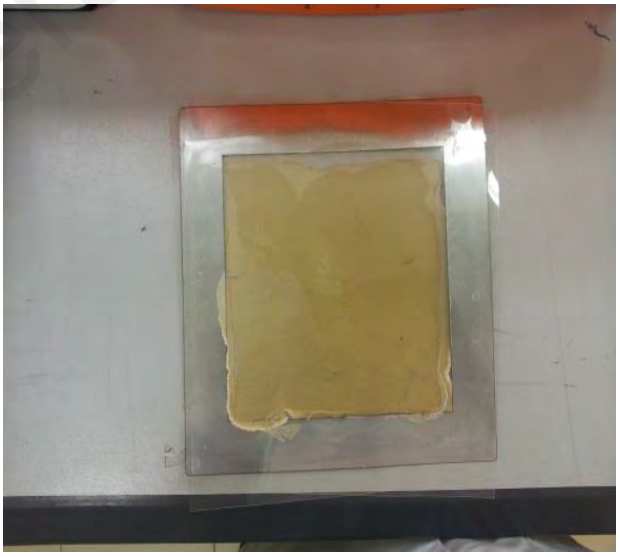

**Figure 5.1:** [(ENR-50)-LiTFSI]$_{dry}$ film

### 5.1.1 Attenuated total reflectance-Fourier transform infrared

ATR-FTIR is an efficient tool to study the local structural changes in polymer electrolytes. The infrared spectra of this system vary according to the salt content and assist in confirming the interaction between the various constituents in the electrolytes. The ATR-FTIR spectrum of $[ENR\text{-}50]_{dry}$ film is shown in Figure 5.2. Again, the focus on this spectrum is the epoxy groups located at 875 and 1251 $cm^{-1}$ which correspond to asymmetrical and symmetrical stretching modes of the epoxide group (Gan and Hamid و 1997(. C-H deformation of $–CH_2-$ and $–CH_3$ are observed at 1449 and 1378 $cm^{-1}$ respectively, whereas the triplet band of C-H stretching modes are observed at 2858, 2918 and 2963 $cm^{-1}$.

Consistent with the results obtained from the wet method presented in Chapter 4, the C-O-C band located at 1251 $cm^{-1}$ disappeared after addition of lithium salt. However, the asymmetrical stretching vibration band of the epoxide group located at 875 $cm^{-1}$ still appears but shifted to lower wavenumbers with increasing salt content as shown in Figure 5.3. Other characteristic bands which are located at 1449 and 1378 $cm^{-1}$ retain their positions. The absence and shifting of bands of epoxy groups show the occurrence of interaction between the polymer and lithium salt.

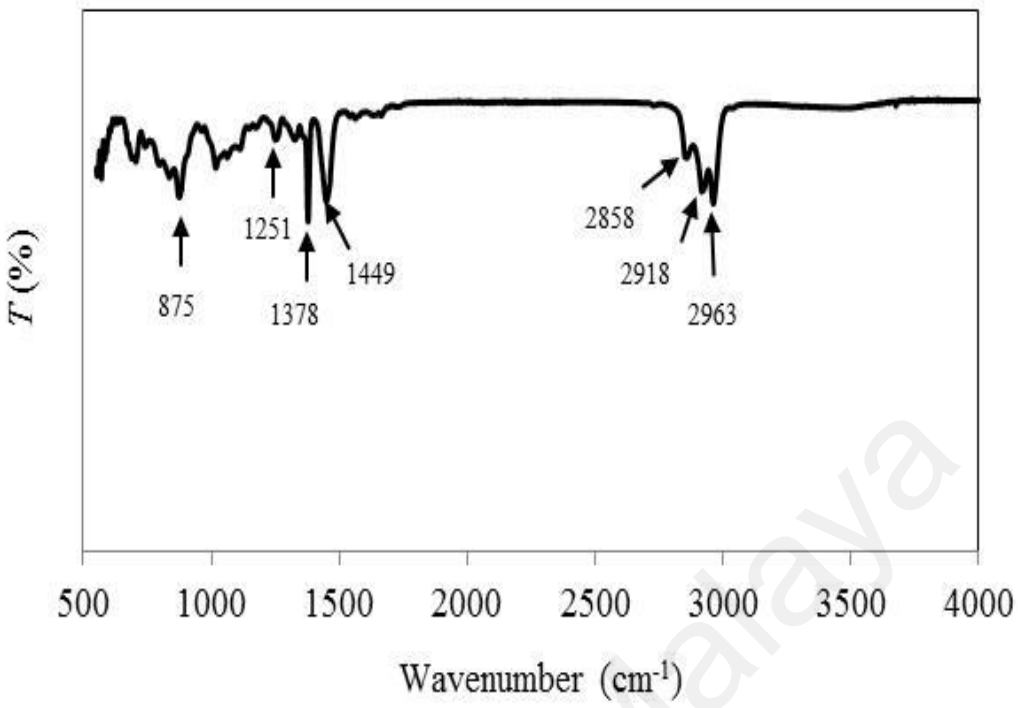


**Figure 5.2:** ATR-FTIR spectrum of DEL0

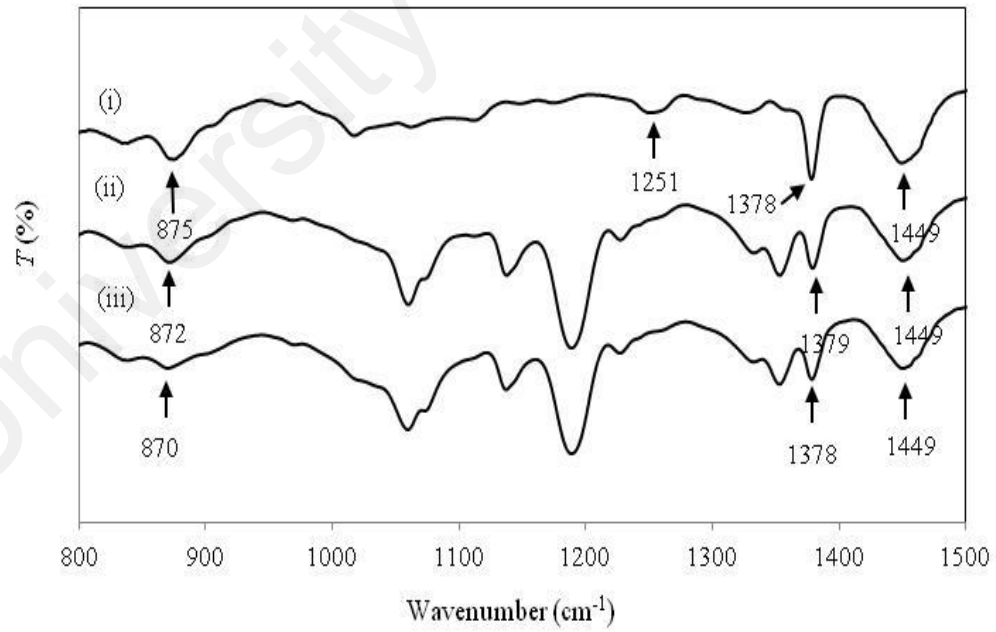


**Figure 5.3:** ATR-FTIR spectra of (i) DEL0, (ii) DEL10 and (iii) DEL20 in the range from 800 to 1500 $cm^{-1}$

### 5.1.2 X-ray photoelectron spectroscopy

Figures 5.4 and 5.5 show the C1s and O1s spectra of DEL0. The strong peak at 284.4 eV is attributed to C-C/C-H bond while the lowest peak at 286.3 eV belong to C-O-C bond as listed in Table 5.1. The O1s spectrum exhibits a dominant peak at 531.4 eV which corresponds to the oxygen and carbon bond of epoxy group from ENR-50.

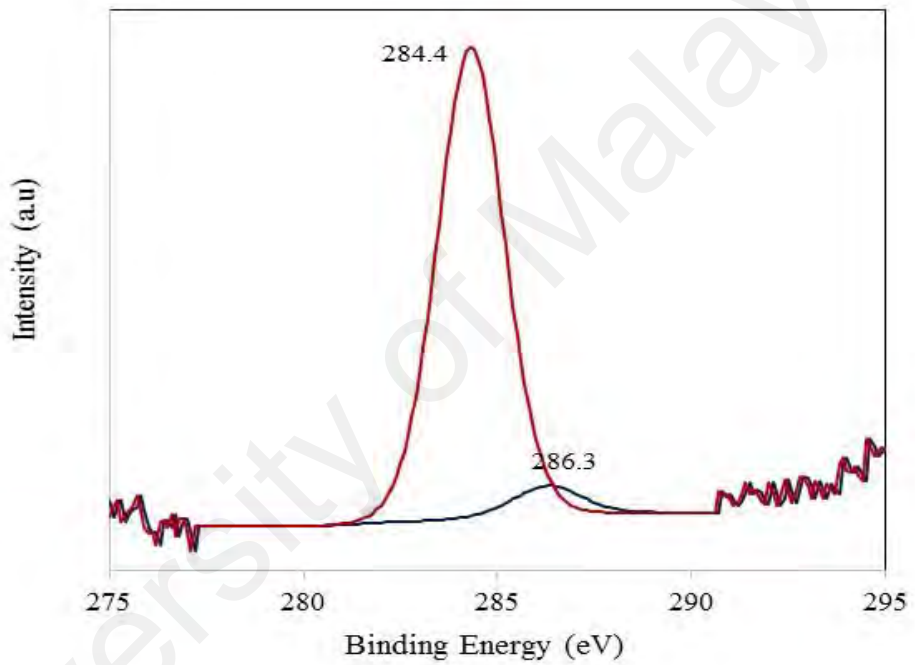


**Figure 5.4:** C1s XPS spectrum for DEL0

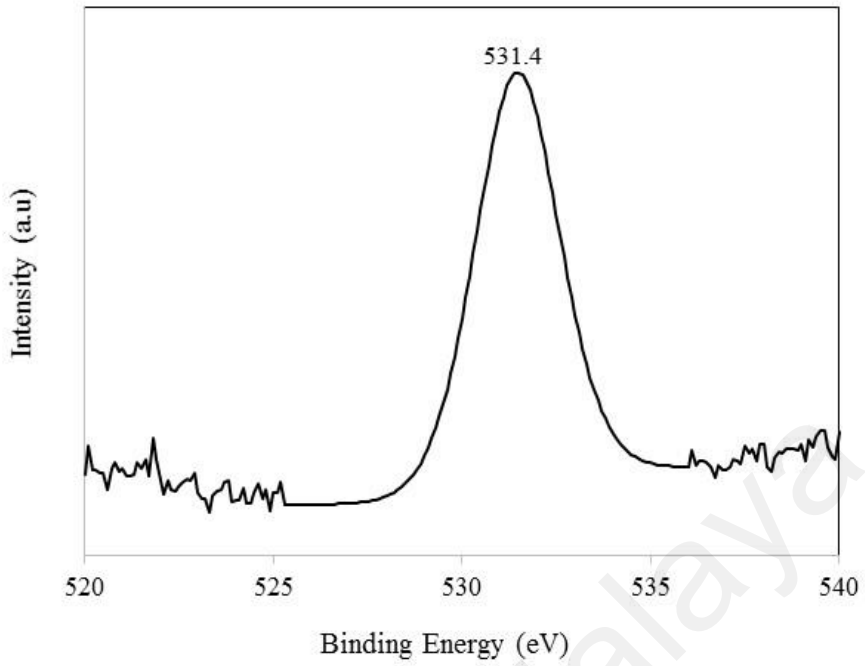


**Figure 5.5**: O1s XPS spectrum for DEL0

**Table 5.1:** C1s and O1s binding energies for $[ENR\text{-}50]_{dry}$

| Spectra | Binding Energy (eV) of DEL0 | Peak (Chemical state) |
|---|---|---|
| C1s | 284.4 | C-C/C-H |
| | 286.3 | C-O-C (epoxy) |
| O1s | 531.4 | O-C |

### 5.1.3 Thermogravimetric Analysis

TGA is a useful technique that has been used to study physical changes encountered by polymer electrolytes during thermal excitation. The technique reveals change in weight attributed to moisture evaporation and degradation of the polymer electrolyte. Figures 5.6 and 5.7 present thermogravimetric responses for the ENR-50 and salted ENR-50 in a temperature range from 30 to 700 °C. From Figure 5.6, the degradation

temperature, $T_d$ of $(ENR\text{-}50)_{dry}$ film starts at ~371 °C which is similar to the $T_d$ of $(ENR\text{-}50)_{wet}$ film. When the lithium salt is added, the thermal stability of the polymer is decreased to ~348 °C. However, this result is consistent with the result obtained for the wet method. Therefore, it can be stated that the thermal stability of (ENR-50)-LiTFSI electrolye materials prepared by both methods show good thermal stability up to 340 °C.

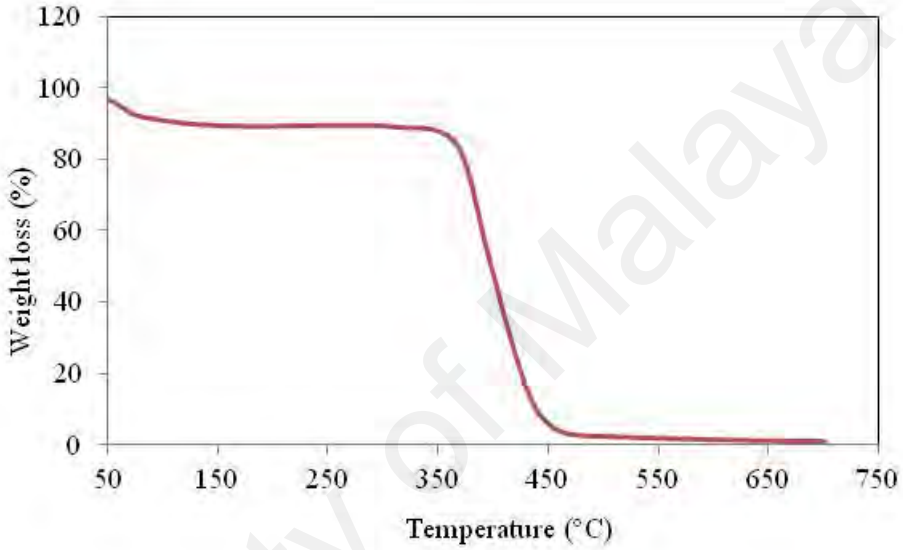


**Figure 5.6:** TGA thermogram of $(ENR\text{-}50)_{dry}$ film

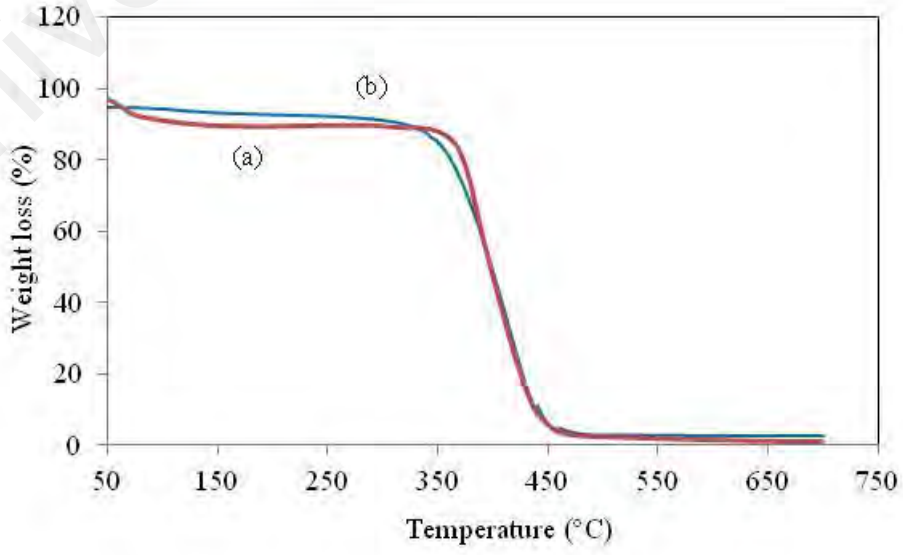


**Figure 5.7:** TGA thermograms of (a) DEL0 and (b) DEL20

### 5.1.4 Differential scanning calorimetry

Figures 5.8 and 5.9 present DSC traces of ENR-50 film and salted ENR-50 films prepared by dry method. The glass transition temperature, $T_g$ of DEL0 is occurred at -18 °C. The $T_g$ obtained from this method is relatively higher compared with the $T_g$ obtained for the ENR-50 film prepared by solution casting method (wet method). This indicates that the solvent used in wet method softened the material thus reduces the glass transition temperature.

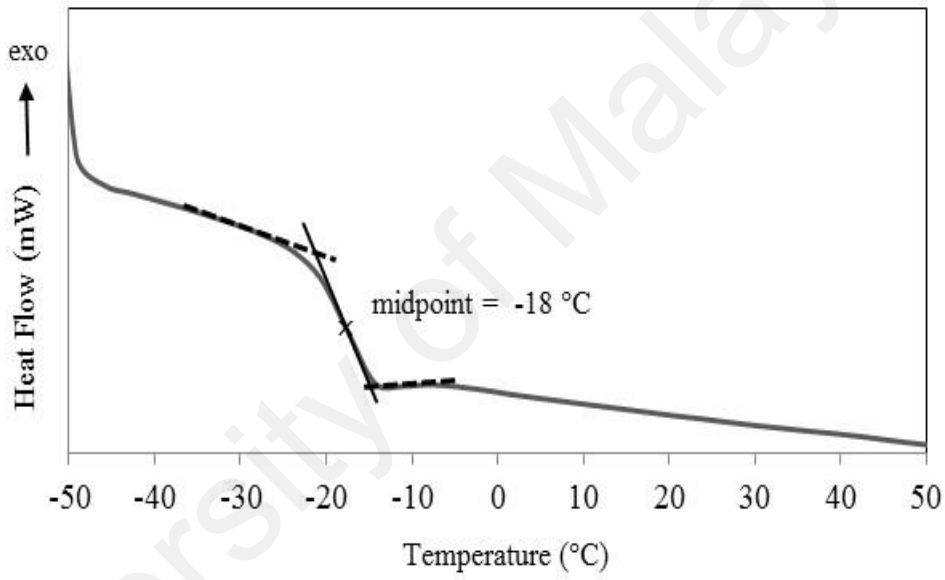


**Figure 5.8:** DSC trace of $[ENR\text{-}50]_{dry}$ film

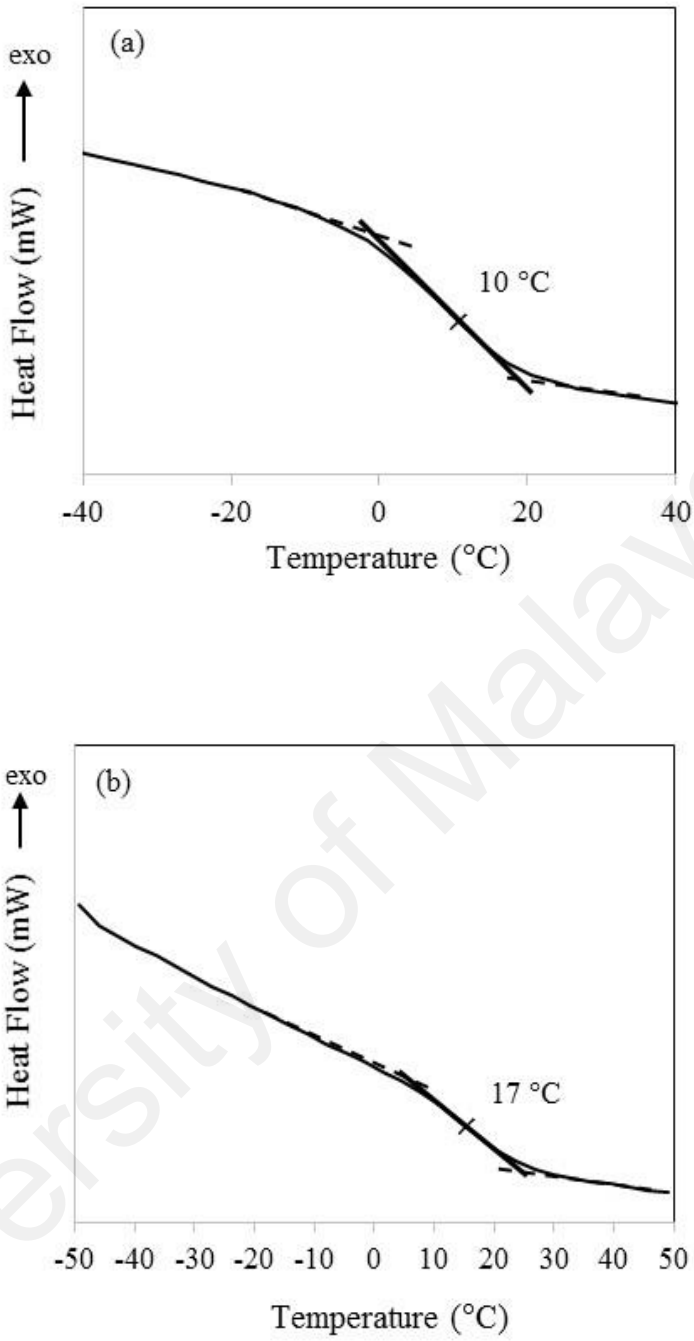


**Figure 5.9:** Glass transition temperature of (a) DEL10 and (b) DEL15

Figure 5.10 shows the glass transition temperature for $[(ENR\text{-}50)\text{-}LiTFSI]_{dry}$ system at various salt content. It is observed that the $T_g$ increases with increasing salt content. This is consistent with the previous work in wet method, which indicates that the solvation of the lithium cation by the polymer arrests the local motion of the polymer segment through the formation of transient cross-links (Hou *et al* (2003); Kim *et al* (2003)).

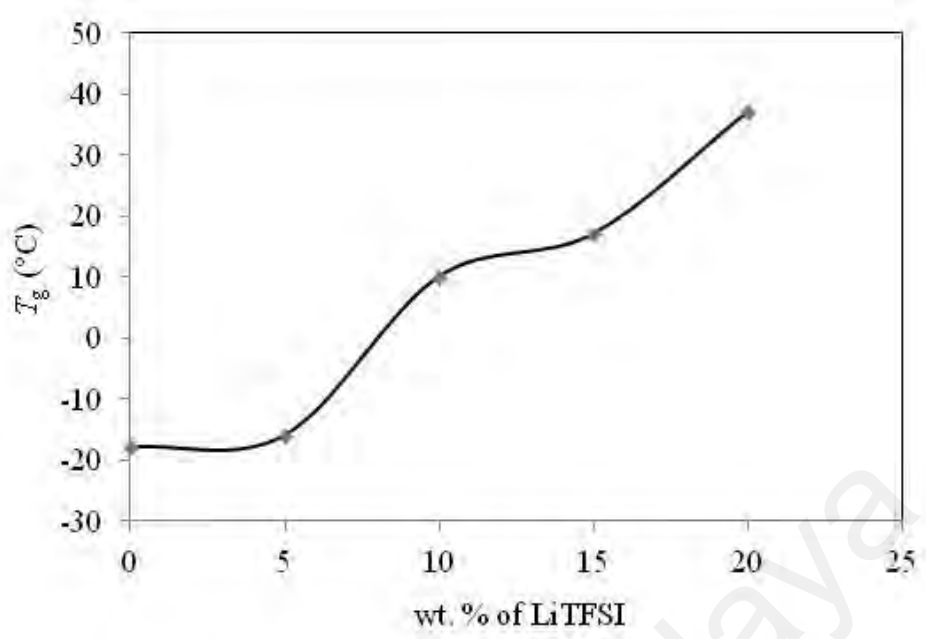


**Figure 5.10:** Glass transition temperatures for $[(ENR\text{-}50)\text{-}LiTFSI]_{dry}$ at different salt content

### 5.1.5 Ionic conductivity

$[(ENR\text{-}50)\text{-}LiTFSI]_{dry}$ electrolyte system was also subjected to impedance spectroscopy to determine the ionic conductivity value. A typical Cole-Cole plot for the electrolyte system is shown in Figure 5.11. The ionic conductivity value was calculated using equation 4.1.

The variation of ionic conductivity of $[(ENR\text{-}50)\text{-}LiTFSI]_{dry}$ with salt content is displayed in Figure 5.12. The ionic conductivity of the system increased by an order of magnitude after addition of 5 wt.% of lithium salt. The increase in ionic conductivity with salt content in this method is not coupled with the glass transition temperature result which shows a decrease in flexibility of polymer chains with increase in salt content. Thus, the increase in ionic conductivity with increase of salt content is due to the increment of the number of charge carriers. However, upon addition of lithium salt, it can be seen that there is a gradual increase in ionic conductivity. As the salt content

increases, there is also an increase in the number of ions. Nevertheless, in this case not all ions contributed to conductivity due to the formation of ion pairs or ion clusters which restricted the mobility of charge carriers in the polymer matrix resulting in low ionic conductivity compared with the result obtained in wet method. Furthermore, the high value of $T_g$ restricted the movement of the polymer, hence reduced the mobility of ions.

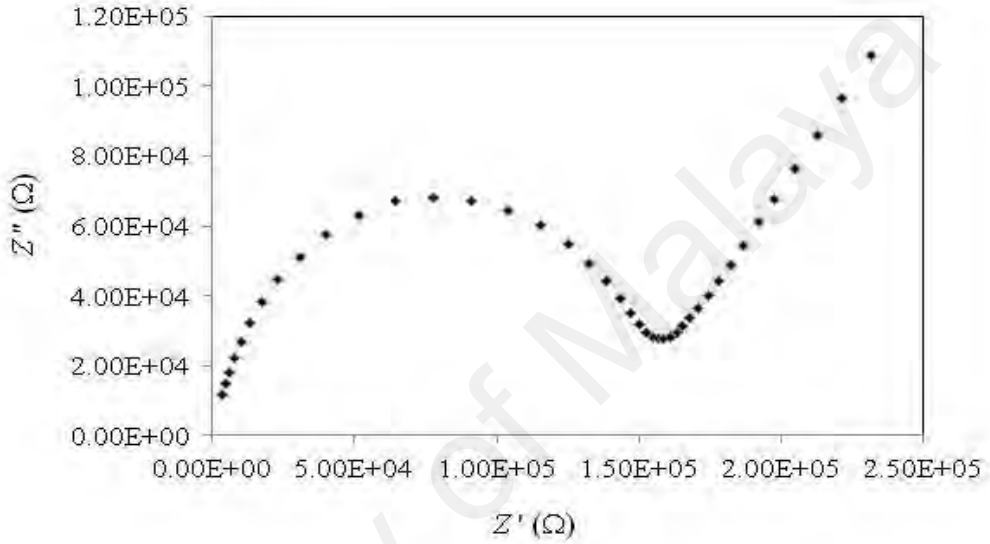


**Figure 5.11:** Cole-Cole plot for DEL20 at ambient temperature

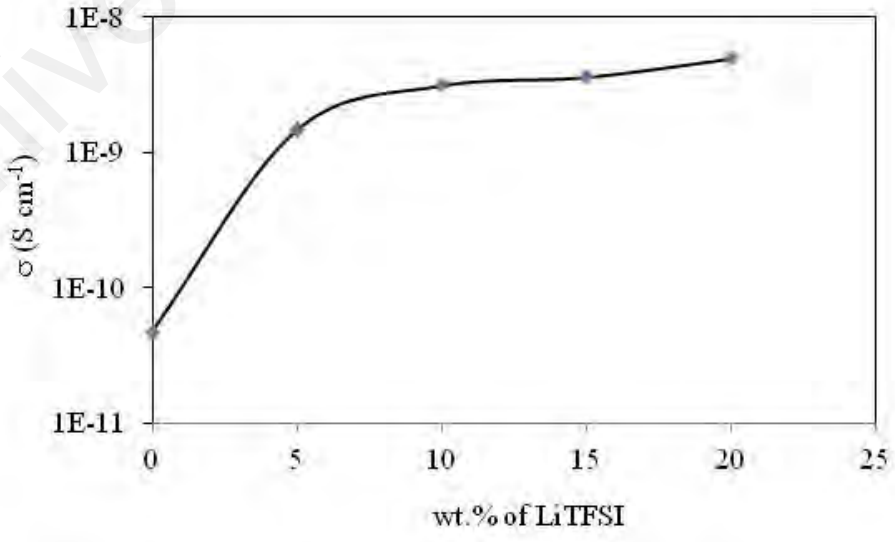


**Figure 5.12:** Ionic conductivity versus salt content of $[(ENR\text{-}50)\text{-}LiTFSI]_{dry}$ electrolyte system at ambient temperature

The temperature dependence of ionic conductivity of the $[(ENR\text{-}50)\text{-}LiTFSI]_{dry}$ system has been studied in the temperature range from 40 °C to 100 °C. Figure 5.13 shows the temperature dependence of conductivity which obeys the VTF relationship in this temperature range. From this Figure, it can be seen that as temperature increases, the conductivity also increases. This is closely related to the polymer chain mobility which induced ion mobility, thus enhanced the ionic conductivity. Furthermore, as temperature increases the viscosity of the material is also expected to decreases.

Conduction activation energy, *B* of the materials was calculated using the VTF relation (equation 4.2). For the highest conducting sample, which is at 20 wt.% of lithium salt, the *B* value is the smallest (3.84 kJ $mol^{-1}$), whereas, for the sample with 5 wt.% of lithium salt, the *B* value is the largest (7.41 kJ $mol^{-1}$). This is in agreement with the ionic conductivity results which show that at 20 wt. % of lithium salt gives the highest ionic conductivity value. The small value of *B* implies high migration rate of charge carriers.

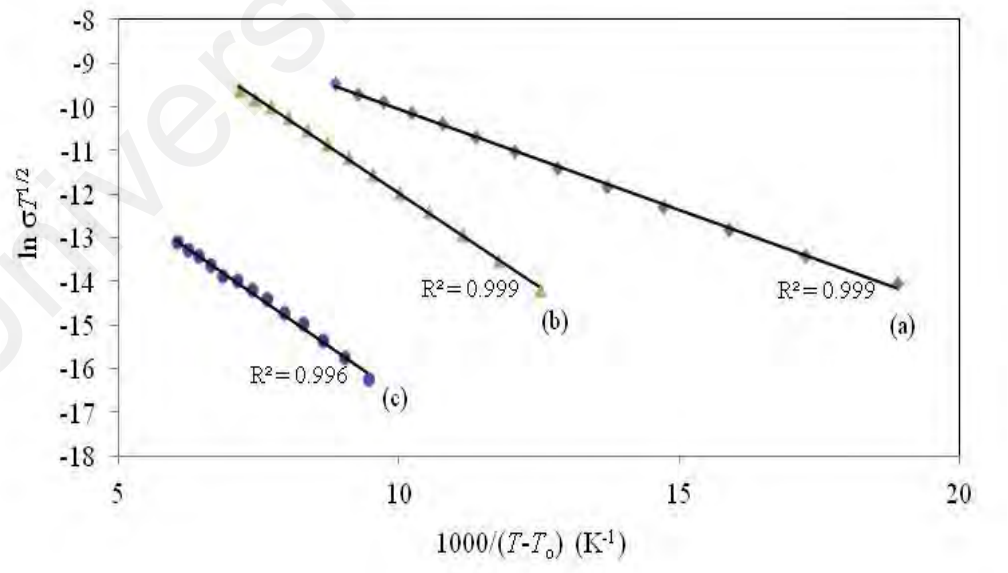


**Figure 5.13:** VTF plots of (a) DEL20 (b) DEL10 and (c) DEL5

## 5.2 System 2: [(ENR-50)-BMITFSI-LiTFSI]$_{dry}$

In this system, the effect of ionic liquid, 1-butyl-3-methylimidazolium bis(trifluoromethanesulfonyl)imide (BMITFSI) was studied mainly to enhance the ionic conductivity and thermal stability of the salted ENR-50 system. Figure 5.14 shows (ENR-50)-BMITFSI-LiTFSI electrolyte film prepared by dry method. The film is quite translucent compared to the ionic liquid – free film.

**Figure 5.14:** [(ENR-50)-BMITFSI-LiTFSI]$_{dry}$ film

### 5.2.1 Attenuated total reflectance-Fourier transform infrared

ATR-FTIR is one of the experimental techniques used to determine the interaction between constituents of a material. In this study, the interactions between polymer, ionic liquid and lithium salt were studied. The ATR-FTIR spectra of [(ENR-50)-BMITFSI-LiTFSI]$_{dry}$ electrolytes in selected regions are shown in Figures 5.15 and 5.16.

As mentioned in Section 5.1.1, the C-O-C vibrations of ENR-50 appear at 875 and 1251 cm$^{-1}$. From Figure 5.15, an asymmetrical stretching vibration band at 875 cm$^{-1}$ appears at a lower wavenumber which indicates weak interaction between polymer and ions. This promotes free ions for ionic transport.. However, the symmetrical stretching

vibration band at 1251 $cm^{-1}$ disappeared after addition of ionic liquid and lithium salt. This is consistent with the ATR-FTIR result obtained in the wet method. When the ionic liquid and lithium salt are mixed with the polymer, there are possibilities that the imidazolium cation ($BMI^+$) of the ionic liquid and lithium cation ($Li^+$) to interact with the epoxy groups of ENR-50 while the other structural units of ENR-50 may not be affected. These epoxy groups are most likely to form bond or complex with ionic liquid cation and lithium cation.

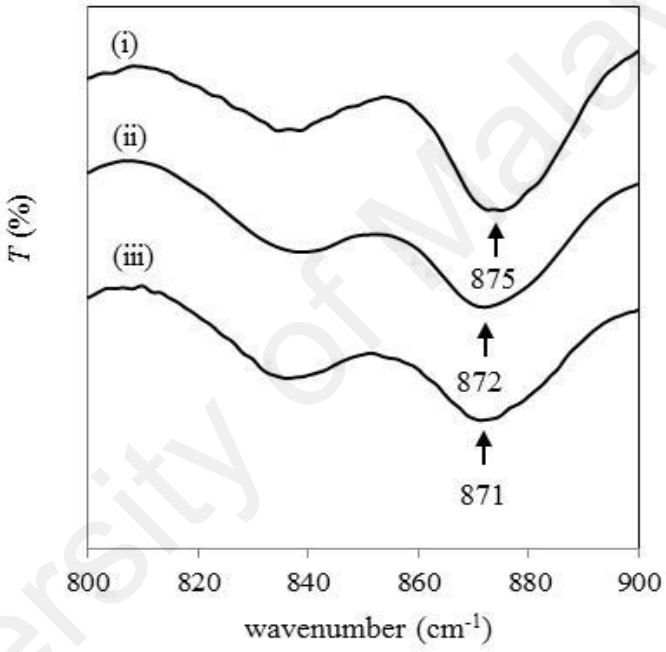


**Figure 5.15:** ATR-FTIR spectra of (i) DEL0, (ii) DEBL5 and (iii) DEBL10 in the range from 800 to 900 $cm^{-1}$

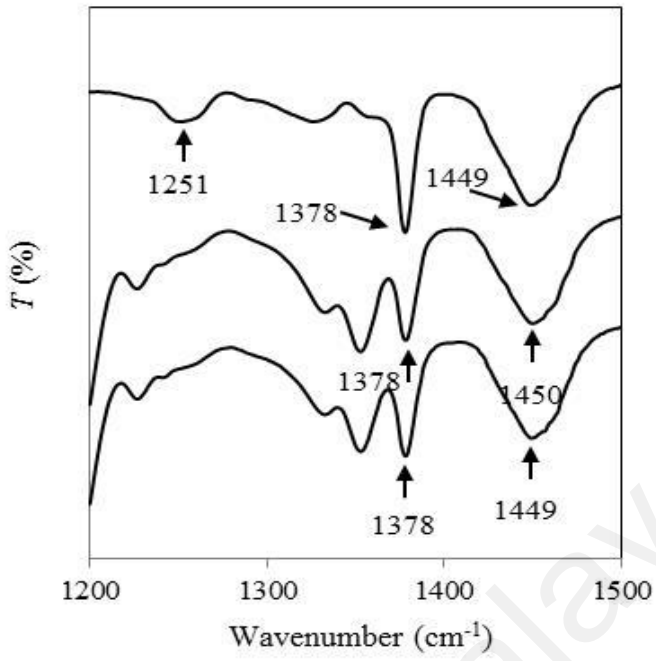


**Figure 5.16**: ATR-FTIR spectra of (i) DEL0, (ii) DEBL5 and (iii) DEBL10 in the range from 1200 to 1500 $cm^{-1}$

### 5.2.2 X-ray photoelectron spectroscopy

The C1s and O1s photoelectron peaks obtained from XPS technique for DEBL0 are shown in Figures 5.17 and 5.18 respectively. The C1s spectrum displays a sharp dominant peak at 284.7 eV due to C-C and/or C-H bonds. The second peak observed at 286.8 eV, which is lower than the first peak, is attributed to the carbon and oxygen bonding from the epoxy group of ENR-50. The carbon and oxygen bonding are also observed in O1s spectrum in Figure 5.18 at 531.3 eV. With addition of ionic liquid, the peak retains its position (compare to DEL0) but reduces in intensity. The decreased intensity is probably due to the interaction between the polymer and ionic liquid. The emission of a new peak which is found at 533.1 eV is related to TFSI anion of the ionic liquid. Table 5.2 lists the binding energies of the corresponding peaks of DEL0 and DEBL0.

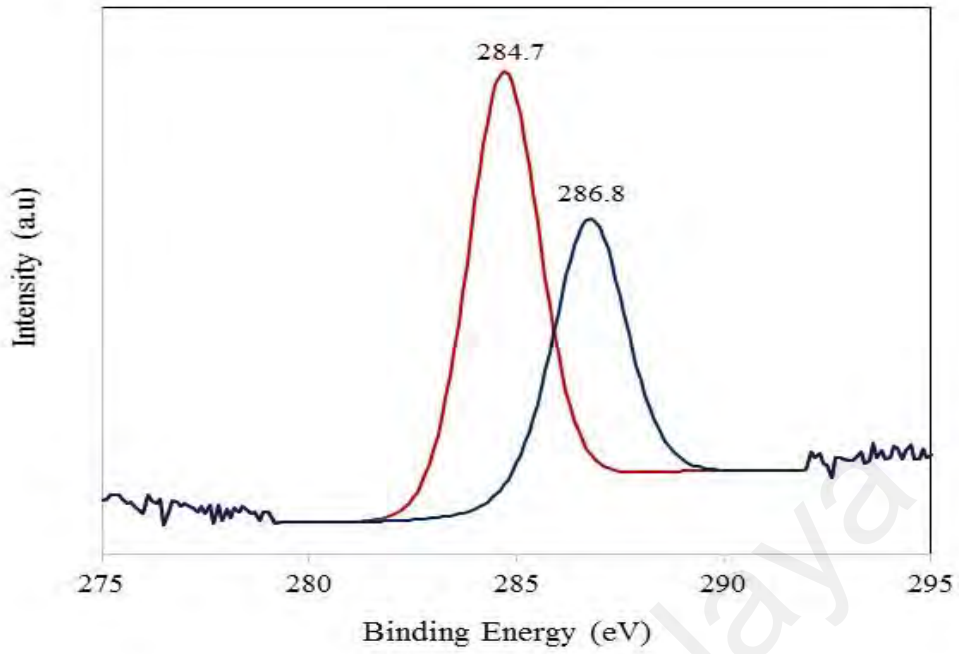


**Figure 5.17:** C1s XPS spectrum for DEBL0

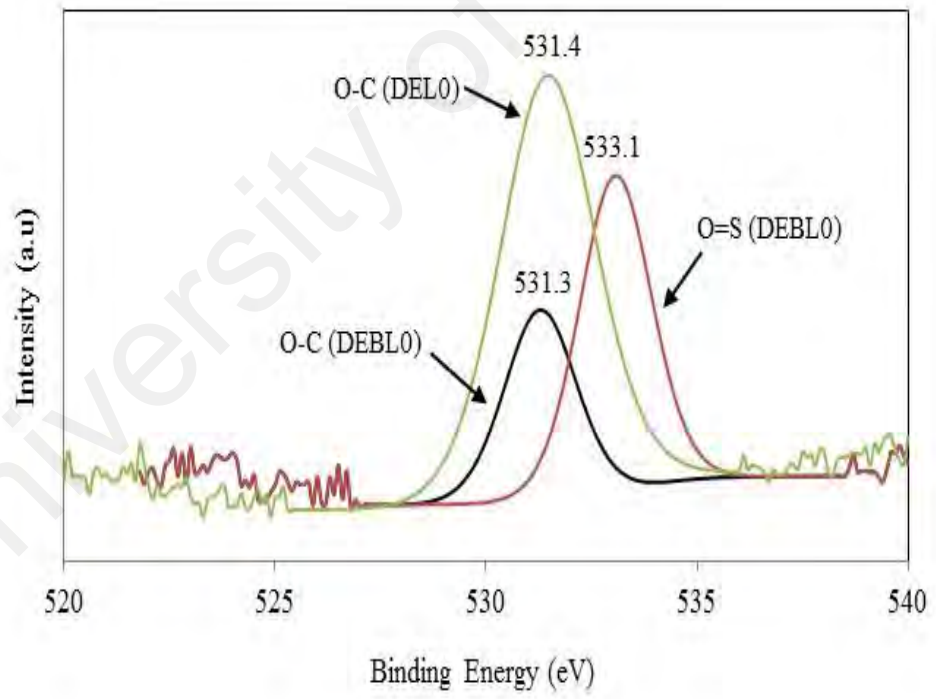


**Figure 5.18**: O1s XPS spectra for DEL0 and DEBL0

**Table 5.2:** C1s and O1s binding energies for $[ENR\text{-}50]_{dry}$ and $[(ENR\text{-}50)\text{-}BMITFSI]_{dry}$

| Spectra | Binding Energy (eV) of DEL0 | Binding Energy (eV) of DEBL0 | Peaks |
|---|---|---|---|
| C1s | 284.4 | 284.7 | C-C/C-H |
| | 286.3 | 286.8 | C-O-C (epoxy) |
| O1s | 531.4 | 531.3 | O-C |
| | - | 533.1 | O=S |

### 5.2.3 Thermogravimetric analysis

The thermal stability of the electrolyte films containing ionic liquid which were prepared by dry method was also studied using TGA over a temperature range from 30 to 700 °C. Figure 5.19 shows that the decomposition temperature for both samples are higher than 360 ºC.

Comparing to Figure 5.7, the degradation of salted film without ionic liquid is lower than the film containing ionic liquid. This result shows that the presence of ionic liquid enhances the thermal stability of the electrolyte film up to more than 10 °C.

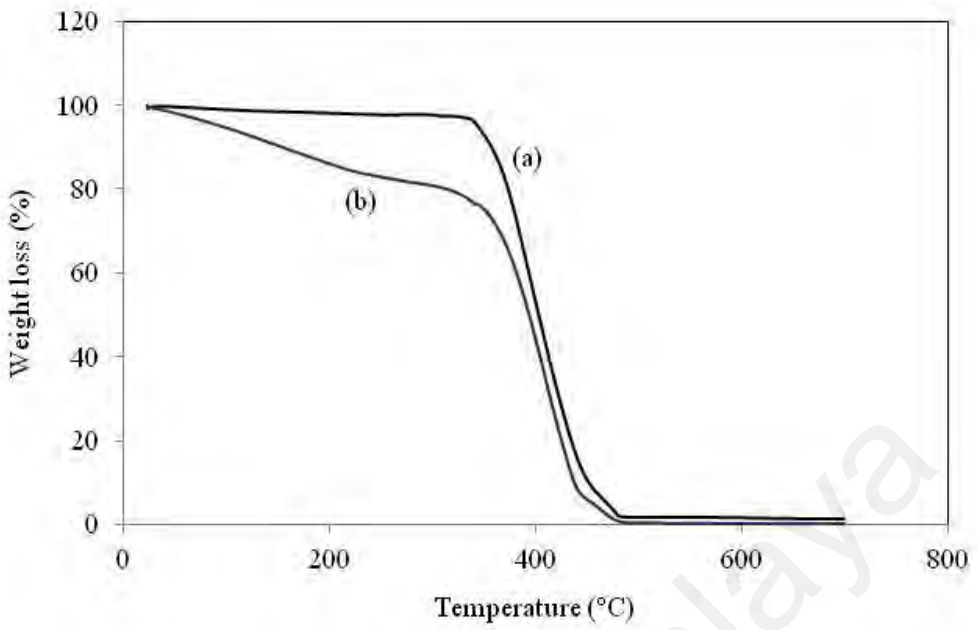


**Figure 5.19:** TGA thermograms of (a) DEBL0 and (b) DEBL10

### 5.2.4 Differential scanning calorimetry

DSC measurement has been performed for (ENR-50)-BMITFSI system with and without the lithium salt. The $T_g$ of (ENR-50)-BMITFSI system without lithium salt is -25 °C. This value is lower than the $T_g$ obtained from pure ENR-50 prepared by the same method. Therefore, it can be stated that the addition of ionic liquid reduces the glass transition temperature of pure ENR-50. This result is also consistent with the wet method's result. Figures 5.20 (a) and (b) depict the glass transition temperature values for the salted system of $[(\text{ENR-50})\text{-BMITFSI}]_{dry}$.

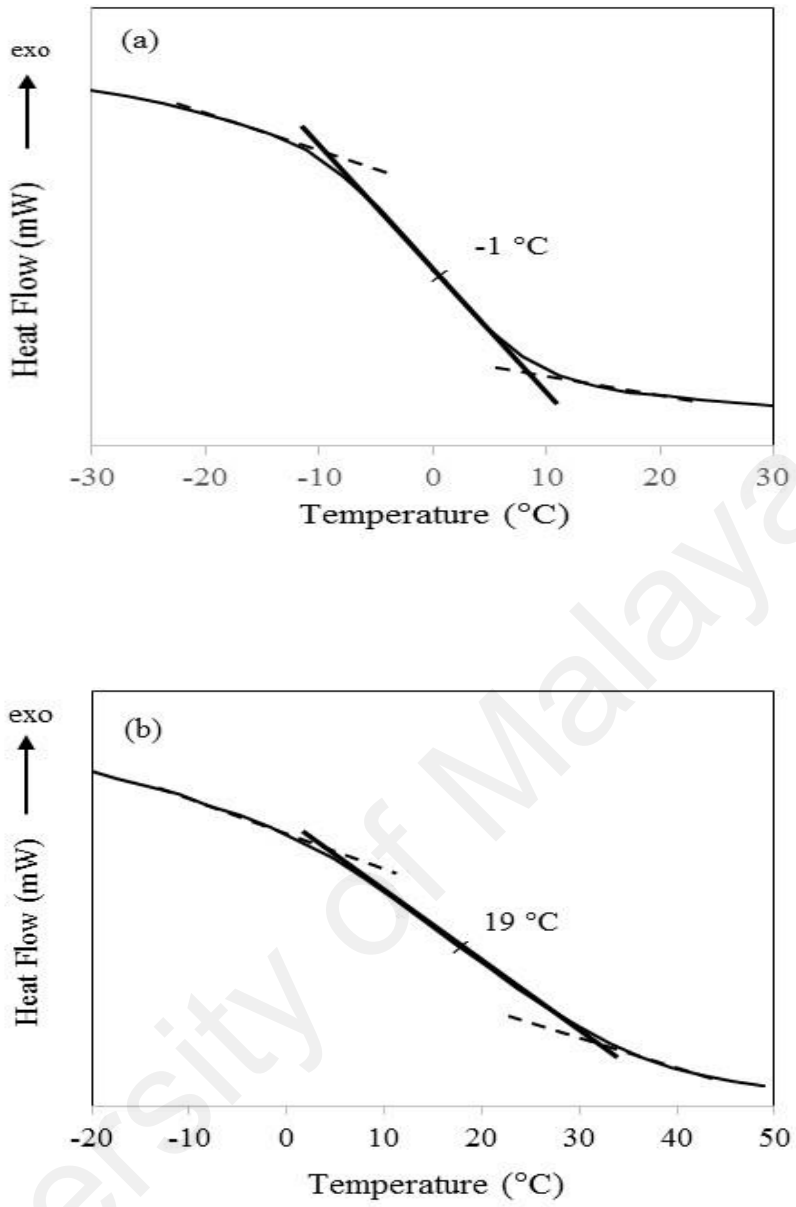


**Figure 5.20:** Glass transition temperature of (a) DEBL10 and (b) DEBL20

Figure 5.21 depicts the variation of $T_g$ with wt. % of lithium salt. The $T_g$ increases with increasing salt content which reflected the presence of cosslinking effect that effectively reduces the chain segmental motion (Hou *et al* (2003) and Kim *et al* (2003)). However, the $T_g$ values obtained from this system are lower compared to the $T_g$ values obtained from ionic liquid - free system. This indicates that the ionic liquid in this system plays a role as plasticizer which improves the segmental mobility of the polymer chain.

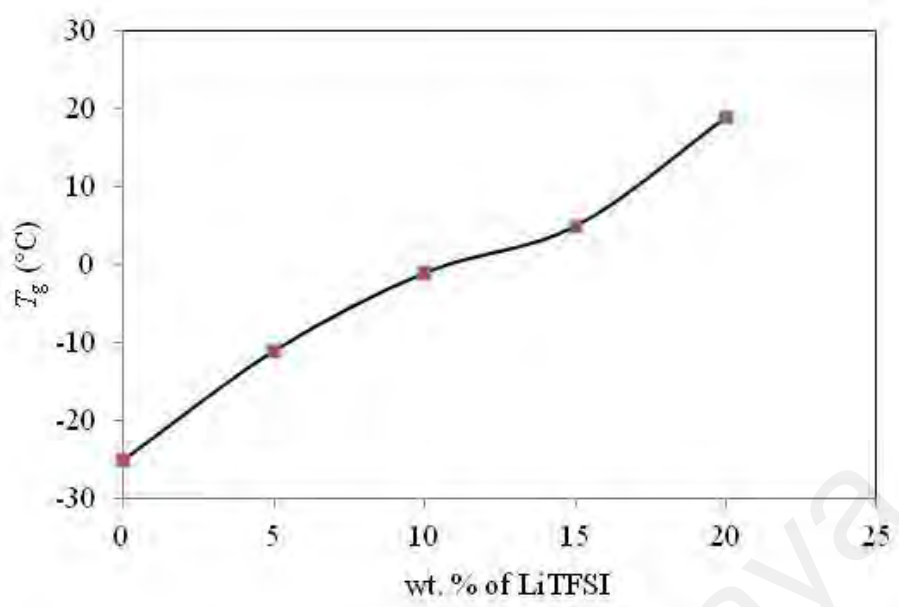


**Figure 5.21:** Graph $T_g$ against salt concentration of $[(ENR\text{-}50)\text{-}BMITFSI\text{-}LiTFSI]_{dry}$ system

### 5.2.5 Ionic Conductivity

Figure 5.22 shows the ionic conductivity against lithium salt content at ambient temperature. The conductivity increases after addition of salt and reaches conductivity value of ~$10^{-7}$ S $cm^{-1}$ at 20 wt.% of LiTFSI. This conductivity value is higher than ionic liquid-free system value at the same amount of LiTFSI. The increase in $T_g$ does not affect the ionic conductivity values. As such, the increase in conductivity could be related to the increasing number of carrier ions (which is usually contributed by lithium cations). Furthermore, the enhancement of ionic conductivity with addition of ionic liquid is also attributed to enhancement of free ions provided by ionic liquid (Singh *et al,* 2009). This is due to high self-dissociating and ion-transporting abilities of the BMITFSI ionic liquid.

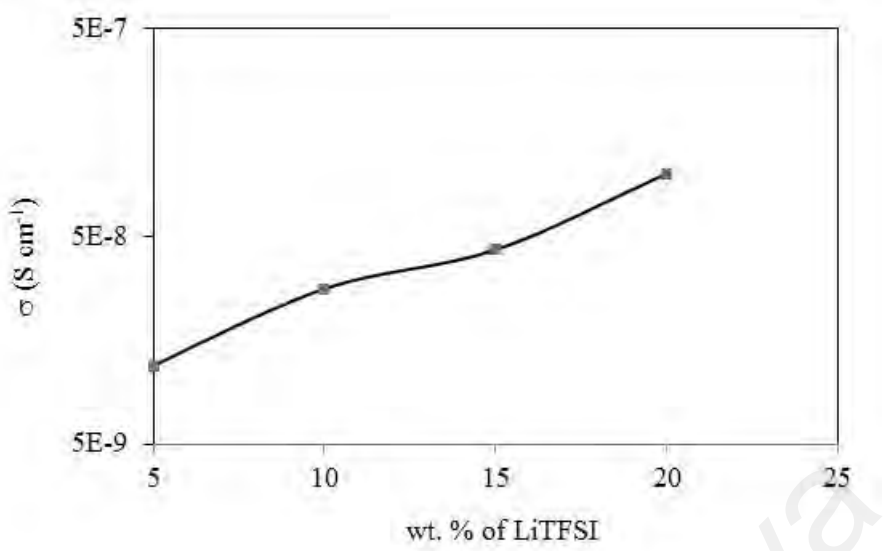


**Figure 5.22:** Ionic conductivity versus salt content of $[(ENR\text{-}50)\text{-}BMITFSI\text{-}LiTFSI]_{dry}$ electrolyte system at ambient temperature

The variation of ionic conductivities with temperature for $[(ENR\text{-}50)\text{-}BMITFSI]_{dry}$ and $[(ENR\text{-}50)\text{-}BMITFSI\text{-}LiTFSI]_{dry}$ are presented in Figure 5.23. It can be seen that the ionic conductivities increase with temperatures and follow the VTF relation suggesting that the ion transportation is coupled with the polymer segmental motion. Generally, such a close correspondence with the VTF equation implies that the ion conduction can be explained in terms of free volume theory (Cohen & Turnbull, 1959). From Figure 5.23, the ionic conductivity of DEBL20 film is the highest among films measured in the same temperature range. The conductivity increases up to two orders of magnitude as the temperature increases (from 40 °C to 100 °C). The conduction activation energy, *B* for all samples fall within 4.6 to 9.9 kJ $mol^{-1}$ with the lowest *B* value corresponds to the film that gives high ionic conductivity value (Figure 5.22). The ionic conductivity of DEBL20 increases up to two order of magnitude when the temperature reached 100 °C. This shows that at higher temperatures, thermal movement of polymer chain segments and the dissociation of salts improved, which increases the ionic conductivity.

Referring to the wet method system, the measurement for ionic conductivity at elevated temperature has been done only up to 80 °C. Conductivity for temperature exceed 80 °C could not be performed due to the instability of the film. However, for dry method system, the measurement has been done at temperature above 80 °C. This shows that this system is suitable for elevated temperature application since it shows high conductivity at high temperature. Furthermore, the system is also stable at high temperature as shown in TGA result.

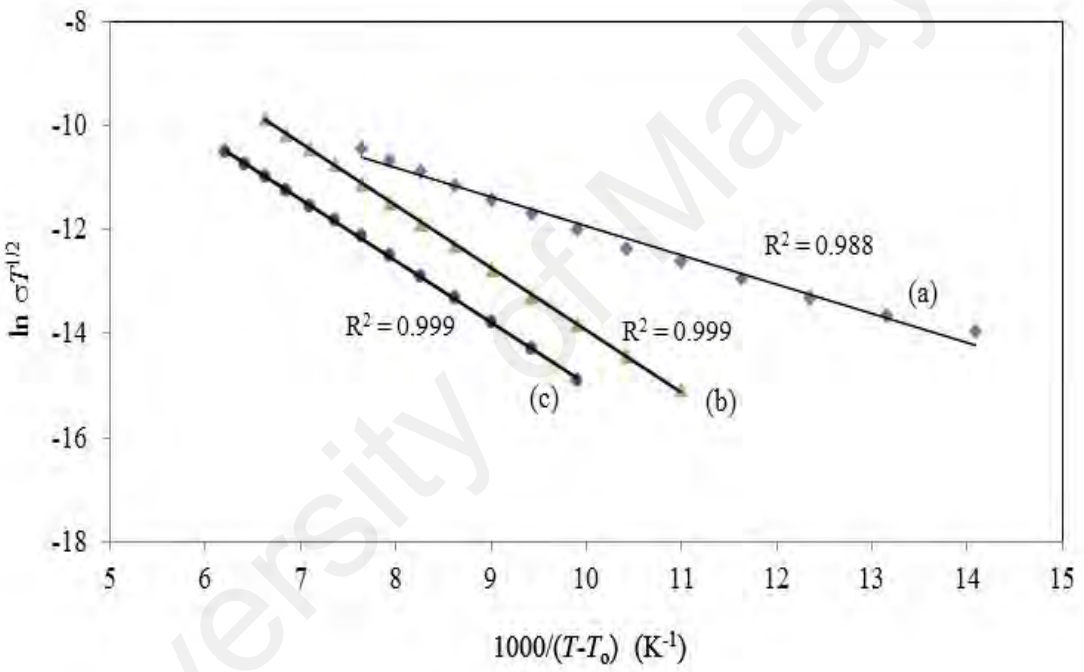


**Figure 5.23:** VTF plots of (a) DEBL20 (b) DEBL10 and (c) DEBL5

# CHAPTER 6: CONCLUSION

## 6.1 Conclusion

The effect of ionic liquid on the thermal properties and ionic conductivity of the electrolyte system based on epoxidized natural rubber 50 added with lithium salt were studied. The results obtained from this research work demonstrated the advantages of the ionic liquid in enhancing the thermal properties and ionic conductivity of the electrolyte materials.

From the ATR-FTIR analysis of both methods, the interactions between ENR-50 with ionic liquid and lithium salt were confirmed by the changes of the vibrational modes of selected bands. The disappearance of C-O-C band at 1255 $cm^{-1}$ (for wet method) and at 1251 $cm^{-1}$ (for dry method) gave an indication that this epoxy group has interacted with ionic liquid and lithium salt. The epoxy group of ENR-50 provided coordination site with Li cation or/and ionic liquid cation/anion to promote ionic conductivity.

The interactions between the epoxy group with ionic liquid and lithium salt were also confirmed by XPS analysis which showed the existence of new peaks after addition of ionic liquid and lithium salt.

It was observed, from both methods, that the decomposition temperatures of the electrolyte films increased after addition of ionic liquid. This indicated that the films containing ionic liquid were more thermally stable (up to 350 °C) compared to ionic liquid free films.

Glass transition temperatures of the electrolyte materials were obtained from DSC measurement. Both methods exhibited a decreasing trend of $T_g$ values after addition of ionic liquid, implying that the incorporation of ionic liquid produced a plasticization effect in the (ENR-50)-lithium salt system.

The increase in $T_g$s' values with increase in salt concentrations were due to the formation of transient cross-linking between ENR-50 and lithium salt. Although the glass transition temperatures increased with salt content, the ionic conductivity values showed an increasing trend for all systems. However, the systems added with ionic liquid gave higher ionic conductivity values compared to ionic liquid free systems. The improvement in ionic liquid can be explained on the basis of interactions between the ionic liquid with both polymer chains and the lithium salt. These interactions weakened the attraction force between the lithium ions and the oxygen atoms in host polymer, thus, causing the lithium ion motion and ultimately improving the ionic conductivity of the electrolytes.

The temperature dependence conductivity plots for all systems suggested that the conductivity behaviour followed VTF behaviour. This indicated that the charge carrier transport mechanism was governed by the polymer chains' motion. In general, a large fractional free volume leads to enhance conductivity due to more facile movement of polymer chains within the free volume. The incorporation of ionic liquid helps to decrease the viscosity of the electrolyte, hence improving the ionic transport, and therefore showing higher ionic conductivity at elevated temperature. In this study, films prepared by dry method system were still stable up to the temperature of 110 °C, but films prepared by wet method could not exceed 80 °C. So, one of the advantages of the films prepared by dry method system was their greater film stability at temperatures higher than 100 °C.

In conclusion, the results in this research work indicated that BMITFSI ionic liquid is suitable to be added in the system containing ENR-50 and lithium salt prepared by both wet and dry methods. This ionic liquid reduced the glass transition temperature and improved the ionic conductivity of the (ENR-50)-LiTFSI electrolyte system. In addition, the electrochemical stability up to 2.7 eV was also obtained for electrolyte film containing BMITFSI. Although EMITFSI gave higher ionic conductivity value for wet method at room temperature, the electrochemical stability could not be determined as their poor film stability. Furthermore, EMITFSI ionic liquid was not suitable for dry method system. This ionic liquid was found to react with certain types of metal used in the sample preparation.

## REFERENCES


Agrawal, R.C. & Pandey, G.P. (2008). Solid polymer electrolytes: materials designing and all-solid-state battery applications: an overview. *Journal of Physics D: Applied Physics, 41*(22), 223001.

Ahmad, A., Rahman, M. Y. A., Low, S. P., & Hamzah, H. (2011). Effect of $LiBF_4$ salt concentration on the properties of plasticized MG49-$TiO_2$ based nanocomposite polymer electrolyte. *ISRN Materials Science*.

Ahmad, A., & Rahman, M. Y. A. (2012). Morphological, infrared, and ionic conductivity studies of poly (ethylene oxide)–49% poly (methyl methacrylate) grafted natural rubber–lithium perchlorate salt based solid polymer electrolytes. *Journal of Applied Polymer Science, 124*(5), 4222-4229.

Ahmad, S., Deepa, M., & Agnihotry, S. A. (2008). Effect of salts on the fumed silica-based composite polymer electrolytes. *Solar Energy Materials and Solar Cells*, *92*(2), 184-189.

Ameen, S., Shin, H. S., Akhtar, M. S., & Song, M. (2013). Metal Oxide Nanomaterials, Conducting Polymers and Their Nanocomposites for Solar Energy. *INTECH Open Access Publisher.*

An, Y., Zuo, P., Cheng, X., Liao, L. & Yin, G. (2011). Preparation and properties of ionic-liquid mixed solutions as a safety electrolyte for lithium ion batteries. *International Journal of Electrochemical Sciences,*)6), 2398-2410.

Appetecchi, G. B., Croce, F., & Scrosati, B. (1995). Kinetics and stability of the lithium electrode in poly (methylmethacrylate)-based gel electrolytes. *Electrochimica Acta*, *40*(8), 991-997.

Aziz, S. B., Abdullah, O. G., Rasheed, M. A., & Ahmed, H. M. (2017). Effect of high salt concentration (HSC) on structural, morphological, and electrical characteristics of chitosan based solid polymer electrolytes. *Polymers, 9, 187*, 1-18.

Bai, J., Lu, H., Cao, Y., Li, X., & Wang, J. (2017). A novel ionic liquid polymer electrolyte for quasi-solid state lithium air batteries. *The Royal Society of Chemistry, 7,* 30603-30609.

Balducci, A., Bardi, U., Caporali, S., Mastragostino, M., & Soavi, F. (2004). Ionic liquids for hybrid supercapacitors. *Electrochemistry communications*, *6*(6), 566-570.

Cao, J., Wang, L., He, X., Fang, M., Gao, J., Li, J..& Fan, S. (2013). In situ prepared nano-crystalline $TiO_2$–poly (methyl methacrylate) hybrid enhanced composite polymer electrolyte for Li-ion batteries. *Journal of Materials Chemistry A*, *1*(19), 5955-5961.

Chaurasia, S.K., Singh, R.K. and Chandra, S. (2011). Structural and transport studies on polymeric membranes of PEO containing ionic liquid, EMIM-TY: Evidence of complexation. *Solid State Ionics,*)183(, 32-39.

Chen-Yang, Y. W., Chen, S. Y., Yuan, C. Y., Tsai, C. H., & Yan, D. P. (2005). Preparation and Characterization of Composite Polymer Electrolytes Based on UV-Curable Vinylic Ether-Containing Cyclotriphosphazene, $LiClO_4$, and α-$Al_2O_3$. *Macromolecules*, *38*(7), 2710-2715.

Cheng, X., Pan, J., Zhao, Y., Liao, M., & Peng, H. (2018). Gel polymer electrolytes for electrochemical energy storage. *Adv. Energy Mater., 8, 1702184*, 1-16.

Chew, K. W., & Tan, K. W. (2011). The effects of ceramic fillers on PMMA-based polymer electrolyte salted with lithium triflate, $LiCF_3SO_3$. *International Journal of Electrochemical Science,* 6, 5792-5801.

Chintapalli, S., & Frech, R. (1996). Effect of plasticizers on ionic association and conductivity in the (PEO) $9LiCF_3SO_3$ system. *Macromolecules*, *29*(10), 3499-3506.

Cho, M.S., Seo, M.S., Nam, J.D. Choi, H.R. Koo, J.C. & Lee, Y. (2007). An electroactive conducting polymer actuator based on NBR/RTIL solid polymer electrolyte. *Smart Materials* and *Structures*, *16*(2), S237-S242.

Choi, J. W., Cheruvally, G., Kim, Y. H., Kim, J. K., Manuel, J., Raghavan, P., ... & Song, C. E. (2007). Poly (ethylene oxide)-based polymer electrolyte incorporating room-temperature ionic liquid for lithium batteries. *Solid State Ionics, 178*(19), 1235-1241.

Cohen, M. H., & Turnbull, D. (1959). Molecular transport in liquids and glasses. *The Journal of Chemical Physics*, *31*(5), 1164-1169.

Deepa, M., Sharma, N., Varshney, P., Agnihotry, S.A. and Chandra, R. (2000). An insight into the interactions between $LiN(CF_3SO_2)_2$ - γBL/DMF – PMMA by FTIR spectroscopy. *Ionics, 6*(5-6), 408-414.

Deraman, S. K., Mohamed, N. S., & Subban, R. H. Y. (2013). Conductivity and Electrochemical Studies on Polymer Electrolytes Based on Poly Vinyl (chloride)-Ammonium Triflate-Ionic Liquid for Proton Battery. *International Journal of Electrochemical. Science*, *8*, 1459-1468.

Dhumal, N. R., Noack, K., Kiefer, J. & Kim, H. J. (2014). Molecular structure and interactions in the ionic liquid 1-ethyl-3 methylimidazolium bis(trifluoromethylsulfonyl)imide. *J. Phys. Chem.A*. 118(13) 2547-2557.

Diederichsen, K. M., Buss, H. G., & McCluskey. (2017) The compensation effect in the Vogel-Tammann-Fulcher (VTF) equation for polymer-based electrolytes. *Macromolecules, 50*, 3831-3840.

Ensling, D., Stjerndahl, M., Nytén, A., Gustafsson, T., & Thomas, J. O. (2009). A comparative XPS surface study of $Li_2FeSiO_4$/C cycled with LiTFSI-and $LiPF_6$-based electrolytes. *Journal of Materials Chemistry, 19*(1), 82-88.

Eschen, T., Kӧst rs, J., Schӧnho f, M., & Stolwijk, N. A. (2012). Ionic transport in polymer electrolytes based on PEO and the PMImI ionic liquid: effects of salt concentration and iodine addition. *The Journal of Physical Chemistry B, 116*(28), 8290-8298.

Fernicola, A., Croce, F., Scrosati, B., Watanabe, T., & Ohno, H. (2007). LiTFSI-BEPyTFSI as an improved ionic liquid electrolyte for rechargeable lithium batteries. *Journal of Power Sources*, *174*(1), 342-348.

Galiński, M., Lewandowski, A., & Stępniak, I. (2006). Ionic liquids as electrolytes. *Electrochimica Acta*, *51*(26), 5567-5580.

Gan, S. N., & Hamid, Z. A. (1997). Partial conversion of epoxide groups to diols in epoxidized natural rubber. *Polymer*, *38*(8), 1953-1956.

Ganesan, S., Muthuraaman, B., Mathew, V., Madhavan, J., Maruthamuthu, P. & Suthanthiraraj, S.A. (2008). Performance of a new polymer electrolyte incorporated with diphenylamine in nanocrystalline dye-sensitized solar cell. *Solar Energy Materials and Solar Cells*, *12*)92), 1718-1722.

Gelling, I.R. & Porter, M. (1985). In: Roberts AD. ed. Natural Rubber Science And Technology. *Oxford : Oxford Press Oxford*.

Glasse, M.D., Idris, R., Latham, R.J., Linford, R.G. & Schlindwein, W.S. (2002). Polymer electrolytes based on modified natural rubber. *Solid State Ionics* )147), 289-294.

Gonzalez, F., Gregorio, V., Rubio, A., Garrido, L., Garcia, N., & Tiemblo, P. (2018). Ionic liquid-based thermoplastic solid electrolytes processed by solvent-free procedures. *Polymers, 10, 124*, 1-17.

Goodrum, J.W. & Geller, D.P. (2002). Rapid thermogravimetric measurements of boiling points and vapour pressure of saturated medium- and long-chain triglycerides. *Bioresource Technology*, *1*(84), 75-80.

Goonctilleke, S. P. P., Silva, S. M. C. E., Witharana, L. P., & Denawake, I. (1991). Chemical modification of natural rubber.

Gorecki, W., Jeannin, M., Belorizky, E., Roux, C., & Armand, M. (1995). Physical properties of solid polymer electrolyte PEO (LiTFSI) complexes. *Journal of Physics: Condensed Matter*, *7*(34), 6823-6832.

Gowda, S. R., Reddy, A. L. M., Shaijumon, M. M., Zhan, X., Ci, L., & Ajayan, P. M. (2010). Conformal coating of thin polymer electrolyte layer on nanostructured electrode materials for three-dimensional battery applications. *Nano letters*, *11*(1), 101-106.

Gracia, B., Lavallée, S., Perron, G., Michot, C., & Armand, M. (2004). Room temperature molten salts as lithium battery electrolyte. *Electrochimica Acta*, *49*(26), 4583-4588.

Han, Z. J & Tay, B. K, (2009) Ti-PS nanocomposites by plasma immersion ion impla deposition. *Nuclear instruments and methods physics research section B: Beam interaction with materials and atoms*, 267(3), 496-501.

Harilal, S. S., Allain, J. P., Hassanein, A., Hensricks, M. R. & Nieto-Perez, M. (2009). Reactivity of lithium exposed graphite surface. *Applied surface science*, 255, 8539-8543.

Hou, W. H., Chen, C. Y., Wang, C. C., & Huang, Y. H. (2003). The effect of different lithium salts on conductivity of comb-like polymer electrolyte with chelating functional group. *Electrochimica acta*, *48*(6), 679-690.

Hussin, N. S., Harun, F., & Chan, C. H. (2017). Thermal properties and conductivity of thermally treated epoxidized natural rubber-based solid polymer electrolytes. *Macromol. Symp., 376, 1700049*, 1-7.

Idris, R., Glasse, M.D., Latham, R.J., Linford, R.G. and Schlindwein, W.S. (2001). Polymer electrolytes based on modified natural rubber for use in rechargeable lithium batteries. *Journal of Power Sources,*)94), 206-211.

Idris, R., Mohd, N.H.N. & Arjan N.M. (2007). Preparation and characterization of the polymer electrolyte system ENR50/PVC/EC/PC/LiN($CF_3SO_2$)$_2$ for electrochemical device applications. *Ionics,* (13) 227-230.

Ishikawa, M., Sugimoto, T., Kikuta, M., Ishiko, E., & Kono, M. (2006). Pure ionic liquid electrolytes compatible with a graphitized carbon negative electrode in rechargeable lithium-ion batteries. *Journal of power sources*, *162*(1), 658-662.

Ismail, H., Tan, S. & Poh, B.T. (2001). Curing and mechanical properties of nitrile and natural rubber blends. *Journal of Elastomers and Plastics*, (33(, 251-262.

Jeon, G.S, Han, M.H. & Seo, G. (1998). Improving adhesion properties between rubber compound and brass-plated steel cord by the addition of epoxidized natural rubber to rubber compound. *Korean Journal of Chemical Engineering, 15*(3), 317-323.

Jiang, J., Gao, D., Li, Z., & Su, G. (2006). Gel polymer electrolytes prepared by in situ polymerization of vinyl monomers in room-temperature ionic liquids. *Reactive and Functional Polymers*, *66*(10), 1141-1148.

Johansson, A., Gogoll, A., & Tegenfeldt, J. (1996). Diffusion and ionic conductivity in Li ($CF_3SO_3$) $PEG_{10}$ and LiN ($CF_3SO_2$)$_2$ $PEG_{10}$. *Polymer*, *37*(8), 1387-1393.

Kang, Y., Lee, W., Suh, D.H. & Lee, C. (2003). Solid polymer electrolytes based on cross-linked polysiloxane-*g*-oligo (ethylene oxide): ionic conductivity and electrochemical properties. *Journal of Power Sources,*)119-121), 448-453.

Karan, N. K., Pradhan, D. K., Thomas, R., Natesan, B., & Katiyar, R. S. (2008). Solid polymer electrolytes based on polyethylene oxide and lithium trifluoro-methane sulfonate (PEO–Li$CF_3SO_3$): Ionic conductivity and dielectric relaxation. *Solid State Ionics, 179*(19), 689-696.

Kim, J. H., Min, B. R., Won, J., & Kang, Y. S. (2003). Analysis of the glass transition behavior of polymer-salt complexes: An extended configurational entropy model. *The Journal of Physical Chemistry B*, *107*(24), 5901-5905.

Kim, H. S., Idris, R., & Moon, S. I. (2004). Synthesis and electrochemical performances of epoxidised natural rubber for lithium-ion polymer batteries. *Bulletin of Electrochemistry, 20*(10), 465-469.

Kim, J. K., Cheruvally, G., Li, X., Ahn, J. H., Kim, K. W., & Ahn, H. J. (2008). Preparation and electrochemical characterization of electrospun, microporous membrane-based composite polymer electrolytes for lithium batteries. *Journal of Power Sources, 178*(2), 815-820.

Kim, S. and Park, S.J. (2009). Preparation and electrochemical properties of composite polymer electrolytes containing 1-ethyl-3-methylimidazolium tetrafluroborate salts. *Electrochimica Acta*, )54(, 3775-3780.

Klinklai, W., Kawahara, S., Marwanta, E., Mizumo, T., Isono, Y., & Ohno, H. (2006). Ionic conductivity of highly deproteinized natural rubber having various amount of epoxy group mixed with lithium salt. *Solid State Ionics, 177*(37), 3251-3257.

Koch, V. R., Nanjundiah, C., Appetecchi, G. B., & Scrosati, B. (1995). The Interfacial Stability of Li with Two New Solvent-Free Ionic Liquids: 1, 2-Dimethyl-3-propylimidazolium Imide and Methide. *Journal of the Electrochemical Society*, *142*(7), L116-L118.

Kumutha, K., Alias, Y., & Said, R. (2005). FTIR and thermal studies of modified natural rubber based polymer electrolytes. *Ionics, 11*(5-6), 472-476.

Lassègues, J. C., Grondin, J., Aupetit, C., & Johansson, P. (2008). Spectroscopic identification of the lithium ion transporting species in LiTFSI-doped ionic liquids. *The Journal of Physical Chemistry A, 113*(1), 305-314.

Lee, S. Y., Yong, H. H., Lee, Y. J., Kim, S. K., & Ahn, S. (2005). Two-cation competition in ionic-liquid-modified electrolytes for lithium ion batteries. *The Journal of Physical Chemistry B*, *109*(28), 13663-13667.

Lewandowski, A., & Świderska, A. (2004). New composite solid electrolytes based on a polymer and ionic liquids. *Solid State Ionics*, *169*(1), 21-24.

Lin, K. J. & Maranas, J. K, (2013). Does increasing ion-ion association improve cation mobility in single ion conductors?. *Phys. Chem. Chem. Phys*., (15) 16143-16151.

Liu, Y., Lee, J.Y. and Hong, L. (2002). Functionalized $SiO_2$ in poly(ethylene oxide)-based polymer electrolytes. *Journal of Power Sources*, (109), 507-514.

Long, L., Wang, S., Xiao, M., & Meng, Y. (2016). Polymer electrolytes for lithium polymer batteries. *J. Mater. Chem. A, 4*, 10038-10069.

MacCallum, J.R & Vincent, C.A (1989). Polymer electrolyte review (Vol.2). *Springer*.

McFarlane, D.R., Sun, J., Golding, J., Meakin, P., & Forsyth, M. (2000). High conductivity molten salts based on the imide ion. *Electrochimica acta*, *45*(8), 1271-1278.

Macfarlane, D.R., Forsyth, M., Howlett, P.C., Pringle, J.M., Sun, J., Annat, G., Neil, W. and Izgorodina, E.I. (2007). Ionic liquids in electrochemical devices and processes: Managing interfacial electrochemistry. *Accounts of Chemical Research*, (40(, 1165-1173.

Mahadeva, S. K., Yi, C., & Kim, J. (2011). Electrical and electromechanical properties of 1-butyl-3-methylimidazolium bis (trifluoromethylsulfonyl) imide-blended cellulose. *Ionics, 17*(1), 41-47.

Marzantowicz, M., Dygas, J. R., Krok, F., Łasińska, A., Florjańczyk, Z., & Zygadło-Monikowska, E. (2006). In situ microscope and impedance study of polymer electrolytes. *Electrochimica acta, 51*(8), 1713-1727.

McEwen, A. B., McDevitt, S. F., & Koch, V. R. (1997). Nonaqueous electrolytes for electrochemical capacitors: Imidazolium cations and inorganic fluorides with organic carbonates. *Journal of The Electrochemical Society*, *144*(4), L84-L86.

Miao, R., Liu, B., Zhu, Z., Liu, Y., Li, J., Wang, X., & Li, Q. (2008). PVDF-HFP-based porous polymer electrolyte membranes for lithium-ion batteries. *Journal of Power Sources, 184*(2), 420-426.

Miranda, R., Yang, J., Roy, C., & Vasile, C. (2001). Vacuum pyrolysis of commingled plastics containing PVC I. Kinetic study. *Polymer Degradation and Stability, 72*(3), 469-491.

Misenan, M. S. M., Ali, E. S., & Khiar, A. S. A. (2018). Conductivity, dielectric and modulus study of chitosan-methyl cellulose-BMIMTFSI polymer electrolyte doped with cellulose nano crystal. *AIP Conference Proceedings, 1972, 030010*, 1-5.

Mobarak, N. N., Ahmad, A., Abdullah, M.P., Ramli, N. & Rahman, M.Y.A. (2013). Conductivity enhancement via chemical modification of chitosan based green polymer electrolyte. *Electrochimica Acta*, *92*, 161-167.

Mohamed, S.N., Johari, N.A., Ali, A.M.M., Harun, M.K., & Yahya, M.Z.A., (2008). Electrochemical studies on epoxidised natural rubber-based gel polymer electrolytes for lithium-air cells. *Journal of Power Sources, 183*, 351-354.

Mohammad, S. F., Zainal, N., Ibrahim, S., & Mohamed, N. S. (2013). Conductivity enhancement of (epoxidized natural rubber 50)/poly (ethyl methacrylate)–ionic liquid-ammonium triflate. *International Journal of Electrochemical Science,* 8, 6145-6153.

Morita, M., Shirai, T., Yoshimoto, N., & Ishikawa, M. (2005). Ionic conductance behavior of polymeric gel electrolyte containing ionic liquid mixed with magnesium salt. *Journal of power sources, 139*(1), 351-355.

Mustafa, M. F., Ridwan, N. I. M., Hatta, F. F., & Yahya, M. Z. A. (2012). Effect of Dimethyl Carbonate Plasticizer on Ionic Conductivity of Methyl Cellulose-Based Polymer Electrolytes. *International Atomic Energy Agency (IAEA*).

Nakajima, H. & Ohno, H. (2005). Preparation of thermally stable polymer electrolytes from imidazolium-type ionic liquid derivatives. *Polymer*, *46*, 11499-11504.

Nanbu, N., Sasaki, Y. & Kitamura, F. (2003). In situ FT-IR spectroscopic observation of a room-temperature molten salt | gold electrode interphase. *Electrochemistry Communications*, 5, 383-387.

Nazir, K., Aziz, A. F., Yahya, M. Z. A., & Ali, A. M. M. (2017). Ionic conductivity of epoxidized poly (methyl methacrylate)-grafted natural rubber based gel polymer electrolyte for dye sensitized polymer solar cell. *AIP Conference Proceedings, 1877, 040003*, 1-8.

Nejati, S. & Lau, K. K. (2011). Integration of polymer electrolytes in dye sensitized solar cells by initiated chemical vapor deposition. *Thin Solid Films*, *519*(14), 4551-4554.

Nguyen, C. A., Xiong, S., Ma, J., Lu, X., & Lee, P. S. (2011). High ionic conductivity P (VDF-TrFE)/PEO blended polymer electrolytes for solid electrochromic devices. *Physical Chemistry Chemical Physics*, *13*(29), 13319-13326.

Noack, K., Schulz, P.S., Paape, N., Kiefer, J., Wasserscheid, P. & Leipertz, A. (2010). The role of the C2 position in interionic interactions of imidazolium based ionic liquids: a vibrational and NMR spectroscopic study. *Physical Chemistry Chemical Physics*, *12*, 14153-14161.

Noda, A., & Watanabe, M. (2000). Highly conductive polymer electrolytes prepared by in situ polymerization of vinyl monomers in room temperature molten salts. *Electrochimica Acta*, *45*(8), 1265-1270.

Noda, A., Hayamizu, K., & Watanabe, M. (2001). Pulsed-gradient spin-echo 1H and 19F NMR ionic diffusion coefficient, viscosity, and ionic conductivity of non-chloroaluminate room-temperature ionic liquids. *The Journal of Physical Chemistry B*, *105*(20), 4603-4610.

Osada, R., Hoshino, T., Okada, K., Ohmasa, Y., & Yao, M. (2009). Surface tension of room temperature ionic liquids measured by dynamic light scattering. *The Journal of Chemical Physics*, *130*(18), 184705.

Park, M. J., Choi, I., Hong, J., & Kim, O. (2013). Polymer electrolytes integrated with ionic liquids for future electrochemical devices. *Journal of Applied Polymer Science, 129*(5), 2363-2376.

Peng, C., Yang, L., Zhang, Z., Tachibana, K. & Yang, Y. (2007). Anodic bahavior of Al current collector in 1-alkyl-3-methylimidazolium bis[(trifluoromethyl)sulfonyl] amide ionic liquid electrolytes. *Journal of Power Sources*, *173*, 510-517.

Pradhan, D. K., Choudhary, R. N. P., & Samantaray, B. K. (2008). Studies of dielectric relaxation and AC conductivity behavior of plasticized polymer nanocomposite electrolytes. *International Journal of Electrochemical Science, 3*(5), 597-608.

Rajendran, S., Sivakumar, M., & Subadevi, R. (2003). Effect of salt concentration in poly (vinyl alcohol)-based solid polymer electrolytes. *Journal of Power Sources*, *124*(1), 225-230.

Rajendran, S., Sivakumar, P., & Babu, R. S. (2006). Investigation on poly (vinylidene fluoride) based gel polymer electrolytes. *Bulletin of Materials Science, 29*(7), 673-678.

Rajendran, S., Prabhu, M. R., & Rani, M. U. (2008). Ionic conduction in poly (vinyl chloride)/poly (ethyl methacrylate)-based polymer blend electrolytes complexed with different lithium salts. *Journal of Power Sources, 180*(2), 880-883.

Ramesh, S., & Lu, S. C. (2008). Effect of nanosized silica in poly (methyl methacrylate)–lithium bis (trifluoromethanesulfonyl) imide based polymer electrolytes. *Journal of Power Sources*, *185*(2), 1439-1443.

Ramesh, S., Liew, C. W., & Ramesh, K. (2011). Evaluation and investigation on the effect of ionic liquid onto PMMA-PVC gel polymer blend electrolytes. *Journal of Non-Crystalline Solids, 357*(10), 2132-2138.

Rao, M., Geng, X., Liao, Y., Hu, S., & Li, W. (2012). Preparation and performance of gel polymer electrolyte based on electrospun polymer membrane and ionic liquid for lithium ion battery. *Journal of Membrane Science*, *399*, 37-42.

Ratner, M. A., Johansson, P., & Shriver, D. F. (2000). Polymer electrolytes: ionic transport mechanisms and relaxation coupling. *Materials Research Society, 25*(03), 31-37.

Razali, I. & Wan Siti Nor, W.A.H. )2007). Characterization of plasticized and nonplasticized epoxidized natural rubber based polymer electrolyte systems. *Solid State Science and Technology 15*(1), 147-155.

Rudziah, S., Ahmad, A., Ahmad, I., & Mohamed, N.S. (2015). Biopolymer electrolytes based on blend of kappa-carrageenan and cellulose derivatives for potential application in dye sensitized solar cell. *Electrochimica Acta, 175*, 162-168.

Sakaebe, H., & Matsumoto, H. (2003). *N*-Methyl-*N*-propylpiperidinium bis (trifluoromethanesulfonyl) imide (PP13–TFSI)–novel electrolyte base for Li battery. *Electrochemistry Communications*, *5*(7), 594-598.

Sato, T., Maruo, T., Marukane, S., & Takagi, K. (2004). Ionic liquids containing carbonate solvent as electrolytes for lithium ion cells. *Journal of Power Sources*,*138*(1), 253-261.

Scott, M. P., Rahman, M., & Brazel, C. S. (2003). Application of ionic liquids as low-volatility plasticizers for PMMA. *European polymer journal*, *39*(10), 1947-1953.

Sekhon, S. S., Krishnan, P., Singh, B., Yamada, K., & Kim, C. S. (2006). Proton conducting membrane containing room temperature ionic liquid. *Electrochimica acta*, *52*(4), 1639-1644.

Seki, S., Susan, M.A.B.H., Kaneko, T., Tokuda, H., Noda, A. & Watanabe, M. (2005). Distinct difference in ionic transport behaviour in polymer electrolytes depending on the matrix polymers and incorporated salts, *Journal of Physical Chemistry B*, *109*, 3886-3892.

Sheha, E., Khoder, H., Shanap, T. S., El-Shaarawy, M. G., & El Mansy, M. K. (2012). Structure, dielectric and optical properties of p-type (PVA/CuI) nanocomposite polymer electrolyte for photovoltaic cells. *Optik-International Journal for Light and Electron Optics, 123*(13), 1161-1166.

Shin, J.H., Henderson, W.A. & Passerini, S. (2003). Ionic liquids to the rescue? Overcoming the ionic conductivity limitations of polymer electrolytes. *Electrochemistry Communications, 5*, 1016-1020.

Shin, J. H., Henderson, W. A., & Passerini, S. (2005). PEO-based polymer electrolytes with ionic liquids and their use in lithium metal-polymer electrolyte batteries. *Journal of The Electrochemical Society, 152*(5), A978-A983.

Singh S., B., & Sekhon, S. S. (2005). Polymer electrolytes based on room temperature ionic liquid: 2, 3-dimethyl-1-octylimidazolium triflate. *The Journal of Physical Chemistry B*, *109*(34), 16539-16543.

Singh, P. K., Kim, K. W., & Rhee, H. W. (2009). Quantum dot doped solid polymer electrolyte for device application. *Electrochemistry Communications*, *11*(6), 1247-1250.

Stephan, A. M., Saito, Y., Muniyandi, N., Renganathan, N. G., Kalyanasundaram, S., & Elizabeth, R. N. (2002). Preparation and characterization of PVC/PMMA blend polymer electrolytes complexed with $LiN(CF_3SO_2)_2$. *Solid State Ionics, 148*(3), 467-473.

Subban, R.H.Y. (2004). Some properties of plasticized and composite PVC-based polymer electrolytes and $LiCoO_2$/ PVC-$LiCF_3SO_3$-$SiO_2$/MCMB electrochemical cells. *Ph.D Thesis* University of Malaya.

Sukri, N., Mohamed, N. S., & Subban,R. H. Y. (2017). Dielectric and conduction mechanism studies of PEMA/ENR-50 blend with $LiCF_3SO_3$ salt. *AIP Conference Proceedings, 1877, 060002*, 1-8.

Tokuda, H., Hayamizu, K., Ishii, K., Susan, M. A. B. H., & Watanabe, M. (2004). Physicochemical properties and structures of room temperature ionic liquids. 1. Variation of anionic species. *The Journal of Physical Chemistry B*, *108*(42), 16593-16600.

Tong, Y., Xu, Y., Chen, D., Xie, Y., Chen, L. Que, M., & H, Y. (2017). Deformable and flexible electrospun nanofiber-supported cross-linked gel polymer electrolyte membranes for high safety lithium-ion batteries. *RSC Adv., 7*, 22728-22734.

Triolo, A., Russina, O., Fazio, B., Appetecchi, G. B., Carewska, M., & Passerini, S. (2009). Nanoscale organization in piperidinium-based room temperature ionic liquids. *The Journal of chemical physics*, *130*(16), 164521-164521.

Tsuzuki, S., Tokuda, H., Hayamizu, K., & Watanabe, M. (2005). Magnitude and directionality of interaction in ion pairs of ionic liquids: Relationship with ionic conductivity. *The Journal of Physical Chemistry B*, *109*(34), 16474-16481.

Turner, M.B., Spear, S.K., Holbrey, J.D., Daly, D.T. & Rogers, R.D. (2005). Ionic liquid-reconstituted cellulose composites as solid support matrices for biocatalyst immobilization. Biomacromolecules, *6*, 2497-2502.

Ueki, T., & Watanabe, M. (2008). Macromolecules in ionic liquids: progress, challenges, and opportunities. *Macromolecules*, *41*(11), 3739-3749.

Vuk, A.S., Jovanovski, V., Pollet-Villart, A., Jerman, I. & Orel, B. (2008). Imidazolium-based ionic liquid derivatives for application in electrochromic devices. *Solar Energy Materials & Solar Cells*, *92*, 126-135.

Wang, W., & Alexandridis, P. (2016). Composite polymer electrolytes : Nanoparticles affect structure and properties. *Polymers, 8, 387*, 1-36.

Wang, Y., Chen, K. S., Mishler, J., Cho, S. C., & Adroher, X. C. (2011). A review of polymer electrolyte membrane fuel cells: technology, applications, and needs on fundamental research. *Applied Energy*, *88*(4), 981-1007.

Wang, Y., Zaghib, K., Guerfi, A., Bazito, F. F., Torresi, R. M., & Dahn, J. R. (2007). Accelerating rate calorimetry studies of the reactions between ionic liquids and charged lithium ion battery electrode materials. *Electrochimica Acta*, *52*(22), 6346-6352.

Watanabe, M., & Mizumura, T. (1996). Conductivity study on ionic liquid/polymer complexes. *Solid State Ionics*, *86*, 353-356.

Wilson, J., Ravi, G. & Kulandainathan, M.A. (2006). Electrochemical studies on inert filler incorporated poly(vinylidene fluoride-hexafluoropropylene)(PVDF-HFP) composite electrolytes. *Polimeros, 16*, 88-93.

Xu, C., Sun, B., Gustafsson, T., Edstrom, K., Brandell, D., & Hahlin, M. (2013). Interface layer formation in solid polymer electrolyte lithium batteries: an XPS study. *Journal of Materials Chemistry A, 00, 1-3*, 1-9.

Xuan, L., An, Y., Fang, W., Liao, L., Ma, Y., Ren, Z., & Yin, G. (2011). Organic Electrolyte Improving the Performance of Ionic Liquid-PEO Polymer Electrolyte Based Lithium Ion Batteries. *International Journal of Electrochemical Science, 6*(12), 6590-6598.

Yoshida, A., Honda, S., Goto, H., & Sugimoto, H. (2014). Synthesis of H-shaped carbon-dioxide-derived poly (propylene carbonate) for topology-based reduction of the glass transition temperature. *Polymer Chemistry*, *5*(6), 1883-1890.

Zhengxi, Z, Xuhui, G & Li, Y. (2005). Electrochemical properties of room temperature ionic liquids incorporating $BF_4^-$ and $TFSI^-$ anions as green electrolytes. *Chinese Science Bulletin*, *50*)18), 2005-2009.

Zhu, C., Cheng, H. & Yang, Y. (2008). Electrochemical characterization of two types of PEO-based polymer electrolytes with room temperature ionic liquids. *Journal of Electrochemical Society, 155*(8(, A569-A575.

## LIST OF PUBLICATIONS AND PAPERS PRESENTED

### Publications

1. **Zainal, N**., Mohamed, N.S. (2013), Properties of ENR-50 Based Electrolyte System. *Sains Malaysiana* 42(4): 481-485.

2. **Zainal, N**., Idris, R. & Mohamed, N.S. (2012), Studies of ENR-50 and $LiN(SO_2CF_3)_2$ electrolyte system. *Advanced Materials Research* 545, 303-307.

3. **Zainal, N**., Idris, R. & Mohamed, N.S. (2011), Characterization of (ENR-50)-ionic liquid-LiTFSI electrolyte system. *Advanced Materials Research: Applications of Engineering Materials* 287-290:424-427.

### Conferences

1. The 16th International Meeting on Lithium Batteries, 17th-22nd June 2012, ICC Jeju Korea.
   **Title**: Characterization of (ENR-50)-ionic liquid based electrolyte system.
   (Poster presenter)

2. Malaysia Polymer International Conference (MPIC 2011), 19th-20th October 2011, Equatorial Hotel, Bangi Putrajaya.
   **Title**: Properties of ENR-50 Based Electrolyte System.
   (Poster presenter)

3. International Conference on Advanced Engineering Materials and Technology, 29th-31st July 2011, Sanya China.
   **Title**: Characterization of (ENR-50)-ionic liquid-LiTFSI electrolyte system.
   (Oral presenter)

4. International Conference on Advanced Engineering Materials and Technology, 29th Nov-1st Dec 2010, Prince Hotel, Kuala Lumpur.
   **Title**: Studies of ENR-50 and $LiN(SO_2CF_3)_2$ electrolyte system.
   (Poster presenter)